

Power-enhanced leading-logarithmic QED corrections to $B_q \rightarrow \mu^+ \mu^-$

MARTIN BENEKE^a, CHRISTOPH BOBETH^a AND ROBERT SZAFRON^a

^a*Physik Department T31,
James-Frank-Straße 1, Technische Universität München,
D-85748 Garching, Germany*

Abstract

We provide a systematic treatment of the previously discovered power-enhanced QED corrections to the leptonic decay $B_q \rightarrow \mu^+ \mu^-$ ($q = d, s$) in the framework of soft-collinear effective theory (SCET). Employing two-step matching on SCET_I and SCET_{II}, and the respective renormalization group equations, we sum the leading-logarithmic QED corrections and the mixed QED–QCD corrections to all orders in the couplings for the matrix element of the semileptonic weak effective operator Q_9 . We propose a treatment of the B -meson decay constant and light-cone distribution amplitude in the presence of process-specific QED corrections. Finally we include ultrasoft photon radiation and provide updated values of the non-radiative and radiative branching fractions of $B_q \rightarrow \mu^+ \mu^-$ decay that include the double-logarithmic QED and QCD corrections.

Contents

1	Introduction	1
2	Preliminaries	4
2.1	$\Delta B = 1$ effective theory for $b \rightarrow q\ell^+\ell^-$	4
2.2	Kinematics of $B_q \rightarrow \ell^+\ell^-$ and power counting	5
2.3	SCET: Definitions and conventions	7
2.4	Heuristic discussion	7
3	SCET_I	11
3.1	Operators	11
3.2	Matching	12
3.3	RG evolution	13
4	SCET_{II}	15
4.1	Operators	15
4.2	Renormalization	17
4.3	Matching	25
5	QED effects and the B-meson decay constant and LCDA	26
6	Resummed power-enhanced $B_q \rightarrow \ell^+\ell^-$ amplitude	29
6.1	Factorization of the amplitude	29
6.2	Resummed amplitude	31
7	$B_q \rightarrow \mu^+\mu^-$ decay width	34
7.1	Tree-level amplitude to $B_q \rightarrow \mu^+\mu^-$	34
7.2	Decay width and ultrasoft photons	36
8	Numerical results	38
8.1	Resummation effects for power-enhanced amplitude	39
8.2	Branching fractions $B_q \rightarrow \mu^+\mu^-$	42
8.3	Rate asymmetries in $B_q \rightarrow \mu^+\mu^-$	46
9	Summary and conclusions	48
A	SCET conventions and results	50
A.1	Lagrangians	50
A.2	Renormalization conventions	53
A.3	SCET _I renormalization	54
A.4	SCET _{II} renormalization	55
B	SCET operators	57
	References	62

1 Introduction

The purely leptonic B -meson decays $B_u \rightarrow \ell \bar{\nu}_\ell$ and $B_{d,s} \rightarrow \ell^+ \ell^-$ ($\ell = e, \mu, \tau$) are among the most valuable probes of the quark-mixing parameters in the Standard Model (SM), namely the parameters of the Cabibbo-Kobayashi-Maskawa (CKM) matrix. The charged-current mediated tree-level decays $B_u \rightarrow \ell \bar{\nu}_\ell$ give direct access to the CKM element $|V_{ub}|$, whereas the flavour-changing neutral-current-mediated $B_{d,s} \rightarrow \ell^+ \ell^-$ decays allow to determine the combination $|V_{tb} V_{td,ts}^*|$ up to a perturbatively calculable short-distance factor that depends on the top-quark mass [1]. Moreover the helicity suppression of the decay rate leads to a high sensitivity to scalar- and pseudo-scalar interactions beyond the SM.

Their importance derives from the fact that the nonperturbative hadronic bound-state effects of the B_q mesons due to the strong interaction (QCD) appear in theoretical predictions at leading order (LO) in electromagnetic (QED) interactions only in the form of the B -meson decay constant f_{B_q} . The most recent lattice-QCD values of $f_{B_{u,d}}$ and f_{B_s} of the FNAL/MILC Collaboration [2] have now reached the relative precision of about 0.7 % and 0.5 %, respectively. It is expected that this precision will be confirmed by other lattice groups and reduced even further in the future thus paving the way to very precise determinations of CKM parameters in the SM. Such a degree of theoretical control on the QCD hadronic uncertainties in FCNC flavour physics is currently only available for $K \rightarrow \pi \nu \bar{\nu}$ decays [3] and will be for the mass differences ΔM_q in neutral B -meson mixing once lattice calculations achieve the required precision.

Given the small uncertainties due to f_{B_q} , it is mandatory to control all other corrections, which arise from several energy scales spanned by the SM, at the percent level. Such control is already achieved for perturbatively calculable higher-order QCD and electroweak (EW) corrections in the framework of the effective theory (EFT) of electroweak interactions of the SM for $\Delta B = 1$ decays [4]. This comprises *i*) the decoupling of the heavy W and Z bosons and the top quark at the electroweak scale $\mu_W \sim m_W$ for $b \rightarrow u \ell \bar{\nu}_\ell$ [5–7] and $b \rightarrow q \ell^+ \ell^-$ [8,9] and *ii*) the resummation of large logarithms under evolution of QCD and QED down to the scale $\mu_b \sim m_b$ of the order of the bottom-quark mass using renormalization-group (RG) improved perturbation theory [10,11].

On the other hand, a consistent simultaneous treatment of QCD and QED corrections is lacking for scales below μ_b . On general grounds, it is well understood that only a suitably defined decay rate $\Gamma[B_q \rightarrow \ell^+ \ell^-] + \Gamma[B_q \rightarrow \ell^+ \ell^- + n \gamma(E_\gamma < \Delta E)]$ that includes real and virtual photon radiation is infrared-finite and well-defined. It is subject to the experimental setup in the form of a photon-energy cutoff ΔE that requires to include in theoretical predictions an arbitrary number of additional undetected real photons with energy $E_\gamma < \Delta E$. The soft-photon emission from the final-state leptons is currently simulated in experimental analyses [12–17] with tools like PHOTOS [18], such that the measured branching fraction is interpreted as the non-radiative one [19]. Further, the soft initial-state radiation has been estimated to be very small based on heavy-hadron chiral perturbation theory (HH χ PT) [20] provided $\Delta E \lesssim 60$ MeV. Thus the present knowledge of QED corrections below the scale μ_b is restricted to very low (ultrasoft) scales $\mu_{us} \ll \Lambda_{\text{QCD}}$ below the QCD confinement scale, where virtual photons cannot resolve partons in the B_q meson. Moreover, it relies entirely

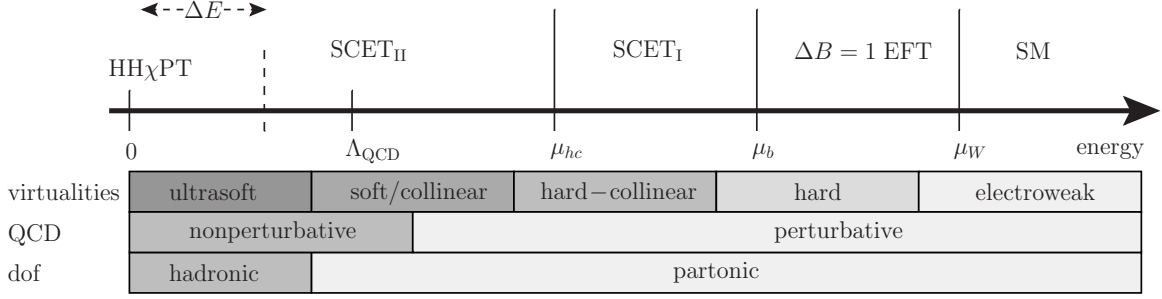


Figure 1: Scheme of the multiple scales and the respective tower of effective theories applicable to $B_q \rightarrow \ell^+ \ell^-$ transitions and more generally also other b -hadron decays. See text for more explanations. The range of ΔE is indicated for the case $\Delta E \ll \Lambda_{\text{QCD}}$ that we consider here. The degrees of freedom (dof) are hadronic at low energies in $\text{HH}\chi\text{PT}$.

on a description in terms of hadronic degrees of freedom (i.e. mesons), which, although it permits a perturbative treatment of QED effects, requires in principle the knowledge of low-energy constants (LEC). The LECs include the impact of the dynamics above the ultrasoft scales, but conceptually little is known of the consistent theoretical treatment of the scales up to μ_b to reliably control the theoretical uncertainties to the percent level. Although one might work perturbatively in a partonic picture even below scales μ_b , at least at the (hard-collinear) scale $\mu_{hc} \sim 1$ GeV, a nonperturbative regime sets in below μ_{hc} that still requires to use the partonic picture because photons continue to resolve the constituents of the hadrons. In the nonperturbative regime, QED corrections need the evaluation of non-local time-ordered products of the electromagnetic quark currents. This spoils naive factorization of the QED and QCD effects based on the soft-photon approximation. A more elaborate treatment based on effective field theory (EFT) approach is necessary to perform the systematic expansion of the higher-order QED matrix elements in powers of Λ_{QCD}/m_b . The theoretical treatment will also depend on the actual magnitude of ΔE and its place within the hierarchy of the above scales. The above discussion is summarized schematically in Figure 1. The nonperturbative matching to $\text{HH}\chi\text{PT}$ and hence the hadronic picture at very low virtualities is optional if one parameterizes the low-energy physics in terms of matrix elements of the previous EFT, SCET_{II} . However, in this case the point-like coupling of ultrasoft photons to mesons is not manifest.

The first step towards a systematic treatment of QED effects below the scale μ_b has been taken in [21] exploiting the special kinematic situation of the $B_q \rightarrow \mu^+ \mu^-$ decays. The final-state muons are energetic, low mass (“collinear”) modes. Their dynamics at scales below μ_b is described by soft-collinear effective theory (SCET). In a two-step decoupling, similar to the treatment of QCD effects in heavy-to-light form factors and hadronic decays (see, for instance, the review [22]), first hard virtualities $\mathcal{O}(m_b^2)$ and subsequently hard-collinear virtualities $\mathcal{O}(m_b \Lambda)$ are removed perturbatively to arrive at SCET_{II} that describes muons with (collinear or soft) virtualities of at most $\mathcal{O}(\Lambda^2)$. The scale $\Lambda \sim \mathcal{O}(100 \text{ MeV})$ represents a typical scale for the muon mass, the spectator quark mass and at the same time hadronic bound-state effects Λ_{QCD} .

The one-loop calculation of electromagnetic corrections below the scale μ_b performed in [21] resulted in the expression (notation explained there)

$$\begin{aligned}
i\mathcal{A} = & m_\ell f_{B_q} \mathcal{N} C_{10} [\bar{\ell} \gamma_5 \ell] + \frac{\alpha_{\text{em}}}{4\pi} Q_\ell Q_q m_\ell m_{B_q} f_{B_q} \mathcal{N} [\bar{\ell} (1 + \gamma_5) \ell] \\
& \times \left\{ \int_0^1 du (1-u) C_9^{\text{eff}}(u m_b^2) \int_0^\infty \frac{d\omega}{\omega} \phi_+(\omega) \left[\ln \frac{m_b \omega}{m_\ell^2} + \ln \frac{u}{1-u} \right] \right. \\
& \left. - Q_\ell C_7^{\text{eff}} \int_0^\infty \frac{d\omega}{\omega} \phi_+(\omega) \left[\ln^2 \frac{m_b \omega}{m_\ell^2} - 2 \ln \frac{m_b \omega}{m_\ell^2} + \frac{2\pi^2}{3} \right] \right\} + \dots
\end{aligned} \tag{1.1}$$

for the $B_s \rightarrow \mu^+ \mu^-$ decay amplitude. A surprising feature of the electromagnetic correction in this expression is that in the expansion Λ/m_b it is *power-enhanced* by a factor of m_b/Λ relative to the well-known amplitude in the absence of QED effects, thereby partially compensating the suppression with the electromagnetic coupling α_{em} . The virtual photon exchange between the final-state leptons and the spectator quark in the B_q meson leads to a non-local annihilation over distances $(m_b \Lambda)^{-1/2}$ inside the B_q meson, different from the local annihilation through weak currents. Whereas the latter is described by f_{B_q} , the former involves the B -meson light-cone distribution amplitude (LCDA) $\phi_+(\omega)$, showing that strong interaction effects cannot be solely described in terms of f_{B_q} once QED effects below the scale μ_b are included. The power-enhanced QED contribution involves two competing terms in the curly brackets, one from the semileptonic operator Q_9 and one from the dipole operator Q_7 . Both terms are further enhanced by large logarithms $\ln(m_b \omega/m_\ell^2) \sim \ln(m_b \Lambda/m_\ell^2)$, and interfere destructively, which reduces the size of the power enhancement. It was also found that in $b \rightarrow u \ell \bar{\nu}_\ell$ the structure of the semi-leptonic weak currents does not give rise to such a power enhancement in $B_u \rightarrow \mu \bar{\nu}_\mu$.

In the present work, the SCET interpretation underlying the above result, which was only briefly mentioned in [21], is provided in detail, together with the EFT treatment of QED and the summation of logarithms. The SCET approach to QED differs from standard QCD applications in several details and factorization theorems for QED effects are not well established, unlike the case for the pure QCD corrections. Two crucial differences are the presence of masses for leptons that regularize the collinear divergences in QED, and the presence of electromagnetically charged external states. Additionally, the soft-photon cutoff is typically below the scale of lepton masses, and thus real collinear photon radiation may be excluded, while virtual collinear corrections can be still present. An additional challenge is related to the proper treatment of QED radiation from light quarks, where nonperturbative QCD has to be consistently treated. Here we use SCET to resum the leading logarithms for the power-enhanced contribution, which arises entirely from virtual effects between the hard and soft/collinear scales. We focus on the contribution of the semileptonic operator Q_9 , since one of the two logarithms enhancing the dipole operator Q_7 term is not a standard RG logarithm, in which case the summation with SCET methods is presently not understood. However, from the numerical point of view, our main finding is that higher-order QED logarithms appear to be negligibly small. The principal effect of

resummation arises from QCD evolution on top of the one-loop QED effect shown above. This observation will allow us to also estimate the effect of resummation on the contribution of the dipole operator.

As a by-product of this investigation, we find that hadronic matrix elements in the presence of QED are less universal than is usually assumed. For example, the nonperturbative matrix elements defining “the” B -meson decay constant and the LCDA depend on the charges and directions of the outgoing energetic particles through light-like electromagnetic Wilson lines.

The outline of the paper is as follows. After a short introduction to the conventions for the $\Delta B = 1$ EFT of $b \rightarrow q\ell^+\ell^-$ decays in Section 2.1, we introduce the power counting set by the external kinematics of $B_q \rightarrow \ell^+\ell^-$ decays in Section 2.2 and provide the power-counting of the SCET fields in Section 2.3. Section 2.4 briefly recapitulates and interprets the findings of the fixed-order calculation [21] relevant to the SCET approach and provides a short outlook on the various contributions in SCET, discussed in the main part later. We proceed with the decoupling of hard virtualities and the RG evolution in SCET_I in Section 3 and further the decoupling of hard-collinear virtualities and the RG evolution in SCET_{II} in Section 4. The definition of the B -meson decay constant and LCDA in the presence of QED corrections is discussed in Section 5. The factorization of the power-enhanced amplitude is presented in Section 6 and the combination with the leading amplitude together with the ultrasoft parts given in Section 7. Eventually we present the numerical impact of QED corrections and updated calculations of the non-radiative and radiative branching fractions in Section 8. Technical details on SCET conventions and definitions as well as the construction of SCET operators have been relegated to appendices.

2 Preliminaries

2.1 $\Delta B = 1$ effective theory for $b \rightarrow q\ell^+\ell^-$

The effective theory for $|\Delta B| = 1$ decays $b \rightarrow q\ell^+\ell^-$ with $q = d, s$ in the framework of the SM,

$$\mathcal{L}_{\Delta B=1} = \mathcal{N}_{\Delta B=1} \left[\sum_{i=1}^{10} C_i(\mu_b) Q_i + \frac{V_{ub}V_{uq}^*}{V_{tb}V_{tq}^*} \sum_{i=1}^2 C_i(\mu_b) (Q_i^u - Q_i^c) \right] + \text{h.c.}, \quad (2.1)$$

includes operators Q_i , which are charged-current ($i = 1, 2$), QCD-penguin operators ($i = 3, \dots, 6$), dipole operators ($i = 7, 8$) and semileptonic operators ($i = 9, 10$). These operators are sufficient for the treatment of the QED effects in $B_q \rightarrow \ell^+\ell^-$ discussed in this paper. We follow the operator definitions of [23] and give only those of the three most relevant operators for our purposes

$$Q_7 = \frac{e}{(4\pi)^2} \bar{m}_b [\bar{q}\sigma^{\mu\nu} P_R b] F_{\mu\nu}, \quad (2.2)$$

$$Q_9 = \frac{\alpha_{\text{em}}}{4\pi} (\bar{q}\gamma^\mu P_L b) \sum_\ell \bar{\ell}\gamma_\mu \ell, \quad (2.3)$$

$$Q_{10} = \frac{\alpha_{\text{em}}}{4\pi} (\bar{q} \gamma^\mu P_L b) \sum_\ell \bar{\ell} \gamma_\mu \gamma_5 \ell, \quad (2.4)$$

where $\alpha_{\text{em}} \equiv e^2/(4\pi)$ and \bar{m}_b denotes the running $\overline{\text{MS}}$ b -quark mass. The overall normalization factor is $\mathcal{N}_{\Delta B=1} \equiv 2\sqrt{2}G_F V_{tb} V_{ts}^*$. The term proportional to $V_{ub} V_{uq}^*$ enters $B_q \rightarrow \ell^+ \ell^-$ only through the QED correction. The Wilson coefficients $C_i(\mu_b)$ and running quark masses need to be evaluated at the renormalization scale $\mu_b \sim m_b$ of the order of the b -quark mass. In the SM they include NNLO QCD matching corrections [9, 24] at the electroweak scale $\mu_W \sim m_W$ of the order of the W -boson mass, and C_{10} further includes the NLO EW matching corrections [8]. The resummation of large logarithms between the scales μ_W and μ_b has been taken into account to the corresponding order following [10, 11], see also [8] for further details. Especially the inclusion of NLO EW corrections [8] to C_{10} requires care in the choice of the numerical input of the electroweak parameters. It must respect the adopted renormalization scheme as for example m_W is not an independent parameter any more.

2.2 Kinematics of $B_q \rightarrow \ell^+ \ell^-$ and power counting

The two-body decay $B_q(p_B) \rightarrow \ell^+(p_{\bar{\ell}}) \ell^-(p_\ell)$ implies lepton energies $E_\ell = E_{\bar{\ell}} = m_{B_q}/2$, such that for light leptons $\ell = e, \mu$ the hierarchy $m_\ell \ll E_\ell$ implies that the leptons are actually “collinear” particles. At the partonic level,

$$b(p_b) + q(l_q) \rightarrow \ell^+(p_{\bar{\ell}}) + \ell^-(p_\ell), \quad (2.5)$$

the mesonic bound state restricts the initial-state quarks to be soft. Writing $p_b = m_b v + l_b$, both quarks move inside the B_q meson with soft residual momenta $l_b, l_q \sim \Lambda_{\text{QCD}}$ of the order of the strong binding energy Λ_{QCD} . In the decomposition of p_b , v is a normalized time-like vector, $v^2 = 1$, which can be interpreted as the four-velocity of the B_q meson. The soft scaling of the residual b - and light-quark momenta can be expressed as

$$l_b, l_q \sim m_b \lambda_s^2 \quad (2.6)$$

in terms of the small dimensionless quantity

$$\lambda_s = \sqrt{\frac{\Lambda_{\text{QCD}}}{m_b}} \ll 1 \quad \text{for} \quad \Lambda_{\text{QCD}} \approx (0.2 - 0.4) \text{ GeV}. \quad (2.7)$$

In this picture both quarks are bound in the B_q and annihilate via the $\Delta B = 1$ operators (2.1). The energy stored in the b -quark mass is released in the form of the energetic lepton pair, which is emitted back-to-back in the B_q rest frame thereby singling out a particular direction. This direction can be described by a pair of light-like vectors $n_+^2 = n_-^2 = 0$ and $n_+ \cdot n_- = 2$ and any four-vector can be decomposed as

$$p^\mu = (n_+ p) \frac{n_-^\mu}{2} + p_\perp^\mu + (n_- p) \frac{n_+^\mu}{2}. \quad (2.8)$$

The components $p \sim (n_+p, p_\perp^\mu, n_-p)$ of the lepton momenta then exhibit the scaling

$$p_\ell \sim m_b(1, \lambda_\ell^2, \lambda_\ell^4), \quad p_{\bar{\ell}} \sim m_b(\lambda_\ell^4, \lambda_\ell^2, 1), \quad (2.9)$$

referred to as collinear and anti-collinear, respectively. Here we introduced the small dimensionless quantity

$$\lambda_\ell = \sqrt{\frac{m_\ell}{m_b}} \ll 1 \quad \text{for} \quad \ell = e, \mu. \quad (2.10)$$

The two cases of $\ell = e$ and $\ell = \mu$ are quite different, given that

$$\lambda_e \ll \lambda_s, \quad \lambda_\mu \approx \lambda_s \equiv \lambda. \quad (2.11)$$

Subsequently we focus on $\ell = \mu$. We note that experimental prospects are best for the decays $B_q \rightarrow \mu^+ \mu^-$, in particular for the CKM-enhanced mode $q = s$. The following different virtualities are set by the kinematic invariants

$$p_b^2 \sim p_\ell \cdot p_{\bar{\ell}} \sim p_b \cdot p_{\ell, \bar{\ell}} \sim m_b^2, \quad (2.12)$$

$$p_b \cdot l_q \sim l_q \cdot p_{\ell, \bar{\ell}} \sim m_b \Lambda, \quad (2.13)$$

$$l_q^2 \sim p_\ell^2 \sim p_{\bar{\ell}}^2 \sim \Lambda^2, \quad (2.14)$$

where $\Lambda = (m_\mu, \Lambda_{\text{QCD}})$ stands for either of the two small scales, the muon mass m_μ or Λ_{QCD} , which we assume to be parametrically of same size. Besides the hard virtuality m_b^2 and the soft and collinear virtuality Λ^2 there is also the hard-collinear virtuality $m_b \Lambda$. In consequence we will go through a two-step matching of EFTs,

$$\begin{array}{ccccc} \text{full QED} & \rightarrow & \text{SCET}_\text{I} & \rightarrow & \text{SCET}_\text{II} \\ \text{hard: } \mu_b^2 \sim m_b^2 & & \text{hard-collinear: } \mu_{hc}^2 \sim m_b \Lambda & & \text{soft/collinear: } \mu_s^2 \sim \mu_c^2 \sim \Lambda^2 \end{array}$$

involving two versions of SCET. We note that given the symmetry of the final state under an exchange of n_+ and n_- , whenever a (hard-) collinear contribution exists the corresponding (hard-) anti-collinear contribution from the configuration with lepton and anti-lepton interchanged is implied.

The decay rate into the exclusive final state $\ell^+ \ell^-$ discussed up to now is not infrared (IR) safe in the presence of QED. The IR-safe definition includes the emission of real photons with energies below a certain value ΔE . Throughout we will restrict the discussion to the case of $\Delta E \ll \Lambda$ that is we assume ΔE to be below the soft and collinear scale of SCET_II . Therefore only virtual corrections need to be considered above and at the scale Λ , and for the most part of the paper we therefore focus on the non-radiative amplitude. Ultra-soft photons, i.e. photons with virtuality much smaller than $\mu_{s,c}^2 \sim \Lambda^2$, will be taken into account at the very end when we put together the final expression for the QED-corrected decay width.

Field	heavy quark	light quark			leptons		photon (gluon)		
	h_v	χ_C	χ_c	q_s	ℓ_C	ℓ_c	$A_C (G_C)$	$A_c (G_c)$	$A_s (G_s)$
Scaling	λ^3	λ	λ^2	λ^3	λ	λ^2	$(1, \lambda, \lambda^2)$	$(1, \lambda^2, \lambda^4)$	$\lambda^2(1, 1, 1)$

Table 1: Fields and their power counting in SCET. In addition there are anti-hard-collinear ($\chi_{\overline{C}}, \ell_{\overline{C}}$) and anti-collinear ($\chi_{\overline{c}}, \ell_{\overline{c}}$) quark and lepton fields with the same scaling as their (hard)-collinear counterparts. The components for the photon field are $(n_+ A, A_\perp^\mu, n_- A)$ and the gauge-invariant building blocks $\mathcal{A}_{C\perp}^\mu$ and $\mathcal{A}_{c\perp}^\mu$ scale as the \perp -components of the fields $A_{C\perp} \sim \lambda$ and $A_{c\perp} \sim \lambda^2$, respectively. The light quark and lepton masses scale as $m_{q,\ell} \sim \lambda^2$.

2.3 SCET: Definitions and conventions

A systematic approach to the construction of SCET_I operator bases was discussed in [25]. In this paper, we apply the same method, and we follow the same conventions and those of [26] when possible. Capital letters C (\overline{C}) refer to hard-collinear (anti-hard-collinear) SCET_I fields, respectively, which we assume to contain both, the hard-collinear SCET_I modes and the collinear SCET_{II} modes. Collinear (anti-collinear) fields in SCET_{II} are denoted by the index c (\overline{c}); these fields contain only collinear modes and thus the power-counting of the SCET_{II} fields is homogeneous. The index s denotes the soft fields. The λ scaling of the heavy b -quark, light spectator quark as well as the lepton fields in SCET_I and SCET_{II} is summarized in Table 1.

The masses of leptons and light quarks scale like λ^2 . Accordingly, in SCET_I collinear mass terms are part of the power-suppressed collinear Lagrangian, while in SCET_{II} they are included in the leading-power collinear Lagrangian. Mass factors may also appear explicitly in the operators. More details on the relevant parts of the SCET Lagrangian are given in Appendix A.1. For definitions of renormalization constants we refer to Appendix A.2.

2.4 Heuristic discussion

Before we begin the detailed formal discussion of resummation and factorization in SCET, we recapitulate and interpret the main finding (1.1) of the one-loop calculation [21] in the framework of SCET.

The starting point is the one-loop virtual photon correction to the matrix elements of the operators $Q_{7,9,10}$ at the scale μ_b . The analysis based on the method of expansion by regions [27, 28] shows that only the diagrams where the photon is exchanged between the soft spectator quark and either of the final-state leptons can be power-enhanced, and that the power-enhancement cannot originate from the hard loop-momentum region. Examples are shown by the first two diagrams in Figure 2. The calculation of these diagrams in full QED, solving first the integrals analytically in full generality¹ and performing the expansion in λ only afterwards confirms this result. The one-loop expression contains logarithms of the ratio of hard-collinear over collinear virtualities, $\ln(\mu_{hc}/\mu_c)$, for insertions of Q_9 and

¹The analytic solutions of the one-loop integrals were also obtained with “Package X” [29, 30].

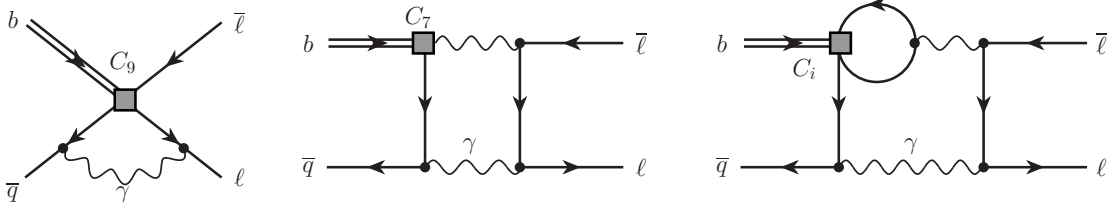


Figure 2: Feynman diagrams that contain the power-enhanced electromagnetic correction. Symmetric diagrams with order of vertices on the leptonic line interchanged are not displayed.

even double-logarithms $\ln^2(\mu_{hc}/\mu_{c,s})$ for Q_7 . Note that the virtual corrections do not lift the helicity suppression of the leptonic $B_q \rightarrow \ell^+ \ell^-$ decays.

The SCET approach is used here to factorize the short-distance contributions perturbatively to the leading non-vanishing order in the expansion in λ and to resum the arising logarithms. Since the one-loop power-enhanced terms do not arise from the hard region, the matching from full QED to SCET_I operators relevant to these terms proceeds at tree-level. Thereby the field content of the semileptonic and dipole operators changes

$$Q_{9,10} \sim [\bar{q} \dots b][\bar{\ell} \dots \ell] \quad \rightarrow \quad \mathcal{O}_i \sim [\bar{\chi}_{C,\bar{C}} \dots h_v][\bar{\ell}_C \dots \ell_{\bar{C}}] \sim \lambda^6, \quad (2.15)$$

$$Q_7 \sim [\bar{q} \dots b]F^{\mu\nu} \quad \rightarrow \quad \mathcal{O}_i \sim [\bar{\chi}_{C,\bar{C}} \dots h_v]\mathcal{A}_{C\perp,C\perp}^\mu \sim \lambda^5, \quad (2.16)$$

where the b -quark is represented by a heavy-quark h_v in HQET and the spectator quark is (anti-) hard-collinear $\chi_{C,\bar{C}}$, whereas the lepton $\bar{\ell}_C$ is hard-collinear and the anti-lepton $\ell_{\bar{C}}$ is anti-hard-collinear. In the case of Q_7 the photon $\mathcal{A}_{C\perp}$ in (2.16) is anti-hard-collinear for hard-collinear χ_C and vice versa. \mathcal{O}_i from (2.15) also appears in the matching of Q_7 . The scaling of these operators in λ follows from the scaling of the fields as summarized in Table 1. The large logarithms between the hard and hard-collinear scales are then resummed with the aid of RG equations (RGEs) in SCET_I, as will be shown below. These logarithms appear only in higher orders, i.e. they dress the diagrams shown Figure 2.

Let us briefly remark on the two-loop diagram in Figure 2, which is generated by the four-quark operators Q_{1-6} in the effective Lagrangian (2.1). It is well-known from $B \rightarrow X_s \ell^+ \ell^-$ decays that the quark loop can be fully absorbed into effective Wilson coefficients $C_9^{\text{eff}}(q^2)$ and C_7^{eff} , so that these diagrams should be considered as one-loop QED corrections, as has been done in (1.1). This is implicitly understood when we refer to tree-level matching of $Q_{7,9,10}$.

The second matching step from SCET_I to SCET_{II} produces the one-loop logarithms. In the case of $Q_{9,10}$ (first diagram in Figure 2) there is a hard-collinear and a collinear momentum region. The first belongs to a one-loop matching coefficient, while the second must be reproduced by the matrix element of a SCET_{II} operator. The SCET_I operator \mathcal{O}_i from (2.15) contains a C -antiquark, which is converted into the external soft spectator antiquark through the subleading-power SCET_I interaction $\mathcal{L}_{\xi q}^{(1)}$ [31], see (A.13), by emission

of a transverse hard-collinear or collinear photon $\mathcal{A}_{C\perp}$. The relevant SCET_{II} operators are

$$[\bar{\chi}_C \dots h_v][\bar{\ell}_C \dots \ell_{\bar{C}}] \rightarrow \mathcal{J}_{\mathcal{A}_\chi}^{B1}, \mathcal{J}_{m_\chi}^{A1}, \quad (2.17)$$

where

$$\mathcal{J}_{\mathcal{A}_\chi}^{B1} \sim [\bar{q}_s(in_- \overleftarrow{\partial})^{-1} \dots h_v][\bar{\ell}_c \mathcal{A}_{c\perp} \dots \ell_{\bar{c}}] \sim \lambda^{10}, \quad (2.18)$$

$$\mathcal{J}_{m_\chi}^{A1} \sim m_\ell [\bar{q}_s(in_- \overleftarrow{\partial})^{-1} \not{p}_- P_L h_v][\bar{\ell}_c P_R \ell_{\bar{c}}] \sim \lambda^{10}. \quad (2.19)$$

To reproduce the C_9^{eff} term in (1.1), the matching to the first of these operators is needed at tree-level. Its one-loop SCET_{II} matrix element accounts for the collinear region. The matching coefficient of the second operator is needed at the one-loop level to reproduce the hard-collinear region. This leads to two important observations. First, the power-enhanced contribution to $B_q \rightarrow \ell^+ \ell^-$ decays requires a power-suppressed interaction in SCET, because the usual, non-enhanced $B_q \rightarrow \ell^+ \ell^-$ amplitude involving Q_{10} (first term on the right-hand side of (1.1)) is in fact doubly suppressed due to helicity conservation *and* the point-like annihilation of the heavy quark with a soft anti-quark. Second, even in the collinear loop, the anti-quark propagator has hard-collinear virtuality – only the lepton and photon propagators have collinear virtuality. This enables the perturbative calculation of the collinear contribution including the non-logarithmic terms.

Note that in SCET_I \rightarrow SCET_{II} matching, C -fields in the SCET_I operator change to fields with collinear virtualities (denoted by c) in SCET_{II}, thereby increasing the power of the SCET_{II} operators in λ . In the above two SCET_{II} operators we included the inverse soft derivative in their definition to explicitly indicate the correct scaling of the operator.² One might have expected that an operator $[\bar{q}_s \gamma_\mu^\perp P_L h_v][\bar{\ell}_c \gamma_\perp^\mu \gamma_5 \ell_{\bar{c}}] \sim \lambda^{10}$ is generated by tree-level leading-power matching, but this operator has no overlap with the pseudo-scalar B -meson in the process $B_q \rightarrow \ell^+ \ell^-$. An additional helicity suppression of $m_\ell \sim \lambda^2$ is required. In fact, also the operator (2.18) has no overlap with the external states of $B_q \rightarrow \ell^+ \ell^-$ because of the additional photon field $\mathcal{A}_{c\perp}$. However, this operator mixes under QED renormalization with $\mathcal{J}_{m_\chi}^{A1}$, which has the correct chiral properties, but nevertheless scales as λ^{10} due the compensating λ^{-2} power from the inverse soft derivative. It is precisely the anomalous dimension of this operator-mixing that reproduces the logarithms $\ln(\mu_{hc}/\mu_c)$ in the one-loop QED correction (1.1). Below we will employ the RGEs of SCET_{II} to resum these logarithms.

The two-step matching of the operators $Q_{9,10}$ and the RG evolution are schematically summarized in Figure 3. In the remainder of this work, we will derive the resummed result in detail for these operators.

Before proceeding, we comment on why we do not discuss the summation of logarithms for the electromagnetic dipole operator Q_7 . The relevant diagram is now the second one in Figure 2. While at first sight the hard-collinear and collinear regions appear similar to

²Later on, we will move this enhancement factor to the coefficient function [32], which is more convenient for calculations. This factor is responsible for the appearance of the $1/\omega$ moment of the B -meson LCDA in (1.1).

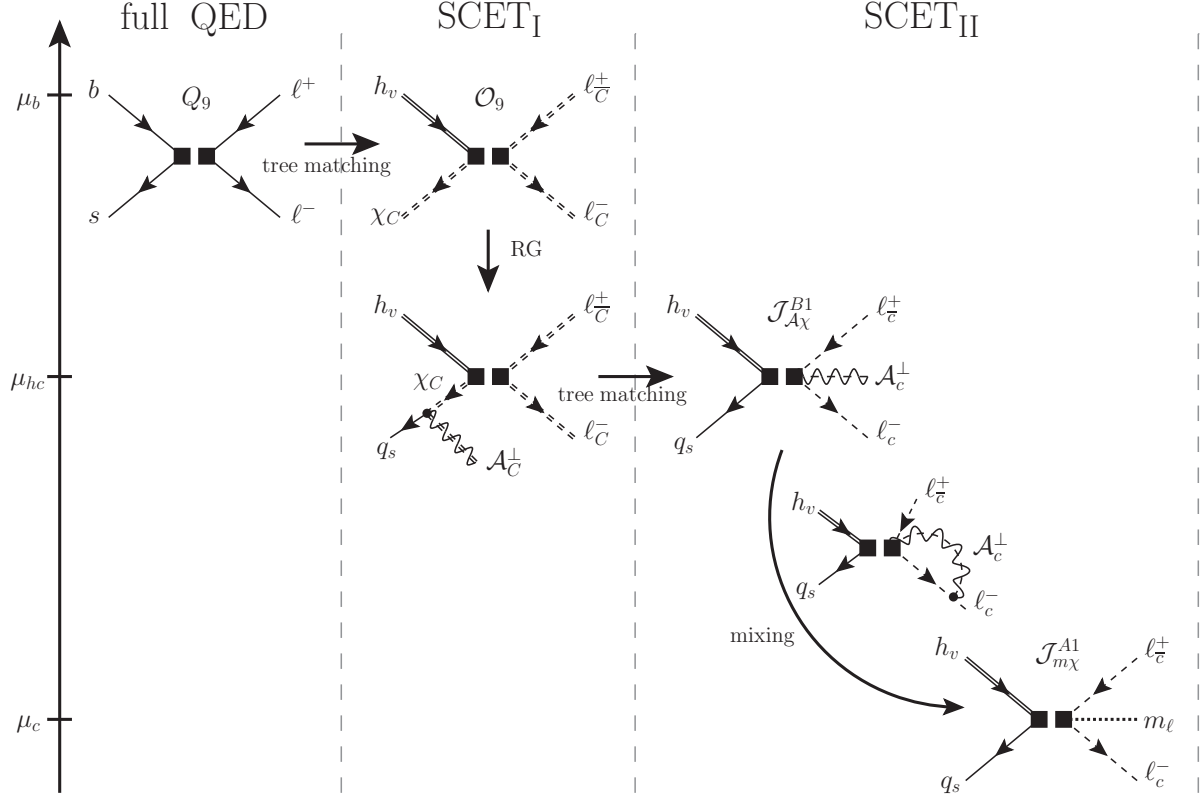


Figure 3: The scheme shows the tree-level matching steps from full QED \rightarrow SCET_I \rightarrow SCET_{II} at the two scales μ_b and μ_{hc} horizontally from left to right. Vertically the RG evolution in SCET_I involves only self-mixing, whereas in SCET_{II} a mixing takes place of the operators $\mathcal{J}_{A_X}^{B1}$ into $\mathcal{J}_{m_X}^{A1}$. The notation and scaling of the SCET fields are given in Table 1. The propagators of the fields are chosen as double-solid for the heavy quark h_v , double-dashed for hard-collinear fermions in SCET_I, whereas single-dashed for collinear fermions in SCET_{II}. The double- and single-dashed lines accompanied by a wavy line depict the hard-collinear and collinear photon fields in SCET_I and SCET_{II}, respectively. The single-solid line depicts the soft spectator quark q_s . The dotted line in $\mathcal{J}_{m_X}^{A1}$ indicates that this operator contains a factor of the lepton mass m_ℓ .

the case discussed above, one finds that the additional photon propagator attached to the dipole operator vertex causes an endpoint-singularity as u , that is, the virtuality um_b^2 of the photon, goes to zero in the hard-collinear and collinear convolution integrals for the box diagram. In this limit, the hard photon from the electromagnetic dipole operator becomes hard-collinear. The singularity is cancelled by a soft contribution (virtuality $\Lambda^2 \sim m_\ell^2$), where the leptons in the final state interact with each other through the exchange of a soft lepton [21]. The relevance of soft-fermion exchange is interesting by itself since it is beyond the standard analysis of logarithmically enhanced terms in QED. Moreover, the endpoint or rapidity divergence encountered here is of a form that defies known methods to sum such logarithms, since the breakdown of soft-collinear factorization arises from a singular matching coefficient, rather than the soft or collinear propagators themselves. A very similar

phenomenon has subsequently been encountered in [33, 34]. The double logarithm in the C_7^{eff} term in (1.1) arises from this additional endpoint divergence. At the one-loop order, the endpoint singularity can be regularized by a non-dimensional regulator [25], which renders all integrals well-defined, with the result given in (1.1). We also verified this logarithm from the expansion of the full one-loop amplitude, without using the split-up into regions, as mentioned above. However, it is currently not known how to write down RGEs for suitably defined renormalized objects for this situation, and hence resummation cannot be performed.

3 SCET_I

3.1 Operators

The first decoupling step involves integrating out the hard modes of the light quark and lepton fields, as well as all other fields, in the matching on the SCET_I operators. For processes described by SCET_{II} a complication in the construction of the relevant operators in the intermediate SCET_I appears, namely operators of different λ scaling may contribute to the same order in λ after matching to SCET_{II} [25]. The power-enhanced contribution requires only a single type of SCET_I four-fermion operator where the light quark is either hard-collinear or anti-hard-collinear. In position space, denoted by a tilde, they read for a hard-collinear light quark

$$\tilde{\mathcal{O}}_9(s, t) = g_{\mu\nu}^\perp [\bar{\chi}_C(sn_+) \gamma_\perp^\mu P_L h_v(0)] [\bar{\ell}_C(tn_+) \gamma_\perp^\nu \ell_{\bar{C}}(0)], \quad (3.1)$$

$$\tilde{\mathcal{O}}_{10}(s, t) = i\varepsilon_{\mu\nu}^\perp [\bar{\chi}_C(sn_+) \gamma_\perp^\mu P_L h_v(0)] [\bar{\ell}_C(tn_+) \gamma_\perp^\nu \ell_{\bar{C}}(0)]; \quad (3.2)$$

for a anti-hard-collinear quark

$$\tilde{\mathcal{O}}_{\bar{9}}(s, t) = g_{\mu\nu}^\perp [\bar{\chi}_{\bar{C}}(sn_-) \gamma_\perp^\mu P_L h_v(0)] [\bar{\ell}_C(0) \gamma_\perp^\nu \ell_{\bar{C}}(tn_-)], \quad (3.3)$$

$$\tilde{\mathcal{O}}_{\bar{10}}(s, t) = i\varepsilon_{\mu\nu}^\perp [\bar{\chi}_{\bar{C}}(sn_-) \gamma_\perp^\mu P_L h_v(0)] [\bar{\ell}_C(0) \gamma_\perp^\nu \ell_{\bar{C}}(tn_-)]. \quad (3.4)$$

The definitions of $g_{\mu\nu}^\perp$ and $\varepsilon_{\mu\nu}^\perp$ are given in Appendix A. In the classification scheme of [26, 31] these are operators of the B1-type with two hard-collinear (or anti-hard-collinear) fields in one of the directions, and of the A0-type in the opposite direction. The operators $i = \bar{9}, \bar{10}$ contain an anti-hard-collinear light quark field $\chi_{\bar{C}}$ instead of a χ_C in operators $i = 9, 10$.

The Fourier-transformed SCET_I operators are defined as

$$\mathcal{O}_i(u) = n_+ p_C \int \frac{dr}{2\pi} e^{-iur(n_+ p_C)} \tilde{\mathcal{O}}_i(0, r). \quad (3.5)$$

Hard-collinear momentum conservation has been used to drop the dependence on the total hard-collinear momentum $n_+ p_C = n_+ (p_\chi + p_\ell)$ on the left-hand side and the first argument of $\tilde{\mathcal{O}}_i$ is set to zero. The variable u should be interpreted as the fraction $n_+ p_\ell / n_+ p_C$ of

$n_+ p_C$ carried by the lepton field, while the hard-collinear light anti-quark has momentum fraction $\bar{u} \equiv (1 - u) = n_+ p_\chi / n_+ p_C$. For the operators $\tilde{\mathcal{O}}_{\bar{i}}$ similar definitions apply after replacing n_+ by n_- .

The SCET_I Wilson coefficients of these operators, the so-called “hard functions”, are introduced in momentum space as

$$\mathcal{L}_{\Delta B=1}^{\text{I}} = \sum_i \int du H_i(u, \mu) \mathcal{O}_i(u). \quad (3.6)$$

They are found by matching full QED+QCD \rightarrow SCET_I at the hard scale $\mu = \mu_b \sim \mathcal{O}(m_b)$ as described in Section 3.2 below.

A complete basis of four-fermion operators when naive dimensional regularization with anti-commuting γ_5 is employed would include in addition also operators with Dirac matrices vanishing in four dimensions, the so-called evanescent operators. However, the logarithms that we aim to sum in this paper in SCET_I are derived from one-loop anomalous dimensions, which are given by the pole parts in $1/\epsilon$, where $\epsilon = (4 - D)/2$ in terms of the number of space-time dimension D , of the one-loop diagrams that are independent of the definition of evanescent operators.

3.2 Matching

For the leading logarithmic accuracy it is sufficient to perform only the tree-level matching of Q_9 and Q_{10} operators on the SCET_I operators \mathcal{O}_i . One-loop matching is needed for the four-quark operators Q_i ($i = 1, \dots, 6$), which can be included as is commonly done by the replacement $C_9 \rightarrow C_9^{\text{eff}}$ [35] as mentioned above. The hard matching condition at the scale μ_b is given by

$$\mathcal{N}_{\Delta B=1} \sum_k C_k(\mu_b) Q_k = \sum_i \int du H_i(u, \mu_b) \mathcal{O}_i(u). \quad (3.7)$$

Evaluating this equation in the appropriate matrix element with a hard-collinear (anti-hard-collinear) light quark state, we find, at tree-level

$$\begin{aligned} H_9(u, \mu_b) &= \mathcal{N} C_9^{\text{eff}}(u, \mu_b), & H_{\bar{9}} &= H_9, \\ H_{10}(u, \mu_b) &= \mathcal{N} C_{10}(\mu_b), & H_{\bar{10}} &= H_{10}. \end{aligned} \quad (3.8)$$

Here

$$\mathcal{N} \equiv \mathcal{N}_{\Delta B=1} \frac{\alpha_{\text{em}}(\mu_b)}{4\pi}, \quad (3.9)$$

and

$$\begin{aligned} C_9^{\text{eff}}(u, \mu_b) &= C_9(\mu_b) + Y(us_{\ell\bar{\ell}}, \mu_b) \\ &\quad - \frac{V_{ub}V_{uq}^*}{V_{tb}V_{tq}^*} \left(\frac{4}{3} C_1 + C_2 \right) [h(0, us_{\ell\bar{\ell}}) - h(m_c, us_{\ell\bar{\ell}})], \end{aligned} \quad (3.10)$$

with the dilepton invariant mass $s_{\ell\bar{\ell}} \equiv (n_+ p_\ell)(n_- p_{\bar{\ell}})$. We use the definition of the function $Y(us_{\ell\bar{\ell}})$ from [36]. The function $h(m_q, q^2)$ [24] depends on the light quark masses $m_{u,d}$ that are set to zero, or the charm-quark mass m_c .

3.3 RG evolution

The RGE in SCET_I governs the evolution of the matching coefficient $H_i(u, \mu)$ from the hard scale μ_b to the hard-collinear scale μ_{hc} . The renormalization constants and the anomalous dimensions of the operators \mathcal{O}_i can be computed similarly to the ones for N -jet operators [26, 37], with the addition of a soft heavy-quark field. Our conventions follow [26] and are summarized in Appendix A.2. We take into account both QCD and QED effects. The evolution of the hard function is determined by

$$\frac{dH_i(u, \mu)}{d \ln \mu} = \Gamma_{\text{cusp}}^I \left(\ln \frac{m_{B_q}}{\mu} - \frac{i\pi}{2} \right) H_i(u, \mu) + \int du' \Gamma_i(u', u) H_i(u', \mu). \quad (3.11)$$

The B -meson mass in the cusp logarithm arises from the kinematic constraint $s_{\ell\bar{\ell}} = m_{B_q}^2$. The imaginary parts arise from $\ln[-(s_{\ell\bar{\ell}} + i0^+)/\mu^2] = \ln(m_{B_q}^2/\mu^2) - i\pi$, and will be neglected throughout, as they do not contribute at the leading logarithmic accuracy. For the summation of the leading logarithms (LL) we require the one-loop cusp anomalous dimension

$$\Gamma_{\text{cusp}}^I(\alpha_s, \alpha_{\text{em}}) = \Gamma_c(\alpha_{\text{em}}) + \Gamma_s(\alpha_s, \alpha_{\text{em}}), \quad (3.12)$$

that has been split for later convenience into a part $\Gamma_c \propto Q_\ell^2$ and the remainder Γ_s that includes also the QCD cusp anomalous dimension,

$$\Gamma_c = \frac{\alpha_{\text{em}}}{\pi} 2Q_\ell^2, \quad \Gamma_s = \frac{\alpha_s}{\pi} C_F + \frac{\alpha_{\text{em}}}{\pi} Q_q(2Q_\ell + Q_q), \quad (3.13)$$

expressed in terms of the electric quark and lepton charges, Q_q and Q_ℓ , respectively, and the QCD Casimir $C_F = 4/3$. At the next-to-leading logarithmic (NLL) accuracy one would also include

$$\Gamma_i(x, y) = \frac{\alpha_s C_F}{4\pi} [4 \ln(1-x) - 5] \delta(x-y) + \frac{\alpha_{\text{em}}}{4\pi} \gamma_i(x, y), \quad (i = 9, 10), \quad (3.14)$$

and the two-loop cusp part. The function $\gamma_i(x, y)$ is provided for completeness in (A.31). The general solution of the RGE (3.11) when only the cusp anomalous dimension is kept (and the imaginary part neglected) reads

$$H_i(u, \mu) = \exp \left[\int_{\mu_b}^{\mu} \frac{d\mu'}{\mu'} \Gamma_{\text{cusp}}^I(\mu') \ln \frac{m_{B_q}}{\mu'} \right] H_i(u, \mu_b), \quad (3.15)$$

and amounts to a global, momentum-fraction independent rescaling of the hard functions $H_i(u, \mu)$ by a Sudakov factor. This property is particular to the LL approximation. From

NLL accuracy, when the non-cusp anomalous dimension $\Gamma_i(u', u)$ is included, the QCD logarithms lead to a momentum-fraction dependent rescaling from the $\ln(1-x)$ term in (3.14), while the QED corrections governed by γ_i reshuffle the momentum fractions carried by the spectator quark and lepton.

The integral in (3.15) can in general be evaluated only numerically. When the running of the strong coupling α_s is included, but the one of α_{em} as well as the influence of α_{em} on the QCD running is neglected, we obtain the solution given in (A.33). However, our aim is to sum leading logarithms in QED to all orders. When the solution is written in the form of (3.15) “LL accuracy” is defined by including all terms of the form $\log \times (\alpha \log)^n$ for any n in the exponent, where α can be α_s or α_{em} . The “double logarithmic” approximation corresponds to keeping only the first term $n = 1$ in the LL series.

In the LL approximation the one-loop cusp anomalous dimension is the sum of a QCD and a QED term (not to be confused with the split into Γ_c and Γ_s above, which will be useful later). The exponential factorizes into a QCD and a QED contribution. Even in this approximation it is convenient to perform the integrals numerically, when the coupling runs through flavour thresholds. We shall use such numerical solutions in the final numerical results in Section 8. For the purpose of discussion, we present the analytic solution, when flavour thresholds in the interval $[\mu, \mu_b]$ are neglected,

$$\frac{H_i(u, \mu)}{H_i(u, \mu_b)} = \exp \left[\frac{4\pi}{\alpha_s(\mu_b)} \frac{C_F}{\beta_0^2} g_0(\eta_s) \right] \exp \left[\frac{4\pi}{\alpha_{\text{em}}(\mu_b)} \frac{[2Q_\ell^2 + Q_q(2Q_\ell + Q_q)]}{\beta_{0,\text{em}}^2} g_0(\eta_{\text{em}}) \right], \quad (3.16)$$

where $g_0(x) = 1 - x + \ln x$ and η_i stands for $\eta_i(\mu_b, \mu) \equiv \alpha_i(\mu_b)/\alpha_i(\mu)$ with $i = s, \text{em}$. To obtain this expression from (3.15) we replace m_{B_q} in the cusp logarithm by μ_b and neglect the non-enhanced logarithm $\ln(m_{B_q}/\mu_b)$. The ambiguity in choosing the precise value of the hard-matching scale $\mu_b \sim m_b$ is resolved only beyond the LL approximation.

Neglecting the running of the QED coupling in (3.16) amounts to the QED double-logarithmic (DL) approximation and the approximation $g_0(x) = -(1-x)^2/2 + \mathcal{O}((1-x)^3)$. In the above and similar expressions below we can always switch between the LL (left) and DL (right) QED resummation by the replacement

$$\exp \left[\frac{4\pi}{\alpha_{\text{em}}(\mu_1)} \frac{\mathcal{Q}}{\beta_{0,\text{em}}^2} g_0(\eta_{\text{em}}) \right] \longleftrightarrow \exp \left[-\frac{\alpha_{\text{em}}}{2\pi} \mathcal{Q} \ln^2 \frac{\mu_1}{\mu_2} \right], \quad (3.17)$$

where now η_{em} denotes $\eta_{\text{em}}(\mu_1, \mu_2) = \alpha_{\text{em}}(\mu_1)/\alpha_{\text{em}}(\mu_2)$, and \mathcal{Q} stands for the appropriate charge factor.

For later purposes it is convenient to pull out the part of the exponent with $\Gamma_c \propto \alpha_{\text{em}} Q_\ell^2$ as follows

$$H_i(u, \mu) = \exp [S_\ell(\mu_b, \mu) + S_q(\mu_b, \mu)] H_i(u, \mu_b), \quad (3.18)$$

thereby introducing the Sudakov exponents

$$S_\ell(\mu_b, \mu) = \frac{4\pi}{\alpha_{\text{em}}(\mu_b)} \frac{2Q_\ell^2}{\beta_{0,\text{em}}^2} g_0(\eta_{\text{em}}) \xrightarrow{\text{DL}} -\frac{\Gamma_c}{2} \ln^2 \frac{\mu_b}{\mu}, \quad (3.19)$$

$$\begin{aligned}
S_q(\mu_b, \mu) &= \frac{4\pi}{\alpha_s(\mu_b)} \frac{C_F}{\beta_0^2} g_0(\eta_s) + \frac{4\pi}{\alpha_{\text{em}}(\mu_b)} \frac{[Q_q(2Q_\ell + Q_q)]}{\beta_{0,\text{em}}^2} g_0(\eta_{\text{em}}) \\
&\xrightarrow{\text{DL}} \frac{4\pi C_F}{\alpha_s(\mu_b) \beta_0^2} (1 - \eta_s + \ln \eta_s) - \frac{\alpha_{\text{em}}}{2\pi} [Q_q(2Q_\ell + Q_q)] \ln^2 \frac{\mu_b}{\mu}. \quad (3.20)
\end{aligned}$$

4 SCET_{II}

The above equations are used to evolve the SCET_I operators $\tilde{\mathcal{O}}_{9,10}$, $\tilde{\mathcal{O}}_{\bar{9},\bar{10}}$ to the hard-collinear scale μ_{hc} , at which the hard-collinear modes with virtuality $\mathcal{O}(m_b\Lambda)$ are removed and the SCET_I operators are matched to SCET_{II}.

An important distinction between SCET_I and SCET_{II} for the problem at hand is the treatment of the lepton mass. Parametrically the muon mass is of the same order as the soft/collinear scale $m_\mu \sim \Lambda_{\text{QCD}}$. Thus the lepton mass terms are part of the leading-power collinear Lagrangian in SCET_{II}, see (A.5). In consequence the muon mass is retained in the denominators of the collinear lepton propagators and serves as a regulator of the collinear divergences.

To develop an idea of operator matching to SCET_{II}, we recall that the SCET_I operators \mathcal{O}_i contain hard-collinear light quark fields, while the B -meson contains only soft fields. The hard-collinear field in the SCET_I operators must be converted into a soft quark field through emission of a (hard-) collinear photon by the power-suppressed SCET_I Lagrangian $\mathcal{L}_{\xi q}^{(1)}$ (definition in (A.13)) to obtain a non-vanishing overlap the B -meson state. Therefore, we match the time-ordered product of the SCET_I operators \mathcal{O}_i with $\mathcal{L}_{\xi q}^{(1)}$ to SCET_{II} operators. The tree-level matching relation is depicted in the second line labelled “tree matching” in Figure 3. Starting from the one-loop order, pure four-fermion operators without collinear photons also appear (not shown). The systematic construction of the SCET_{II} operator basis is substantially more complicated than for SCET_I, since one must control the degree of non-locality of soft fields [25]. In the following we discuss the operators, their renormalization and matching coefficients relevant to LL resummation. Some further details are provided in Appendices A and B.

4.1 Operators

We note that, quite generally, in SCET_{II} operators also the soft fields are delocalized along the direction of the light-cone. The small component n_-p of the hard-collinear mode, which is integrated out, is of the same order as the soft momentum, hence the soft field can be at any position in the n_- direction. The roles of n_- and n_+ are reversed when the anti-hard-collinear mode is integrated out.

A power-counting analysis similar to the one performed in [25] for heavy-to-light meson form factors shows that only two different SCET_{II} operators for each collinear direction are relevant to the power-enhanced correction from the Q_9 operator. The two SCET_{II} operators mix under renormalization. The technical arguments can be found in Appendix B. In

position space, the two operators are defined as

$$\tilde{\mathcal{J}}_{m\chi}^{A1}(v) = \bar{q}_s(vn_-)Y(vn_-, 0) \frac{\not{n}_-}{2} P_L h_v(0) [Y_+^\dagger Y_-](0) [\bar{\ell}_c(0)(4m_\ell P_R) \ell_{\bar{c}}(0)], \quad (4.1)$$

$$\begin{aligned} \tilde{\mathcal{J}}_{\mathcal{A}\chi}^{B1}(v, t) &= \bar{q}_s(vn_-)Y(vn_-, 0) \frac{\not{n}_-}{2} P_L h_v(0) [Y_+^\dagger Y_-](0) [\bar{\ell}_c(0)(g_{\mu\nu}^\perp + i\varepsilon_{\mu\nu}^\perp) \mathcal{A}_{c\perp}^\mu(tn_+) \gamma_\perp^\nu \ell_{\bar{c}}(0)] \\ &= \bar{q}_s(vn_-)Y(vn_-, 0) \frac{\not{n}_-}{2} P_L h_v(0) [Y_+^\dagger Y_-](0) [\bar{\ell}_c(0)(2\mathcal{A}_{c\perp}(tn_+) P_R) \ell_{\bar{c}}(0)]. \end{aligned} \quad (4.2)$$

For $\tilde{\mathcal{J}}_{\mathcal{A}\chi}^{B1}$ the second line provides an equivalent representation which makes the chirality of the leptons explicit. The analogous operators generated from the matching of $\mathcal{O}_{\bar{9}, \overline{10}}$ are defined as

$$\tilde{\mathcal{J}}_{m\bar{\chi}}^{A1}(v) = \bar{q}_s(vn_+)Y(vn_+, 0) \frac{\not{n}_+}{2} P_L h_v(0) [Y_+^\dagger Y_-](0) [\bar{\ell}_c(0)(4m_\ell P_R) \ell_{\bar{c}}(0)], \quad (4.3)$$

$$\begin{aligned} \tilde{\mathcal{J}}_{\mathcal{A}\bar{\chi}}^{B1}(v, t) &= \bar{q}_s(vn_+)Y(vn_+, 0) \frac{\not{n}_+}{2} P_L h_v(0) [Y_+^\dagger Y_-](0) [\bar{\ell}_c(0)(g_{\mu\nu}^\perp - i\varepsilon_{\mu\nu}^\perp) \mathcal{A}_{\bar{c}\perp}^\mu(tn_-) \gamma_\perp^\nu \ell_{\bar{c}}(0)] \\ &= \bar{q}_s(vn_+)Y(vn_+, 0) \frac{\not{n}_+}{2} P_L h_v(0) [Y_+^\dagger Y_-](0) [\bar{\ell}_c(0)(2P_R \mathcal{A}_{\bar{c}\perp}(tn_-) \ell_{\bar{c}}(0)]. \end{aligned} \quad (4.4)$$

The A1-type operators are constructed from leading-power building blocks and multiplied by a factor of the lepton mass where the factor of 4 is introduced for convenience. The B1-type operators contain the (anti-) collinear photon field $\mathcal{A}_{c\perp}^\mu(\bar{c}\perp)$. Both operators have the same λ scaling. The product of Wilson lines $[Y_+^\dagger Y_-](0) \equiv Y_+^\dagger(0)Y_-(0)$ appears after decoupling of soft photons from the collinear and anti-collinear leptons in SCET_I, see also (A.15). These electromagnetic Wilson lines are defined as

$$Y_\pm(x) = \exp \left[-ie Q_\ell \int_0^\infty ds n_\mp A_s(x + sn_\mp) \right]. \quad (4.5)$$

For the quark current the usual finite-distance Wilson line

$$Y(x, y) = \exp \left[ie Q_q \int_y^x dz_\mu A_s^\mu(z) \right] \mathcal{P} \exp \left[ig_s \int_y^x dz_\mu G_s^\mu(z) \right] \quad (4.6)$$

appears, which is necessary to maintain the QCD and QED gauge invariance of non-local operators. Here \mathcal{P} is the path-ordering operator and $G_s^\mu = G_s^{\mu A} T^A$ is the soft gluon field. The integral is evaluated along the straight line connecting the points x and y . We define the Fourier transforms

$$\mathcal{J}_i^{A1}(\omega) = \int \frac{dv}{2\pi} e^{i\omega v} \tilde{\mathcal{J}}_i^{A1}(v), \quad (4.7)$$

$$\mathcal{J}_i^{B1}(\omega, w) = (n \cdot p) \int \frac{dv}{2\pi} e^{i\omega v} \int \frac{dt}{2\pi} e^{-i\bar{w}t(n \cdot p)} \tilde{\mathcal{J}}_i^{B1}(v, t) \quad (4.8)$$

of the operators, where w corresponds to the collinear momentum fraction carried by the lepton, and ω may be interpreted as the soft momentum of the light quark along the n_+ or n_- direction, depending on the operator. Further $(n \cdot p) = n_+ p_c = n_+(p_\ell + p_{\mathcal{A}_{c\perp}})$ for $i = \mathcal{A}\chi$ and $(n \cdot p) = n_- p_{\bar{c}} = n_-(p_{\bar{\ell}} + p_{\mathcal{A}_{\bar{c}\perp}})$ for $i = \mathcal{A}\bar{\chi}$, respectively. In this way, after taking the matrix element, $w = n_+ p_\ell / n_+ p_c$ denotes the momentum fraction of $n_+ p_c$ carried by the collinear lepton and analogously for the anti-collinear case with appropriate replacements $n_+ \rightarrow n_-$ and $c \rightarrow \bar{c}$. We further defined $\bar{w} \equiv 1 - w$.

4.2 Renormalization

The SCET_{II} operators (4.1)–(4.4) are composed of soft, collinear and anti-collinear field products

$$\tilde{\mathcal{J}}_i = \hat{\mathcal{J}}_{i,s} \otimes \hat{\mathcal{J}}_{i,c} \otimes \hat{\mathcal{J}}_{i,\bar{c}}, \quad (4.9)$$

where the \otimes symbol indicates potential summation/contractions over spinorial and/or Lorentz indices. In SCET_{II}, the soft, collinear and anti-collinear fields do not interact with one another, which implies that the matrix elements of the SCET_{II} operators factorize accordingly into matrix elements of the separate factors on the right-hand side of (4.9) in the respective soft, collinear and anti-collinear Hilbert space. The UV counterterms can also be defined separately for each sector. However, a rearrangement is necessary due to the factorization anomaly as discussed below. The renormalization of SCET_{II} operators then proceeds similarly to the SCET_I case, see [26, 34, 37]. We next discuss the renormalization of each sector separately and then present the combined result for the SCET_{II} operators.

4.2.1 Soft sector

The soft part of the operators $\mathcal{J}_{m\chi}^{A1}$ and $\mathcal{J}_{\mathcal{A}\chi}^{B1}$,

$$\hat{\mathcal{J}}_s(v) = \bar{q}_s(vn_-) Y(vn_-, 0) \frac{\not{n}_-}{2} P_L h_v(0) [Y_+^\dagger Y_-](0), \quad (4.10)$$

is common to both. We thus omit the subindex i , and write $\hat{\mathcal{J}}_{i,s} = \hat{\mathcal{J}}_s$. The discussion for $\mathcal{J}_{m\chi}^{A1}$ and $\mathcal{J}_{\mathcal{A}\chi}^{B1}$ proceeds analogously after exchanging $n_- \leftrightarrow n_+$ in the $\bar{q}_s[\dots]h_v$ part of the operator. The QED one-loop diagrams due to soft photons from the soft Wilson lines contributing to the renormalization of $\hat{\mathcal{J}}_s(v)$ are shown in Figure 4a. Not shown is the vertex diagram from photon exchange between the heavy and light quark, and the field renormalization contribution. The QCD one-loop diagrams are the same as those that appear in the calculation of the renormalization of the leading-twist B -meson light-cone distribution amplitude [38].

To find the UV poles in dimensional regularization, we evaluate the operator between a heavy-light quark state and the vacuum, and regulate the infrared (IR) divergences by taking the external lines slightly off-shell. See Appendix A.4 for more details. Calculating in Feynman gauge, the dependence on the off-shell IR regulators cancels except for the tadpole-type diagram (6) of Figure 4a. The remaining IR-regulator dependence is cancelled by the

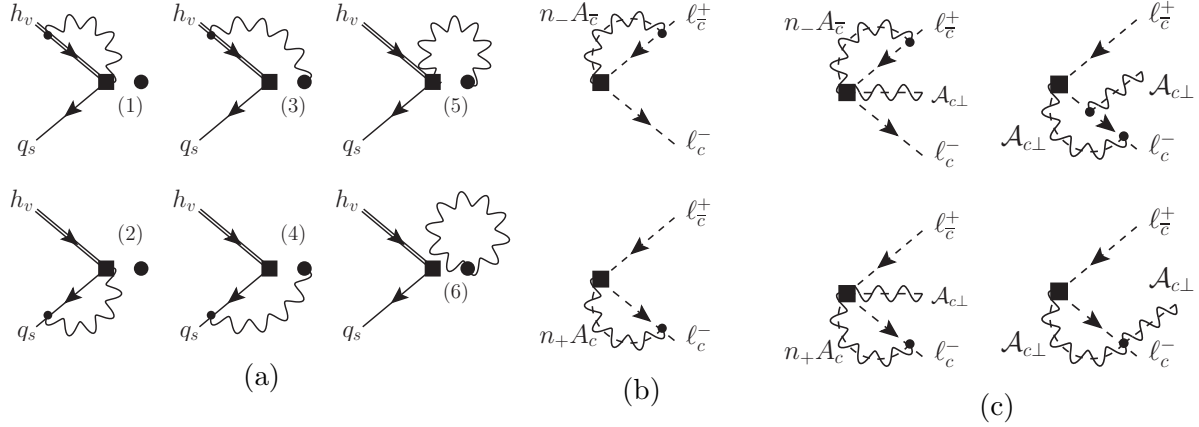


Figure 4: The diagrams in Figure 4a show the parts of the SCET_{II} operators \mathcal{J}_i ($i = m\chi, \mathcal{A}_\chi$) with soft photon exchange (wavy lines) from *i*) the Wilson lines in the soft fields h_v (double line) and q_s (single line) depicted by the square and *ii*) the product of soft Wilson lines $Y_+^\dagger(0)Y_-(0)$ depicted by the solid blob. They contribute to the Z_s^{QED} (diagrams 1 – 5), and $Z_{\chi, \chi}^{(1)}$ and $Z_{\mathcal{A}_\chi, \mathcal{A}_\chi}^{(1)}$ (diagram 6 $\propto Q_\ell^2$). Figure 4b shows diagrams relevant for $Z_{\chi, \chi}^{(1)}$ and Figure 4c diagrams relevant for $Z_{\mathcal{A}_\chi, \mathcal{A}_\chi}^{(1)}$. The dashed lines depict the lepton and anti-lepton and the wavy-dashed lines the (anti-) collinear photons from the corresponding Wilson lines.

diagrams in Figure 4b and Figure 4c with collinear and anti-collinear photons n_+A_c and $n_-A_{\bar{c}}$, respectively. While at first sight, this appears to be in conflict with the factorization of the soft and (anti-) collinear sectors, we can subtract the overlap between soft and collinear and anti-collinear regions by defining and renormalizing the soft operator

$$\tilde{\mathcal{J}}_s(v) \equiv \frac{\hat{\mathcal{J}}_s(v)}{\langle 0 | [Y_+^\dagger Y_-](0) | 0 \rangle}. \quad (4.11)$$

For the operators $i = m\bar{\chi}, \mathcal{A}\bar{\chi}$ we proceed in complete analogy using the respective soft field product. The operator (4.11) is divided by the vacuum expectation value of the gauge-invariant product of Wilson lines

$$\langle 0 | [Y_+^\dagger Y_-](0) | 0 \rangle \equiv R_+ R_-. \quad (4.12)$$

At the one-loop order, this subtraction simply removes the tadpole diagram (6) in Figure 4a from the soft operator. Beyond one-loop it ensures that the UV counterterm for the soft operator is independent of the IR regulator as is required for consistent operator renormalization. Further it ensures that the renormalization of the soft sector does not depend on the structure of the (anti-) collinear parts of the SCET_{II} operators, but only on the total charge of the final state associated to the (anti-) collinear direction.

Using separate IR regulators for collinear and anti-collinear fields, we further factorized the vacuum expectation value of the Wilson lines into factors R_+ and R_- , which depend only on the collinear and anti-collinear IR regulators, respectively. This split can always

be performed. At the one-loop order one obtains the sum of two terms, each of which depends only on one of the regulators; beyond, the one-loop IR divergence exponentiates. There is a freedom in the choice of splitting the product R_+R_- into the separate factors R_+ and R_- , which affects the definition of the collinear and anti-collinear renormalization constants discussed below.³ We adopt the symmetric convention, such that R_+ equals R_- upon exchanging $n_+ \leftrightarrow n_-$. This corresponds to rearranging the SCET_{II} operator (4.9) as

$$\tilde{\mathcal{J}}_i = \frac{\hat{\mathcal{J}}_s}{R_+R_-} \otimes R_+ \hat{\mathcal{J}}_{i,c} \otimes R_- \hat{\mathcal{J}}_{i,\bar{c}} \equiv \tilde{\mathcal{J}}_s \otimes \tilde{\mathcal{J}}_{i,c} \otimes \tilde{\mathcal{J}}_{i,\bar{c}}, \quad (4.13)$$

where now in the soft, collinear and anti-collinear factors $\tilde{\mathcal{J}}$ can be renormalized consistently in contrast to the original $\hat{\mathcal{J}}$.

We denote by Z_s the UV renormalization factor of the Fourier transform $\mathcal{J}_s(\omega) = \int \frac{dv}{2\pi} e^{i\omega v} \tilde{\mathcal{J}}_s(v)$ of the soft operator. At the one-loop order, $Z_s^{(1)}$ is the sum

$$Z_s^{(1)} = \frac{\alpha_{\text{em}}}{4\pi} Z_s^{\text{QED}} + \frac{\alpha_s}{4\pi} Z_s^{\text{QCD}} \quad (4.14)$$

of the QED and QCD contribution. The expressions for Z_s^{QED} and Z_s^{QCD} are given in (A.36) and (A.37), respectively. As explained above, the tadpole diagram 6 of Figure 4a cancels with the corresponding diagram in the denominator of (4.11). With the help of (A.28), the corresponding anomalous dimension reads

$$\begin{aligned} \Gamma^s(\omega, \omega') = & \left[-\Gamma_s \ln \frac{\omega}{\mu} - 5 \left(\frac{\alpha_s}{4\pi} C_F + \frac{\alpha_{\text{em}}}{4\pi} Q_q^2 \right) \right] \delta(\omega - \omega') \\ & - 4 \left[\frac{\alpha_s}{4\pi} C_F + \frac{\alpha_{\text{em}}}{4\pi} Q_q(Q_q + Q_\ell) \right] F(\omega, \omega'), \end{aligned} \quad (4.15)$$

where $F(\omega, \omega')$ is given in (A.38). The anomalous dimension contains the cusp part Γ_s , which appeared already in the anomalous dimension (3.13) of the SCET_I operators. However, here it enters with the opposite sign and is multiplied by $\ln(\omega/\mu)$. Note that the QED part of the anomalous dimension is proportional to the light-quark charge Q_q .

The soft operator fulfils the RGE⁴

$$\frac{d}{d \ln \mu} \mathcal{J}_s(\omega; \mu) = - \int d\omega' \Gamma^s(\omega, \omega') \mathcal{J}_s(\omega'; \mu), \quad (4.16)$$

which at the LL accuracy, i.e. keeping only the cusp part of the anomalous dimension, admits a solution of the form

$$\mathcal{J}_s(\omega; \mu) = U_s(\mu, \mu_s; \omega) \mathcal{J}_s(\omega; \mu_s). \quad (4.17)$$

³We note the similarity to the factorization of the soft function in the definition of the transverse momentum-dependent parton distribution functions, see, for example, [39].

⁴The minus sign on the right-hand side appears in accordance with the general convention (A.29) for the RGEs of operators and coefficient functions.

The LL soft RG evolution factor U_s from an initial soft scale $\mu_s \sim \omega$ to μ is given by

$$U_s(\mu, \mu_s; \omega) = \exp \left[\frac{4\pi}{\alpha_s(\mu_s)} \frac{C_F}{\beta_0^2} \left(g_0(\eta_s) + \frac{\alpha_s(\mu_s)}{2\pi} \beta_0 \ln \eta_s \ln \frac{\omega}{\mu_s} \right) \right] \\ \times \exp \left[\frac{4\pi}{\alpha_{\text{em}}(\mu_s)} \frac{Q_q(2Q_\ell + Q_q)}{\beta_{0,\text{em}}^2} \left(g_0(\eta_{\text{em}}) + \frac{\alpha_{\text{em}}(\mu_s)}{2\pi} \beta_{0,\text{em}} \ln \eta_{\text{em}} \ln \frac{\omega}{\mu_s} \right) \right] \quad (4.18)$$

$$\xrightarrow{\text{DL}} \exp \left[\frac{\Gamma_s}{2} \left(\ln^2 \frac{\omega}{\mu_s} - \ln^2 \frac{\omega}{\mu} \right) \right], \quad (4.19)$$

where for soft evolution η_i stands for $\eta_i(\mu_s, \mu) \equiv \alpha_i(\mu_s)/\alpha_i(\mu)$ with $i = s, \text{em}$. In the last line we have taken the double-logarithmic approximation of the QCD and QED factor, but we will not make use of this approximation later on.

The above result can be simplified by noting that $\omega, \mu_s \sim \Lambda$, hence $\ln(\omega/\mu_s)$ is never a large logarithm. Similar to the solution of the SCET_I evolution equation, we may drop such $\mathcal{O}(1)$ logarithms. In the present case, this renders the evolution factor independent of the momentum variable ω , resulting in

$$U_s(\mu, \mu_s) = \exp \left[\frac{4\pi}{\alpha_s(\mu_s)} \frac{C_F}{\beta_0^2} g_0(\eta_s) \right] \exp \left[\frac{4\pi}{\alpha_{\text{em}}(\mu_s)} \frac{Q_q(2Q_\ell + Q_q)}{\beta_{0,\text{em}}^2} g_0(\eta_{\text{em}}) \right] \\ \xrightarrow{\text{DL}} \exp \left[\frac{4\pi}{\alpha_s(\mu_s)} \frac{C_F}{\beta_0^2} g_0(\eta_s) \right] \exp \left[-\frac{\alpha_{\text{em}}}{2\pi} [Q_q(2Q_\ell + Q_q)] \ln^2 \frac{\mu_s}{\mu} \right]. \quad (4.20)$$

We note the same form as (3.16) for the hard-collinear evolution, except now the evolution starts at μ_s , and there is no Q_ℓ^2 term in the anomalous dimension.

4.2.2 Anti-collinear sector

The anti-collinear sector is the same for both operators and given by the anti-collinear lepton field $\widehat{\mathcal{J}}_{\bar{c}} = \ell_{\bar{c}}(0)$.⁵ We define the anti-collinear operator

$$\mathcal{J}_{\bar{c}} \equiv \mathcal{J}_{i,\bar{c}} = R_- \ell_{\bar{c}}(0), \quad (4.21)$$

including the R_- factor from the soft subtraction. The operator has a single open spinor index which is omitted for simplicity, as the anomalous dimension is diagonal.

The one-loop diagrams needed to compute the anomalous dimension of the above operator correspond to the anti-collinear part of the two diagrams in Figure 4b and Figure 4c involving $n_- A_{\bar{c}}$. The factor R_- , which originates from the soft tadpole diagram (6), ensures the cancellation of the off-shell IR regulator in the UV divergent part. We introduce the renormalization constant $Z_{\bar{c}}$ associated with the UV counterterm, for which the one-loop result is given in (A.40).

⁵We note that this refers to the field including the anti-collinear Wilson line, which is invariant under anti-collinear gauge transformations, see (A.10).

The anti-collinear part obeys the RG equation

$$\frac{d}{d \ln \mu} \mathcal{J}_{\bar{c}}(\mu) = -\Gamma_{\bar{c}} \mathcal{J}_{\bar{c}}(\mu), \quad (4.22)$$

with the one-loop anomalous dimension

$$\Gamma_{\bar{c}} = \frac{\Gamma_c}{2} \left(\ln \frac{m_{B_q}}{\mu} - \frac{i\pi}{2} \right) - \frac{\alpha_{\text{em}}}{4\pi} 3Q_\ell^2, \quad (4.23)$$

and the cusp anomalous dimension Γ_c previously defined in (3.13). The solution to LL accuracy is

$$\mathcal{J}_{\bar{c}}(\mu) = U_{\bar{c}}(\mu, \mu_c) \mathcal{J}_{\bar{c}}(\mu_c), \quad (4.24)$$

with

$$U_{\bar{c}}(\mu, \mu_c) = \exp \left[-\frac{4\pi}{\alpha_{\text{em}}(\mu_c)} \frac{Q_\ell^2}{\beta_{0,\text{em}}^2} \left(g_0(\eta_{\text{em}}) + \frac{\alpha_{\text{em}}(\mu_c)}{2\pi} \beta_{0,\text{em}} \ln \eta_{\text{em}} \ln \frac{m_{B_q}}{\mu_c} \right) \right] \quad (4.25)$$

$$\xrightarrow{\text{DL}} \exp \left[-\frac{\Gamma_c}{4} \left(\ln^2 \frac{m_{B_q}}{\mu_c} - \ln^2 \frac{m_{B_q}}{\mu} \right) \right]. \quad (4.26)$$

Here η_{em} is $\eta_{\text{em}}(\mu_c, \mu) = \alpha_{\text{em}}(\mu_c)/\alpha_{\text{em}}(\mu)$ for (anti-) collinear evolution. Note that we cannot neglect the first term in the exponent in this case, since $\ln(m_{B_q}/\mu_c)$ is a large logarithm.

4.2.3 Collinear sector

The collinear part of operators (4.1) and (4.2) consists of the two operators

$$\mathcal{J}_c^{A1} \equiv \mathcal{J}_{m_\chi, c}^{A1} = R_+ \bar{\ell}_c(0) 4m_\ell P_R, \quad (4.27)$$

$$\mathcal{J}_c^{B1}(w) \equiv \mathcal{J}_{\mathcal{A}_\chi, c}^{B1} = R_+ (n_+ p) \int \frac{dt}{2\pi} e^{-i\bar{w}t n_+ p} \bar{\ell}_c(0) 2\mathcal{A}_{c\perp}(tn_+) P_R, \quad (4.28)$$

with $\bar{w} \equiv 1 - w$, which mix under renormalization. Similar to the anti-collinear part, the factor R_+ must be included to cancel the IR regulator dependence in the anomalous dimension. The 2×2 renormalization matrix has the structure

$$\begin{pmatrix} [\mathcal{J}_c^{A1}]_{\text{ren}} \\ [\mathcal{J}_c^{B1}]_{\text{ren}} \end{pmatrix} = \begin{pmatrix} Z_{m_\chi}^c & 0 \\ Z_{\mathcal{A}_\chi, m_\chi}^c & Z_{\mathcal{A}_\chi}^c \end{pmatrix} \otimes_{w'} \begin{pmatrix} [\mathcal{J}_c^{A1}]_{\text{bare}} \\ [\mathcal{J}_c^{B1}]_{\text{bare}} \end{pmatrix}, \quad (4.29)$$

where $\otimes_{w'}$ indicates the presence of the convolution with respect to the collinear momentum fraction. Both operators have in common the collinear lepton field $\bar{\ell}_c(0)$, for which the associated one-loop diagrams due to the collinear Wilson lines are the diagrams in Figure 4b and Figure 4c which involve $n_+ A_c$. Further, the operator \mathcal{J}_c^{A1} contains an explicit factor of m_ℓ in the $\overline{\text{MS}}$ scheme, which we assign to the collinear sector as can be motivated by the

one-loop matching calculation for this operator in Section 4.3. The operator \mathcal{J}_c^{B1} contains the additional collinear photon field $\mathcal{A}_{c\perp}^\mu(tn_+)$, which gives two more one-loop diagrams shown in Figure 4c. The one-loop result of the diagonal elements $Z_{m_\chi}^{c,(1)}$ and $Z_{\mathcal{A}_\chi}^{c,(1)}$ are given in (A.41) and (A.42), respectively.

For massless fermions in SCET_I, the mixing of B1-type operators into A1-type operators is absent. In SCET_{II} with non-zero fermion mass, we find the non-vanishing one-loop off-shell collinear matrix element of B1-type operator shown as the middle diagram in the column labelled “SCET_{II}” in Figure 3. Its divergent part is proportional to the tree-level matrix element of the mass-suppressed A1-type operator. Explicitly, the matrix element is given by

$$\begin{aligned} n_+ p \int \frac{dt}{2\pi} e^{-i\bar{w}t(n_+p)} \langle \ell(p) | \bar{\ell}_c(0) \mathcal{A}_{c\perp}^\mu(tn_+) | 0 \rangle \\ = -\frac{\alpha_{\text{em}}}{4\pi} Q_\ell \bar{w} \left[\frac{1}{\epsilon} + \ln \frac{\mu^2}{\bar{w}(m_\ell^2 - p^2 w)} \right] m_\ell \bar{u}_c(p) \gamma_\perp^\mu, \end{aligned} \quad (4.30)$$

yielding the mixing counterterm

$$Z_{\mathcal{A}^\mu_{\chi\alpha}, m_{\chi\beta}}^{c(1)}(w) = \frac{\alpha_{\text{em}}}{4\pi} \frac{Q_\ell}{\epsilon} \bar{w} [\gamma_\perp^\mu]_{\alpha\beta} \quad (4.31)$$

for the general case with open Dirac and Lorentz indices. Contracting them with $2\gamma^{\perp\mu} P_R$, the SCET_{II} mixing counterterm pertinent to the operators (4.27) and (4.28) is

$$Z_{\mathcal{A}_\chi, m_\chi}^{c(1)}(w) = \frac{\alpha_{\text{em}}}{4\pi} \frac{Q_\ell}{\epsilon} \bar{w}. \quad (4.32)$$

The renormalization of the collinear fields leads to the coupled system of RGEs,

$$\frac{d}{d \ln \mu} \begin{pmatrix} \mathcal{J}_c^{A1}(\mu) \\ \mathcal{J}_c^{B1}(w; \mu) \end{pmatrix} = - \begin{pmatrix} \Gamma_{m_\chi}^c & 0 \\ \Gamma_{\mathcal{A}_\chi, m_\chi}^c & \Gamma_{\mathcal{A}_\chi}^c \end{pmatrix} \otimes_{w'} \begin{pmatrix} \mathcal{J}_c^{A1}(\mu) \\ \mathcal{J}_c^{B1}(w'; \mu) \end{pmatrix}, \quad (4.33)$$

with the one-loop collinear anomalous dimensions given by⁶

$$\Gamma_{m_\chi}^c = \frac{\Gamma_c}{2} \left(\ln \frac{m_{B_q}}{\mu} - \frac{i\pi}{2} \right) + \frac{\alpha_{\text{em}}}{4\pi} 3Q_\ell^2, \quad (4.34)$$

$$\Gamma_{\mathcal{A}_\chi, m_\chi}^c(w) = \frac{\alpha_{\text{em}}}{4\pi} 2Q_\ell \bar{w}, \quad (4.35)$$

$$\Gamma_{\mathcal{A}_\chi}^c(w, w') = \delta(w - w') \left[\frac{\Gamma_c}{2} \left(\ln \frac{m_{B_q}}{\mu} - \frac{i\pi}{2} \right) + \frac{\alpha_{\text{em}}}{4\pi} Q_\ell^2 (4 \ln w - 6) \right]$$

⁶A very similar operator mixing calculation appears in the SCET analysis of power-suppressed two-jet operators sourced by a new heavy particle [33]. In this application, the insertion of an external Higgs field operator corresponds to the lepton mass factor. The off-diagonal anomalous dimension in [33] misses the factor \bar{w} , because the one-particle reducible diagram with the Higgs insertion on the external leg was not included.

$$-\frac{\alpha_{\text{em}}}{4\pi} 2Q_\ell^2 \gamma_{\mathcal{A}_\chi, \mathcal{A}_\chi}(w, w'). \quad (4.36)$$

The non-cusp anomalous dimension $\gamma_{\mathcal{A}_\chi, \mathcal{A}_\chi}(w, w')$ is provided for completeness in (A.43). The opposite sign of the non-cusp term in (4.34) compared to (4.23) arises from the anomalous dimension of the $\overline{\text{MS}}$ lepton mass in the definition of \mathcal{J}_c^{A1} .

At LL accuracy, keeping only the cusp anomalous dimension terms, the system of RGEs (4.33) is easily solved first for $\mathcal{J}_c^{A1}(\mu)$, and subsequently for $\mathcal{J}_c^{B1}(w, \mu)$, yielding

$$\mathcal{J}_c^{A1}(\mu) = U_c(\mu, \mu_c) \mathcal{J}_c^{A1}(\mu_c), \quad (4.37)$$

$$\mathcal{J}_c^{B1}(w; \mu) = U_c(\mu, \mu_c) \left[\mathcal{J}_c^{B1}(w; \mu_c) - \frac{Q_\ell \bar{w}}{\beta_{0,\text{em}}} \ln \eta_{\text{em}} \mathcal{J}_c^{A1}(\mu_c) \right]. \quad (4.38)$$

Here η_{em} equals $\eta_{\text{em}}(\mu_c, \mu) = \alpha_{\text{em}}(\mu_c)/\alpha_{\text{em}}(\mu)$ and $U_c(\mu, \mu_c) = U_{\bar{c}}(\mu, \mu_c)$ defined in (4.24) with LL accuracy, because the cusp part of the anomalous dimensions $\Gamma_{m_\chi}^c, \Gamma_{\mathcal{A}_\chi}^c$ is the same as of Γ^c in (4.23).

Naively, the second term in the bracket in (4.38) appears suppressed as it contains α_{em} times a single logarithm. However, the tree-level matrix element of the operator $\mathcal{J}_c^{B1}(\mu_c)$ vanishes for $B_q \rightarrow \mu^+ \mu^-$. Hence, the second term is actually the leading term, as outlined in Figure 3. The matrix element of the B1-operator contributes at the one-loop order, and does not contain large logarithms because it is evaluated at the collinear scale. For the LL accuracy, it is then enough to choose the initial condition $\mathcal{J}_c^{B1}(w; \mu_c) = 0$. In the double-logarithmic approximation, we could further replace

$$\frac{1}{\beta_{0,\text{em}}} \ln \eta_{\text{em}} \xrightarrow{\text{DL}} \frac{\alpha_{\text{em}}}{2\pi} \ln \frac{\mu}{\mu_c}. \quad (4.39)$$

4.2.4 Complete SCET_{II} operator and evolution

For convenience, we summarize the renormalization and RGEs for the full SCET_{II} operators $\mathcal{J}_{m_\chi}^{A1}$ and $\mathcal{J}_{\mathcal{A}_\chi}^{B1}$. The operator mixing in the collinear sector leads to a 2×2 renormalization matrix

$$\begin{pmatrix} [\mathcal{J}_{m_\chi}^{A1}]_{\text{ren}} \\ [\mathcal{J}_{\mathcal{A}_\chi}^{B1}]_{\text{ren}} \end{pmatrix} = \begin{pmatrix} Z_{m_\chi, m_\chi} & 0 \\ Z_{\mathcal{A}_\chi, m_\chi} & Z_{\mathcal{A}_\chi, \mathcal{A}_\chi} \end{pmatrix} \otimes_{\omega', w'} \begin{pmatrix} [\mathcal{J}_{m_\chi}^{A1}]_{\text{bare}} \\ [\mathcal{J}_{\mathcal{A}_\chi}^{B1}]_{\text{bare}} \end{pmatrix}, \quad (4.40)$$

where appropriate convolutions are indicated by \otimes . The renormalization constants are the products of the soft, collinear and anti-collinear factors discussed before,

$$Z_{m_\chi, m_\chi}(\omega, \omega') = Z_s(\omega, \omega') Z_{\bar{c}} Z_{m_\chi}^c, \quad (4.41)$$

$$Z_{\mathcal{A}_\chi, \mathcal{A}_\chi}(\omega, \omega'; w, w') = Z_s(\omega, \omega') Z_{\bar{c}} Z_{\mathcal{A}_\chi}^c(w, w'), \quad (4.42)$$

$$Z_{\mathcal{A}_\chi, m_\chi}(\omega, \omega'; w) = Z_s(\omega, \omega') Z_{\bar{c}} Z_{\mathcal{A}_\chi, m_\chi}^c(w), \quad (4.43)$$

and the anomalous dimension matrix becomes the sum of the soft, collinear, and anti-collinear anomalous dimensions. We can write this in the form

$$\Gamma^{\text{II}} = \Gamma^s(\omega, \omega') \begin{pmatrix} 1 & 0 \\ 0 & \delta(w - w') \end{pmatrix} + \delta(\omega - \omega') \begin{pmatrix} \Gamma^{\bar{c}} + \Gamma_{m\chi}^c & 0 \\ \Gamma_{A\chi, m\chi}^c(w) & \delta(w - w') \Gamma^{\bar{c}} + \Gamma_{A\chi}^c(w, w') \end{pmatrix}, \quad (4.44)$$

with entries defined in (4.15), (4.23) and (4.34)–(4.36). Since the soft part is independent of the collinear and anti-collinear building blocks, it enters only the diagonal entries. Both operators $\mathcal{J}_{m\chi}^{A1}$ and $\mathcal{J}_{A\chi}^{B1}$ contain the cusp anomalous dimension parts Γ_s and Γ_c from (3.13), which appeared already in the anomalous dimension of the SCET_I operators. Contrary to SCET_I, in SCET_{II} Γ_s enters with the opposite sign and is multiplied by $\ln(\omega/\mu)$, but Γ_c is multiplied by $\ln(m_{B_q}/\mu)$ as in SCET_I. Finally we note that the soft and (anti-)collinear anomalous dimensions are separately gauge invariant.

We collect at this point all evolution factors, including the evolution in SCET_I. From $H_i(\mu_b)\mathcal{O}_i(\mu_b) = H_i(\mu)\mathcal{O}_i(\mu)$ and (3.18), we obtain

$$\begin{aligned} \mathcal{O}_i(\mu_b) &= \exp[S_\ell(\mu_b, \mu) + S_q(\mu_b, \mu)] \mathcal{O}(\mu) \\ &= \exp[S_\ell(\mu_b, \mu) + S_q(\mu_b, \mu)] \left[\mathcal{J}_s \otimes \mathcal{J}_c^{B1} \otimes \mathcal{J}_{\bar{c}} \right](\mu). \end{aligned} \quad (4.45)$$

In passing to the second line, we have matched the SCET_I operator at the scale $\mu \ll \mu_b$ at tree level to the SCET_{II} operator. We also omitted the SCET_{II} matching coefficient, which does not change the structure of the result. (The precise matching relation will be given in the following subsection.) Next we use the SCET_{II} evolution factors to write

$$\begin{aligned} \mathcal{O}_i(\mu_b) &= \exp[S_\ell(\mu_b, \mu) + S_q(\mu_b, \mu)] U_s(\mu, \mu_s) \mathcal{J}_s(\mu_s) \otimes U_{\bar{c}}(\mu, \mu_c) \mathcal{J}_{\bar{c}}(\mu_c) \\ &\quad \otimes U_c(\mu, \mu_c) \left[\mathcal{J}_c^{B1}(w; \mu_c) - \frac{Q_\ell \bar{w}}{\beta_{0,\text{em}}} \ln \eta_{\text{em}} \mathcal{J}_c^{A1}(\mu_c) \right] \\ &= \exp[S_\ell(\mu_b, \mu_c)] \exp[S_q(\mu_b, \mu)] U_s(\mu, \mu_s) \mathcal{J}_s(\mu_s) \mathcal{J}_{\bar{c}}(\mu_c) \\ &\quad \otimes \left[\mathcal{J}_c^{B1}(w; \mu_c) - \frac{Q_\ell \bar{w}}{\beta_{0,\text{em}}} \ln \eta_{\text{em}} \mathcal{J}_c^{A1}(\mu_c) \right]. \end{aligned} \quad (4.46)$$

In the final expression we combined the part of the hard-collinear evolution contained in $S_\ell(\mu_b, \mu)$ with the collinear and anti-collinear factors making use of⁷

$$\exp[S_\ell(\mu_b, \mu)] U_{\bar{c}}(\mu, \mu_c) U_c(\mu, \mu_c) = \exp[S_\ell(\mu_b, \mu_c)]. \quad (4.47)$$

This shows that the logarithms proportional to Q_ℓ^2 involving only the final-state leptons arise from uniform evolution from the hard scale m_{B_q} to the collinear scale m_ℓ . In the final

⁷To obtain the following identity exactly, we make use of the freedom to replace m_{B_q} by μ_b in (4.25) in the LL approximation. Alternatively, we may choose $\mu_b = m_{B_q}$.

expression (4.46), we may drop the term $\mathcal{J}_c^{B1}(w; \mu_c)$, since in the LL approximation the initial condition of the B1-operator at the collinear scale can be set to zero, as discussed above. When one takes the matrix element of (4.46), no large logarithms appear in the matrix elements of the \mathcal{J} , since they are evaluated at their natural scale, and all large logarithms are already summed.

4.3 Matching

We match the SCET_I operators \mathcal{O}_i at the hard-collinear scale μ_{hc} on the SCET_{II} operators in momentum space. The matching equations read

$$\mathcal{O}_i(u) = \int d\omega \left[J_m(u; \omega) \mathcal{J}_{m\bar{\chi}}^{A1}(\omega) + \int dw J_A(u; \omega, w) \mathcal{J}_{A\bar{\chi}}^{B1}(\omega, w) \right], \quad (4.48)$$

$$\mathcal{O}_{\bar{i}}(u) = \int d\omega \left[J_{\bar{m}}(u; \omega) \mathcal{J}_{m\bar{\chi}}^{A1}(\omega) + \int dw J_{\bar{A}}(u; \omega, w) \mathcal{J}_{A\bar{\chi}}^{B1}(\omega, w) \right], \quad (4.49)$$

with perturbative matching coefficients J_i , also called “jet functions”, which account for the (anti-) hard-collinear modes. There are no leading-power interactions between soft and hard-collinear fermions in SCET_I, hence to obtain the power-enhanced contribution we must include a single insertion of the power-suppressed Lagrangian $\mathcal{L}_{\xi q}^{(1)}(x)$, given in (A.13), to convert the hard-collinear quark into a soft quark. The jet functions $J_{m, \bar{m}}(u; \omega)$ start at the one-loop order, while $J_{A, \bar{A}}(u; \omega, w)$ coincide at tree level with expressions

$$J_A^{(0)}(u; \omega, w, \mu) = J_{\bar{A}}^{(0)}(u; \omega, w, \mu) = -\frac{Q_q}{\omega} \delta(u - w) \quad (4.50)$$

from the lower diagram depicted in the column labelled “SCET_I” in Figure 3. The explicit calculation shows that both operators \mathcal{O}_i for $i = 9, 10$ contribute equally to $\mathcal{J}_{A\bar{\chi}}^{B1}$, whereas $i = \bar{9}, \bar{10}$ contribute to $\mathcal{J}_{A\bar{\chi}}^{B1}$ with an opposite sign. Summarizing, we find

$$H_9 \otimes_u \mathcal{O}_9 + H_{10} \otimes_u \mathcal{O}_{10} \quad \rightarrow \quad (H_9 + H_{10}) \otimes_u J_A \otimes_{\omega, w} \mathcal{J}_{A\bar{\chi}}^{B1}, \quad (4.51)$$

$$H_{\bar{9}} \otimes_u \mathcal{O}_{\bar{9}} + H_{\bar{10}} \otimes_u \mathcal{O}_{\bar{10}} \quad \rightarrow \quad (H_{\bar{9}} - H_{\bar{10}}) \otimes_u J_{\bar{A}} \otimes_{\omega, w} \mathcal{J}_{A\bar{\chi}}^{B1}. \quad (4.52)$$

Here we anticipate that the relative minus sign in front of H_{10} and $H_{\bar{10}}$ to the right-hand side of the arrows, together with (3.8), is the origin of the cancellation of the Wilson coefficient C_{10} at the amplitude level after adding the collinear and anti-collinear contributions. Thus we reproduce in the SCET approach our previous finding [21] that the power-enhanced contribution (1.1) does not depend on C_{10} .

As an aside, we note that for the charged B -meson leptonic decay $B_u \rightarrow \mu \bar{\nu}_\mu$, the anti-collinear parts are not present because the anti-lepton is replaced by the chargeless neutrino, thus (4.52) will not contribute. Further, there is only a single operator with Wilson coefficient C and the Dirac structure $\gamma_\mu(1 - \gamma_5)$ in the lepton current. This implies the replacements $C_9 = C$ and $C_{10} = -C$, such that $H_9 + H_{10} = 0$ and no power-enhanced contribution arises for this process.

Returning to $B_q \rightarrow \mu^+ \mu^-$, let us briefly discuss also the one-loop matching of the coefficients $J_{m,\bar{m}}(u; \omega)$. The one-loop matrix elements of the left-hand sides of (4.51) and (4.52) in a $\langle \ell \ell | \dots | \bar{q} b \rangle$ state used to extract $J_{m,\bar{m}}(u; \omega)$ contain an IR divergence. This divergence is reproduced on the right-hand side in SCET_{II} by the scaleless one-loop matrix element and the renormalization constant (4.32) convoluted with the tree-level (anti-) hard-collinear jet function (4.50). After we include these contributions in the matching, the IR divergence cancels and we find

$$J_m^{(1)}(u; \omega; \mu) = \frac{\alpha_{\text{em}}}{4\pi} Q_\ell Q_q \frac{1-u}{\omega} \left[\ln \left(\frac{\omega n_+ p_\ell}{\mu^2} \right) + \ln [u(1-u)] \right] \theta(u) \theta(1-u). \quad (4.53)$$

The result for $J_{\bar{m}}^{(1)}$ is obtained by the replacement $n_+ p_\ell \rightarrow n_- p_{\bar{\ell}}$. The cancellation of the IR divergence in the matching of SCET_I on SCET_{II} confirms the short-distance nature of the jet function, and serves as a check of the EFT setup. We note that when $\mu \ll \mu_{hc}$, the one-loop expression above contains a large logarithm. This is precisely the logarithm that is generated by RG evolution and correctly taken into account by the LL result (4.38), (4.39). The non-logarithmic term $\ln [u(1-u)]$ enters (1.1) together with the non-logarithmic contributions from the collinear matrix element (6.4) below.

5 QED effects and the B -meson decay constant and LCDA

Before turning to the factorized matrix element for the power-enhanced part of the $B_q \rightarrow \mu^+ \mu^-$ amplitude, we discuss the hadronic matrix element of the soft operator $\tilde{\mathcal{J}}_s(v)$ (4.11), which is related to the B -meson decay constant and the leading-twist B -meson LCDA [40, 41]. However, the additional soft Wilson lines in the SCET_{II} operators (4.1)–(4.4) and $\tilde{\mathcal{J}}_s(v)$ imply that the hadronic matrix element does not coincide with the universal B -meson LCDA that would appear in the absence of electromagnetic interactions, and indicate a dependence on the final-state particles of the specific process. We discuss these issues in this section.

We thus define the generalized and process-dependent B -meson LCDA $\Phi_+(\omega)$ by the soft matrix element of the operator $\tilde{\mathcal{J}}_s(v)$

$$\begin{aligned} (-4) \langle 0 | \tilde{\mathcal{J}}_s(v) | \bar{B}_q(p) \rangle &= \frac{\langle 0 | \bar{q}_s(v n_-) Y(v n_-, 0) \not{n}_- \gamma_5 h_v(0) Y_+^\dagger(0) Y_-(0) | \bar{B}_q(p) \rangle}{\langle 0 | [Y_+^\dagger Y_-](0) | 0 \rangle} \\ &\equiv i m_{B_q} \int_0^\infty d\omega e^{-i\omega v} \mathcal{F}_{B_q} \Phi_+(\omega). \end{aligned} \quad (5.1)$$

The analogous definition holds for the anti-collinear case after interchanging $n_+ \leftrightarrow n_-$ in the $\bar{q}_s[\dots] h_v$ part of the operator, but with the same function $\Phi_+(\omega)$. As an overall factor we include the generalized process-dependent B -meson decay constant \mathcal{F}_{B_q} in the presence

of electromagnetic corrections, defined through the local matrix element

$$\frac{\langle 0 | \bar{q}_s(0) \gamma^\mu \gamma_5 h_v(0) Y_+^\dagger(0) Y_-(0) | \bar{B}_q(p) \rangle}{\langle 0 | [Y_+^\dagger Y_-](0) | 0 \rangle} = i \mathcal{F}_{B_q} m_{B_q} v^\mu, \quad (5.2)$$

where $p = m_{B_q} v$, and v^μ is the four-velocity label of the heavy-quark field. Since we are working with the heavy quark field in HQET, \mathcal{F}_{B_q} is the so-called static B -meson decay constant. It is related to the decay constant in full QCD and QED by matching corrections at the hard scale. The generalized B -meson LCDA satisfies the RGE (4.16),

$$\frac{d}{d \ln \mu} [\mathcal{F}_{B_q}(\mu) \Phi_+(\omega; \mu)] = - \int_0^\infty d\omega' \Gamma^s(\omega, \omega') \mathcal{F}_{B_q}(\mu) \Phi_+(\omega'; \mu), \quad (5.3)$$

with the anomalous dimension kernel Γ^s given in (4.15) at the one-loop order. Note that it depends on the charges Q_ℓ of the leptons in the final state. Keeping only the cusp part as before, the solution is

$$\mathcal{F}_{B_q}(\mu) \Phi_+(\omega; \mu) = U_s(\mu, \mu_s; \omega) \mathcal{F}_{B_q}(\mu_s) \Phi_+(\omega; \mu_s) \quad (5.4)$$

with $U_s(\mu, \mu_s; \omega)$ from (4.18).

In practice, owing to the smallness of α_{em} , we can treat QED effects on hadronic matrix elements perturbatively. Since we wish to sum logarithmic QED effects to all orders, the expansion of the matrix element in α_{em} must be done at the soft scale $\mu_s \sim \Lambda$, where the matrix element contains no large logarithms. We can then use the RGE including the QED anomalous dimension to sum the large logarithms between the soft and the hard-collinear and hard scale. We therefore define the expansions

$$\mathcal{F}_{B_q}(\mu_s) = \sum_{n=0}^{\infty} \left(\frac{\alpha_{\text{em}}(\mu_s)}{4\pi} \right)^n F_{B_q}^{(n)}(\mu_s), \quad (5.5)$$

$$\mathcal{F}_{B_q}(\mu_s) \Phi_+(\omega; \mu_s) = \sum_{n=0}^{\infty} \left(\frac{\alpha_{\text{em}}(\mu_s)}{4\pi} \right)^n F_{B_q}^{(n)}(\mu_s) \phi_+^{(n)}(\omega; \mu_s), \quad (5.6)$$

of the B -meson decay constant and LCDA. The leading terms in the expansion coincide with the standard B -meson decay constant $F_{B_q}(\mu)$ and LCDA $\phi_+(\omega; \mu)$ defined in the absence of QED *at the soft scale*, that is, $F_{B_q}^{(0)}(\mu_s) \equiv F_{B_q}(\mu_s)$ and $\phi_+^{(0)}(\omega; \mu_s) \equiv \phi_+(\omega; \mu_s)$, respectively. However, they evolve differently to $\mu \gg \mu_s$, since the RGE for $\phi_+(\omega; \mu)$ does not include QED effects. To be specific, write

$$U_s(\mu, \mu_s; \omega, \omega') = U_s^{\text{QCD}}(\mu, \mu_s; \omega, \omega') U_s^{\text{QED}}(\mu, \mu_s; \omega, \omega'), \quad (5.7)$$

where $U_s^{\text{QCD}}(\mu, \mu_s; \omega, \omega')$ is defined as $U_s(\mu, \mu_s; \omega, \omega')$ with the electromagnetic coupling α_{em} set to zero, and $U_s^{\text{QED}}(\mu, \mu_s; \omega, \omega')$ as the rest.⁸ In other words, $U_s^{\text{QED}}(\mu, \mu_s)$ fulfils the RGE

$$\frac{d}{d \ln \mu} U_s^{\text{QED}}(\mu, \mu_s; \omega, \omega') = - \left[\Gamma^s - \Gamma^s|_{\alpha_{\text{em}} \rightarrow 0} \right] U_s^{\text{QED}}(\mu, \mu_s; \omega, \omega') \quad (5.8)$$

⁸Note that this definition implies that in general $U_s^{\text{QED}}(\mu, \mu_s; \omega, \omega')$ depends on the strong coupling, although not at the LL accuracy. It is defined as the additional evolution caused by QED, and therefore includes mixed QED-QCD effects. We also added the second argument ω' , such that these general definitions are valid beyond the LL approximation.

with initial condition $U_s^{\text{QED}}(\mu_s, \mu_s; \omega, \omega') = \delta(\omega - \omega')$. Since $U_s^{\text{QCD}}(\mu, \mu_s; \omega, \omega')$ is the evolution factor for the standard B -meson LCDA in the absence of QED, we have the relation

$$\begin{aligned} F_{B_q}^{(0)}(\mu) \phi_+^{(0)}(\omega; \mu) &= U_s^{\text{QCD}}(\mu, \mu_s; \omega, \omega') U_s^{\text{QED}}(\mu, \mu_s; \omega, \omega') \otimes_{\omega'} [F_{B_q}^{(0)}(\mu_s) \phi_+^{(0)}(\omega; \mu_s)] \\ &= U_s^{\text{QED}}(\mu, \mu_s; \omega, \omega') U_s^{\text{QCD}}(\mu, \mu_s; \omega, \omega') \otimes_{\omega'} [F_{B_q}(\mu_s) \phi_+(\omega; \mu_s)] \\ &= U_s^{\text{QED}}(\mu, \mu_s; \omega, \omega') \otimes_{\omega'} [F_{B_q}(\mu) \phi_+(\omega'; \mu)], \end{aligned} \quad (5.9)$$

at an arbitrary scale.

Higher-order terms in the expansion (5.5), (5.6) define non-universal, non-local QCD (more precisely, HQET) matrix elements that have to be evaluated nonperturbatively. Since α_{em} is small, only a few terms will be needed in practice. For example, the computation of the time-ordered product of the electromagnetic current $j_\mu^{\text{em}}(x)$ with the soft quark fields contained in the SCET_{II} operators contributes to $\phi_+^{(1)}(\omega)$ and $F_{B_q}^{(1)}$. The decay constants $F_{B_q}^{(n)}(\mu_s)$ and LCDAs $\phi_+^{(n)}(\omega)$ at the scale μ_s provide a basis of initial conditions for the systematic inclusion and resummation of QED effects. At the leading and next-to-leading logarithmic (NLL) accuracy, only the universal objects $F_{B_q}(\mu_s)$ and $\phi_+(\omega)$ need to be known. For $N^{k+1}\text{LL}$ or fixed-order $N^k\text{LO}$ accuracy, the expansions (5.5), (5.6) can be truncated at $n = k$.

The above discussion, applicable to $B_q \rightarrow \ell^+ \ell^-$, illustrates some complications related to the factorization of QED corrections for exclusive B -meson decays. Only the leading and next-to-leading QED logarithms can be computed without introducing new QED-specific nonperturbative hadronic matrix elements. To be more explicit on the process dependence of the B -meson LCDA and the decay constant in the presence of QED, we consider defining the QED gauge-invariant generalization of the standard LCDA by

$$\langle 0 | \bar{q}_s(vn_-) Y(vn_-, 0) \not{n}_- \gamma_5 h_v(0) | \bar{B}_q(p) \rangle \equiv i m_{B_q} \int_0^\infty d\omega e^{-i\omega v} \mathcal{F}_{B_q}^0 \Phi_+^0(\omega), \quad (5.10)$$

where the matrix element should be evaluated with the QCD and QED Lagrangians. At least the local matrix elements, defining $\mathcal{F}_{B_q}^0$, could be computed with lattice QCD. This is indeed a valid definition, however, it would be relevant in factorization theorems for processes like $B_q \rightarrow \gamma\gamma$ or $B_q \rightarrow \nu\bar{\nu}$ with no charged particles in the final state. It cannot be used for $B_q \rightarrow \ell^+ \ell^-$. In fact, the functions Φ_+^0 and Φ_+ , when evolved to scales $\mu \gg \mu_s$ differ already in the LL approximation, since they have different cusp anomalous dimensions. The one for Φ_+^0 does not contain the terms proportional to $Q_q Q_\ell$; in particular, at the one-loop order, the diagrams 3–5 in Figure 4a are absent. In general, the presence of non-local Wilson lines even in the definition of naively local objects such as the B -meson decay constant, see (5.2), provides a serious obstacle to any attempt to include QED effects in lattice computations of hadronic matrix elements for processes with energetic, charged particles in the final state.

Another interesting example is the leptonic charged B -meson decay $B_u \rightarrow \ell \bar{\nu}_\ell$. In this case, we need to introduce an auxiliary Wilson line to achieve soft-collinear factorization.

The LCDA is then defined via the soft matrix element

$$\frac{\langle 0 | \bar{q}'_s(vn_-) \tilde{Y}(vn_-, 0) \not{v} \gamma_5 h_v(0) Y_+^\dagger(0) | \bar{B}_u(p) \rangle}{\langle 0 | Y_v(0) Y_+^\dagger(0) | 0 \rangle} \equiv im_{B_u} \int_0^\infty d\omega e^{-i\omega v} \mathcal{F}_{B_u}^\pm \Phi_+^\pm(\omega). \quad (5.11)$$

The QCD+QED Wilson line that ensures gauge invariance is now given by

$$\tilde{Y}(vn_-, 0) = \bar{Y}_{q'+}(vn_-) \bar{Y}_{\text{QCD}+}(vn_-) \bar{Y}_{\text{QCD}+}^\dagger(0) \bar{Y}_{q+}^\dagger(0), \quad (5.12)$$

where $Q_{q'}$ is the charge of the soft u -quark denoted by q'_s in the B_u meson. The explicit definitions of soft Wilson lines can be found in Appendix A.1. The new auxiliary Wilson line $Y_v(0)$ is defined with the time-like vector v and carries the charge of the B_u meson. The dependence of the LCDA on the arbitrary vector v cancels after convolution with the collinear matrix element. It is clear that the arbitrary vector v breaks the boost invariance of the collinear matrix element, which includes the factor $R_{v+} \equiv \langle 0 | Y_v(0) Y_+^\dagger(0) | 0 \rangle$ that was removed above from the soft matrix element. The same breaking occurs also for $B_q \rightarrow \ell^+ \ell^-$ since the boost-invariant vacuum expectation value of the Wilson lines is factorized into the boost non-invariant quantities R_\pm . This is a consequence of the SCET_{II} factorization anomaly [39, 42–44], which frequently appears when there are collinear and soft modes with equal invariant mass, which cannot be uniquely separated in dimensional regularization.

Finally, let us comment on the dipole operator contribution proportional to C_7 . From Appendix B, we expect that for this case yet another generalized LCDA should be defined containing the soft leptons of the operator in (B.16). Thus, the set of required LCDAs is not only process-dependent but also depends on the operator at the hard scale.

6 Resummed power-enhanced $B_q \rightarrow \ell^+ \ell^-$ amplitude

6.1 Factorization of the amplitude

Having defined the soft matrix element in terms of the generalized B -meson LCDA, we now focus on the collinear and anti-collinear matrix elements. As they involve only the leptons and their interactions with collinear/anti-collinear photons, they are free of QCD effects at the considered order. As is the case for other low-energy electromagnetic quantities, hadronic vacuum polarization and other strong interaction effects would become relevant in higher orders in the electromagnetic coupling. In SCET_{II}, the A1-type operators contain either a single collinear (anti-collinear) lepton field, and B1-type operators a product of both collinear (anti-collinear) lepton and photon fields. In each case, we are interested only in the matrix element of $\bar{B}_q(p) \rightarrow \ell^+(p_{\bar{\ell}}) \ell^-(p_\ell)$ with only leptons in the final state.⁹ Thus,

⁹We recall that the power-enhanced QED corrections are purely virtual. By assumption, we define the IR finite observable through a narrow signal window in the di-muon invariant mass around the mass of the B_q meson. This allows photons with ultrasoft energy $E_\gamma < \Delta E \ll \Lambda$ in the final state, but excludes final-state radiation of real collinear photons with virtuality of order Λ^2 . We consider ultrasoft photons in Section 7.

we define the *renormalized* collinear and anti-collinear on-shell matrix elements related to $\mathcal{J}_{m_\chi}^{A1}$ as

$$\langle \ell^-(p_\ell) | R_+ \bar{\ell}_c(0) | 0 \rangle = Z_\ell \bar{u}_c(p_\ell), \quad \langle \ell^+(p_{\bar{\ell}}) | R_- \ell_{\bar{c}}(0) | 0 \rangle = Z_{\bar{\ell}} v_{\bar{c}}(p_{\bar{\ell}}), \quad (6.1)$$

and those related to $\mathcal{J}_{A_\chi}^{B1}$ as

$$\begin{aligned} R_+ \int \frac{dt}{2\pi} e^{-it\bar{w}(n_+p_\ell)} \langle \ell^-(p_\ell) | \bar{\ell}_c(0) \mathcal{A}_{c\perp}^\mu(tn_+) | 0 \rangle &= Z_\ell M_A(w) m_\ell [\bar{u}_c(p_\ell) \gamma_\perp^\mu], \\ R_- \int \frac{dt}{2\pi} e^{-it\bar{w}(n_-p_{\bar{\ell}})} \langle \ell^+(p_{\bar{\ell}}) | \mathcal{A}_{\bar{c}\perp}^\mu(tn_-) \ell_{\bar{c}}(0) | 0 \rangle &= Z_{\bar{\ell}} M_{\bar{A}}(w) m_\ell [\gamma_\perp^\mu v_{\bar{c}}(p_{\bar{\ell}})]. \end{aligned} \quad (6.2)$$

We note that the second equation in (6.1) simply defines the matrix element of $\mathcal{J}_{\bar{c}}$ from (4.21), while the first and (6.2) gives the matrix elements of (4.27), (4.28) after straightforward multiplications and contractions. Explicit computation to the required order gives

$$Z_\ell = Z_{\bar{\ell}} = 1 + \mathcal{O}(\alpha_{\text{em}}), \quad (6.3)$$

$$M_A^{(1)}(w; \mu) = M_{\bar{A}}^{(1)}(w; \mu) = -\frac{\alpha_{\text{em}}}{4\pi} Q_\ell \bar{w} \left(\ln \frac{\mu^2}{m_\ell^2} - \ln \bar{w}^2 \right), \quad (6.4)$$

with $\bar{w} \equiv 1 - w$. In the case of $\mathcal{J}_{A_\chi}^{B1}$, the matrix element starts at the one-loop order, as indicated by the superscript. The bare matrix element is UV divergent and rendered finite by the operator mixing counterterm (4.32). When evaluated at the collinear scale $\mu \sim \Lambda$, the matrix elements do not contain large logarithmic corrections.

With the above collinear matrix elements and the parametrization (5.1) of the soft matrix element at hand, we can now derive the factorized expression for the matrix elements of the Fourier transforms (4.7), (4.8) of the SCET_{II} operators (4.1), (4.2) in the form

$$\langle \ell^+(p_{\bar{\ell}}) \ell^-(p_\ell) | \mathcal{J}_{m_\chi}^{A1}(\omega) | \bar{B}_q(p) \rangle = T_+ m_{B_q} \mathcal{F}_{B_q} \Phi_+(\omega), \quad (6.5)$$

$$\langle \ell^+(p_{\bar{\ell}}) \ell^-(p_\ell) | \mathcal{J}_{A_\chi}^{B1}(\omega, w) | \bar{B}_q(p) \rangle = T_+ M_A(w) m_{B_q} \mathcal{F}_{B_q} \Phi_+(\omega). \quad (6.6)$$

All scale-dependent quantities are understood to be evaluated at the scale μ , and we defined the common factor

$$T_+(\mu) \equiv (-i) m_\ell(\mu) Z_\ell(\mu) Z_{\bar{\ell}}(\mu) [\bar{u}_c(p_\ell) P_R v_{\bar{c}}(p_{\bar{\ell}})]. \quad (6.7)$$

Note that $\langle \mathcal{J}_{m_\chi}^{A1} \rangle$ contributes at tree level, whereas $\langle \mathcal{J}_{A_\chi}^{B1} \rangle$ starts to contribute only from the one-loop order. The same result holds for the anti-collinear operators $i = m_{\bar{\chi}}, \mathcal{A}_{\bar{\chi}}$ owing to (6.4) and the definition of the soft matrix element (5.1).

The complete expression for the power-enhanced $B_q \rightarrow \ell^+ \ell^-$ amplitude due to the operators $Q_{9,10}$ of the effective weak interaction Lagrangian is now obtained by adding the hard ($H_{9,10}$) and hard-collinear ($J_{m,A}$) matching coefficients according to (3.7) and (4.48),

and by summing over all contributions $i = 9, \bar{9}, 10, \bar{10}$ in the general factorized form

$$i\mathcal{A}_9 = T_+ \left[(H_9 + H_{10}) \otimes_u (J_m + J_A \otimes_w M_A) \right. \\ \left. + (H_{\bar{9}} - H_{\bar{10}}) \otimes_u (J_{\bar{m}} + J_{\bar{A}} \otimes_w M_{\bar{A}}) \right] \otimes_\omega m_{B_q} \mathcal{F}_{B_q} \Phi_+, \quad (6.8)$$

where we have suppressed all arguments, which will be shown explicitly below. The formula simplifies considerably when accounting for several relations between the matching coefficients of the collinear and anti-collinear sectors, which show up at tree level: for the hard functions $H_9^{(0)} = H_{\bar{9}}^{(0)}$ and $H_{10}^{(0)} = H_{\bar{10}}^{(0)}$ from (3.8) and for the jet functions $J_A^{(0)} = J_{\bar{A}}^{(0)}$ from (4.50), and $J_m^{(0)} = J_{\bar{m}}^{(0)} = 0$. In fact, higher-order QED corrections are symmetric under the exchange of the collinear and anti-collinear sectors once hard fluctuations are decoupled, such that the relations $H_9 = H_{\bar{9}}$ and $H_{10} = H_{\bar{10}}$ are valid even beyond tree level. Thus the hard functions in both sectors will exhibit the same u -dependence. Concerning the jet functions and matrix elements of the SCET_{II} operators, the explicit one-loop results show that $J_m^{(1)} = J_{\bar{m}}^{(1)}$ upon the identification of $n_+ p_\ell = n_- p_{\bar{\ell}} = m_{B_q}$ in (4.53), while $M_A^{(1)} = M_{\bar{A}}^{(1)}$ according to (6.4). Again we expect these relations to extend to higher orders in QED, because of the symmetry between the collinear and anti-collinear sectors. Making use of these relations we find that (6.8) simplifies to

$$i\mathcal{A}_9 = T_+ \int_0^1 du 2H_9(u) \int_0^\infty d\omega \left[J_m(u; \omega) + \int_0^1 dw J_A(u; \omega, w) M_A(w) \right] m_{B_q} \mathcal{F}_{B_q} \Phi_+(\omega) \quad (6.9)$$

even beyond leading logarithmic approximation. The contribution from the operator Q_{10} has cancelled and a factor of two arises for the Q_9 term, as anticipated earlier. All momentum fraction arguments and convolutions have now been made explicit. Every factor is understood to be evaluated at the same scale μ . In this form there is no value of μ in which not at least one of the factors contains large logarithms. For example, if μ is chosen of order of the soft and collinear scale Λ , large logarithms occur in the hard and hard-collinear coefficients functions. On the other hand, if μ is chosen at the hard-collinear scale $\sqrt{m_b \Lambda}$, $H_9(u)$ and the matrix element factors T_+ , $M_A(w)$ and $\mathcal{F}_{B_q} \Phi_+(\omega)$ contain large logarithms.

6.2 Resummed amplitude

We will now use the solutions to the renormalization group equations derived earlier to convert (6.9) into a formula in which large logarithms are summed. The explicit result is given in the LL approximation, but the essence of the manipulations is general. We shall take the common scale to be the hard-collinear scale $\mu_{hc} \sim \sqrt{m_b \Lambda}$, hence we have to evolve the hard function from $\mu_b \sim m_b$ down to μ_{hc} and the soft and collinear functions up from $\mu_s \sim \mu_c \sim \Lambda$ to μ_{hc} .

To implement this procedure into (6.9), we use (3.18), and include the hard-function evolution to μ_{hc} via the substitution

$$H_9(u) \rightarrow \exp [S_\ell(\mu_b, \mu_{hc}) + S_q(\mu_b, \mu_{hc})] H_9(u, \mu_b). \quad (6.10)$$

For the soft matrix element, we use (5.4), (5.9) to obtain

$$\begin{aligned}\mathcal{F}_{B_q} \Phi_+(\omega) &\rightarrow U_s(\mu_{hc}, \mu_s; \omega) \mathcal{F}_{B_q}(\mu_s) \Phi_+(\omega; \mu_s) \\ &\rightarrow U_s^{\text{QED}}(\mu_{hc}, \mu_s; \omega) F_{B_q}(\mu_{hc}) \phi_+(\omega; \mu_{hc}).\end{aligned}\quad (6.11)$$

After the second arrow, we expressed the initial condition for the generalized B -meson LCDA at the soft scale in terms of the standard LCDA in the absence of QED corrections, which can be done at LL accuracy, as discussed Section 5, and evolved the latter back to the hard collinear scale. The advantage of this procedure is that while pure QED quantities can be evaluated perturbatively at low scales of order $\Lambda \sim m_\ell$, the soft scale is generally nonperturbative in QCD. The above form requires only that the standard B -meson LCDA $\phi_+(\omega; \mu_{hc})$ is provided at the hard-collinear scale by some nonperturbative method, or by extracting it from data directly at this scale [45]. Finally, for the anti-collinear part we use (4.24) to substitute $Z_{\bar{\ell}} \rightarrow U_{\bar{c}}(\mu_{hc}, \mu_c) Z_{\bar{\ell}}(\mu_c)$, which together with (4.37), (4.38) for the collinear part amounts to

$$T_+ \rightarrow U_c(\mu_{hc}, \mu_c) U_{\bar{c}}(\mu_{hc}, \mu_c) T_+(\mu_c), \quad (6.12)$$

$$T_+ M_A(w) \rightarrow U_c(\mu_{hc}, \mu_c) U_{\bar{c}}(\mu_{hc}, \mu_c) T_+(\mu_c) \left[M_A(w; \mu_c) - \frac{Q_\ell \bar{w}}{\beta_{0,\text{em}}} \ln \eta_{\text{em}} \right], \quad (6.13)$$

where $\eta_{\text{em}} = \alpha_{\text{em}}(\mu_c)/\alpha_{\text{em}}(\mu_{hc})$. After these replacements, the result contains the scales μ_b , μ_c and μ_s where the initial conditions of the various evolutions are set. This dependence cancels between the evolution factors, matching coefficients and matrix elements up to residual dependence of higher order than LL accuracy.

Putting this together in (6.9) and making use of (4.47) results in the all-order LL-resummed amplitude

$$\begin{aligned}i\mathcal{A}_9 &= e^{S_\ell(\mu_b, \mu_c)} T_+(\mu_c) \\ &\times \int_0^1 du e^{S_q(\mu_b, \mu_{hc})} 2H_9(u; \mu_b) \int_0^\infty d\omega U_s^{\text{QED}}(\mu_{hc}, \mu_s; \omega) m_{B_q} F_{B_q}(\mu_{hc}) \phi_+(\omega; \mu_{hc}) \\ &\times \left[J_m(u; \omega; \mu_{hc}) + \int_0^1 dw J_A(u; \omega, w; \mu_{hc}) \left(M_A(w; \mu_c) - \frac{Q_\ell \bar{w}}{\beta_{0,\text{em}}} \ln \eta_{\text{em}} \right) \right].\end{aligned}\quad (6.14)$$

We note that the prefactor $\exp[S_\ell(\mu_b, \mu_c)]$ sums the purely leptonic leading-logarithms proportional to Q_ℓ^2 between the hard scale μ_b and the collinear scale μ_c . They originate from virtual QED corrections in SCET_I and SCET_{II}. In Section 7 it will be combined with the remaining final-state contributions due to ultrasoft photons to provide the radiative $B_q \rightarrow \ell^+ \ell^-$ branching fraction including the fully resummed double-logarithmic QED corrections to all orders in perturbation theory.

The resummation of the leading-logarithmic QED (and QCD) corrections to all orders in perturbation theory is achieved by keeping the one-loop expressions of the cusp part of the anomalous dimensions together with tree-level results for the hard and jet functions. In

addition, due to the presence of operator mixing, the leading off-diagonal elements in the anomalous dimension matrix must also be kept. Otherwise, $i\mathcal{A}_9 = 0$, because $M_{A,\bar{A}}^{(0)}(\mu_c) = 0$ and $J_{m,\bar{m}}^{(0)}(\mu) = 0$ for all μ when the one-loop mixing of $\Gamma_{\mathcal{A}_\chi, m_\chi}^c$ in (4.33) is neglected.

In the following we obtain from (6.14) an expression that is both LL-accurate *and* NLO-accurate, thus generalizing the previous NLO result (1.1) to include the leading logarithms to all orders. This can be achieved by keeping the non-logarithmic one-loop corrections to J_m and M_A given in (4.53) and (6.4), respectively. First using (4.50) removes the w -integral in the second line of (6.14), such that the square bracket turns into

$$J_m(u; \omega; \mu_{hc}) - \frac{Q_q}{\omega} J_A(u; \omega, u; \mu_{hc}) \left(M_A(u; \mu_c) - \frac{Q_\ell \bar{u}}{\beta_{0,\text{em}}} \ln \eta_{\text{em}} \right). \quad (6.15)$$

With LL accuracy it is also justified to apply (4.39) with $\mu = \mu_{hc}$ in the last term. Inserting (4.53) and (6.4) produces

$$\frac{\alpha_{\text{em}}}{4\pi} Q_\ell Q_q \frac{1-u}{\omega} \left[\ln \frac{\omega n_{+p\ell}}{\mu_{hc}^2} + \ln u \bar{u} + \left[\ln \frac{\mu_c^2}{m_\ell^2} - 2 \ln \bar{u} \right] + \ln \frac{\mu_{hc}^2}{\mu_c^2} \right]. \quad (6.16)$$

After combining the logarithms and setting $n_{+p\ell} = m_{B_q}$, we recognize the factor that appears in (1.1).¹⁰ This allows us to put (6.14) into the final form

$$\begin{aligned} i\mathcal{A}_9 &= \frac{\alpha_{\text{em}}(\mu_c)}{4\pi} Q_\ell Q_q m_\ell (-i) m_{B_q} f_{B_q} e^{S_\ell(\mu_b, \mu_c)} \mathcal{N}[\bar{u}_c(1 + \gamma_5)v_{\bar{c}}] \\ &\times e^{S_q(\mu_b, \mu_{hc})} \int_0^1 du (1-u) C_9^{\text{eff}}(u, \mu_b) \\ &\times \int_0^\infty \frac{d\omega}{\omega} U_s^{\text{QED}}(\mu_{hc}, \mu_s; \omega) \phi_+(\omega; \mu_{hc}) \left[\ln \frac{\omega m_{B_q}}{m_\ell^2} + \ln \frac{u}{1-u} \right]. \end{aligned} \quad (6.17)$$

At LL accuracy the scale of the overall factor of α_{em} is arbitrary and we have chosen the collinear scale. Within the same LL approximation, we can also replace the HQET decay constant by the QCD decay constant f_{B_q} . The one-loop QED result of [21] in (1.1) is obtained from the above expression when setting the Sudakov exponentials and the soft evolution factor U_s^{QED} to unity, apart from the term proportional to C_7^{eff} that was not considered up to now. The explicit result for $S_\ell(\mu_b, \mu_c)$ and $S_q(\mu_b, \mu_{hc})$ can be inferred from (3.19) and (3.20), respectively. The residual QED evolution from the B -meson LCDA is obtained from (4.18) or the simpler version (4.20) by setting $\alpha_s = 0$, see (5.8). Explicitly

$$\begin{aligned} U_s^{\text{QED}}(\mu_{hc}, \mu_s; \omega) &= \exp \left[\frac{4\pi}{\alpha_{\text{em}}(\mu_s)} \frac{Q_q (2Q_\ell + Q_q)}{\beta_{0,\text{em}}^2} \left(g_0(\eta_{\text{em}}) + \frac{\alpha_{\text{em}}(\mu_s)}{2\pi} \beta_{0,\text{em}} \ln \eta_{\text{em}} \ln \frac{\omega}{\mu_s} \right) \right] \\ &\xrightarrow{\text{DL}} \exp \left[\frac{\Gamma_s^{\text{QED}}}{2} \left(\ln^2 \frac{\omega}{\mu_s} - \ln^2 \frac{\omega}{\mu_{hc}} \right) \right], \end{aligned} \quad (6.18)$$

¹⁰The present analysis clarifies that m_{B_q} should appear in the logarithm, because it arises from the kinematic lepton momentum rather than the bottom quark mass.

where for soft evolution η_{em} stands for $\eta_{\text{em}}(\mu_s, \mu_{hc}) \equiv \alpha_{\text{em}}(\mu_s)/\alpha_{\text{em}}(\mu_{hc})$, or, more simply, by dropping the $\mathcal{O}(1)$ logarithm of ω/μ_s ,

$$U_s^{\text{QED}}(\mu_{hc}, \mu_s) = \exp \left[\frac{4\pi}{\alpha_{\text{em}}(\mu_s)} \frac{Q_q(2Q_\ell + Q_q)}{\beta_{0,\text{em}}^2} g_0(\eta_{\text{em}}) \right] \\ \xrightarrow{\text{DL}} \exp \left[- \frac{\alpha_{\text{em}}}{2\pi} [Q_q(2Q_\ell + Q_q)] \ln^2 \frac{\mu_s}{\mu_{hc}} \right]. \quad (6.19)$$

Here, similarly to (5.8), $\Gamma_s^{\text{QED}} \equiv \Gamma_s(\alpha_s, \alpha_{\text{em}}) - \Gamma_s(\alpha_s, \alpha_{\text{em}} = 0)$ is obtained at the one-loop order from Γ_s in (3.13) by setting $\alpha_s = 0$.

7 $B_q \rightarrow \mu^+ \mu^-$ decay width

In the decay $B_q \rightarrow \mu^+ \mu^-$ we encounter the peculiar situation that the numerically leading amplitude at tree-level in α_{em} , discussed in more detail below as $\mathcal{A}_{10} \propto C_{10}$, is power-suppressed compared to the amplitude \mathcal{A}_9 in (6.9), which on the other hand is suppressed by α_{em} , hence

$$\mathcal{A}_{10} \sim 1 \cdot \lambda^{12}, \quad \mathcal{A}_9 \sim \frac{\alpha_{\text{em}}}{\pi} \cdot \lambda^{10} \cdot \ln \frac{\mu_{hc}}{\mu_c}. \quad (7.1)$$

Indeed the hierarchy $\alpha_{\text{em}}/\pi \sim 1/420$ compared to $\lambda^2 \sim \Lambda_{\text{QCD}}/m_b \sim 1/20$ confirms that \mathcal{A}_{10} is numerically the most relevant amplitude, but in an imaginary world with a much larger value of m_b or a much larger electromagnetic coupling, the amplitude \mathcal{A}_9 would be largest. As the decay width is proportional to $|\mathcal{A}_{10} + \mathcal{A}_9|^2$, the dominant effect of \mathcal{A}_9 is the interference with \mathcal{A}_{10} . The investigation of the full QED effects at the subleading power in $1/m_b$, as would be required for \mathcal{A}_{10} in the SCET approach, is a rather daunting task and we leave it for the future. However, based on our derivations in the previous sections, we discuss the leading effect, which requires only tree-level matching and leading-logarithmic resummation.

7.1 Tree-level amplitude to $B_q \rightarrow \mu^+ \mu^-$

Here we derive the LL resummation of the formally power-suppressed but numerically dominant amplitude \mathcal{A}_{10} for $B_q \rightarrow \ell^+ \ell^-$. At this accuracy it is sufficient to match at tree level and to employ the one-loop cusp anomalous dimensions of the relevant operators. The fact that we restrict ourselves to the operators obtained from tree-level matching in α_{em} simplifies the operator structure; in particular it implies that in the SCET_I operator the light quark field must be soft, since otherwise the operator could not overlap with the B -meson state at tree level. Due to the chiral structure of the weak EFT operators, the lepton-mass term appears already after the hard matching leading to the well-known helicity suppression of the amplitude. Hence, the relevant SCET_I operator is

$$\tilde{\mathcal{O}}_m = m_\ell [\bar{q}_s(0) P_R h_v(0)] [\bar{\ell}_C(0) \gamma_5 \ell_{\bar{C}}(0)], \quad (7.2)$$

with the matching coefficient

$$H_m(\mu_b) = \mathcal{N} \frac{2 C_{10}(\mu_b)}{m_{B_q}} \quad (7.3)$$

at the hard scale μ_b . As one works to subleading order in λ , one must use the $\mathcal{O}(\lambda)$ relation between the full theory fields and SCET fields, as derived for example in [25], to obtain the above result. The SCET_I RGE of the coefficient H_m at LL accuracy, i.e. neglecting non-cusp parts of the anomalous dimension and possible operator mixing, reads

$$\frac{d}{d \ln \mu} H_m(\mu) = \Gamma_c \ln \frac{m_{B_q}}{\mu} H_m(\mu). \quad (7.4)$$

It is governed by the collinear cusp anomalous dimension (3.13) encountered previously for the power-enhanced amplitude in SCET_I and SCET_{II}.

The decoupling of the hard-collinear modes of SCET_I is trivial and yields the SCET_{II} operator (in position space)

$$\tilde{\mathcal{J}}_m^{A1} = m_\ell \bar{q}_s(0) P_R h_v(0) [Y_+^\dagger Y_-](0) [\bar{\ell}_c(0) \gamma_5 \ell_{\bar{c}}(0)], \quad (7.5)$$

with unit matching coefficient. Note that the jet function cannot depend on the soft quark position along the light-cone at tree level, hence the operator remains local, unlike for SCET_I to SCET_{II} matching of the power-enhanced amplitude \mathcal{A}_9 . The RG evolution of the matrix element of $\tilde{\mathcal{J}}_m^{A1}$ is governed by the same cusp anomalous dimension as in SCET_I in (7.4). The amplitude in SCET_{II} at the collinear scale is then given by

$$\begin{aligned} i \mathcal{A}_{10} &= \frac{1}{2} (-i) m_{B_q} \mathcal{F}_{B_q}(\mu_{hc}) m_\ell [Z_\ell Z_{\bar{\ell}}](\mu_{hc}) H_m(\mu_{hc}) [\bar{u}_c(p_\ell) \gamma_5 v_{\bar{c}}(p_{\bar{\ell}})] \\ &= \frac{1}{2} (-i) m_{B_q} m_\ell f_{B_q} e^{S_\ell(\mu_b, \mu_c)} H_m(\mu_b) [\bar{u}_c(p_\ell) \gamma_5 v_{\bar{c}}(p_{\bar{\ell}})]. \end{aligned} \quad (7.6)$$

In the first line the hard function is meant to be evaluated at the hard-collinear scale by means of its SCET_I RGE and further a SCET_{II} RG evolution is implied for the matrix element of $\langle \tilde{\mathcal{J}}_m^{A1} \rangle \propto Z_\ell Z_{\bar{\ell}} \mathcal{F}_{B_q}$ from the soft and collinear scale to the hard-collinear scale. In the second line, we make use of the LL solution of the RGEs discussed in Section 6.2 and set $[Z_\ell Z_{\bar{\ell}}](\mu_c) = 1$. In particular, the same Sudakov factor $e^{S_\ell(\mu_b, \mu_c)}$ between the hard and collinear scales as in the power-enhanced amplitude (6.14) appears as an overall factor. Moreover the hard function H_m enters now at the hard scale with value given in (7.3). The static B -meson decay constant $\mathcal{F}_{B_q}(\mu_{hc}) = F_{B_q}^{(0)}(\mu_{hc}) + \alpha_{\text{em}}/(4\pi) F_{B_q}^{(1)}(\mu_{hc}) + \mathcal{O}(\alpha_{\text{em}}^2)$ contains the term $F_{B_q}^{(1)}$ that contributes at the same order in α_{em} as \mathcal{A}_9 , but is power-suppressed by λ^2 compared to \mathcal{A}_9 , and for this reason will be omitted. Further we replace $F_{B_q}^{(0)}(\mu_{hc})$ by $F_{B_q}(\mu_{hc})$, the static decay constant in the absence of QED, because the difference in RG evolution does not contribute double logarithms. For the same reason, we equate $F_{B_q}(\mu_{hc})$ to the full QCD decay constant f_{B_q} , which is usually calculated on the lattice within QCD.¹¹ This is exact to the considered accuracy of tree-level matching at the hard scale μ_b .

¹¹The lattice calculation [2] includes electromagnetic contributions to meson masses to fix quark masses, which leads to some isospin breaking for the B_q meson decay constants.

Since both, \mathcal{A}_9 and \mathcal{A}_{10} , share the same overall leptonic Sudakov factor, it proves advantageous for later purposes to factor it from the sum of both amplitudes. We write

$$i(\mathcal{A}_{10} + \mathcal{A}_9) \equiv e^{S_\ell(\mu_b, \mu_c)} \left(A_{10} [\bar{u}_c \gamma_5 v_{\bar{c}}] + A_9 [\bar{u}_c (1 + \gamma_5) v_{\bar{c}}] \right), \quad (7.7)$$

where we introduced the scalar reduced amplitudes $A_{9,10}$, which can be extracted from (6.14) and (7.6). An analogous reduced amplitude A_7 is defined for the part of the amplitude proportional to C_7^{eff} . Its non-resummed one-loop expression can be read off from (1.1). Moreover, the resummation of the leading logarithmic QCD (but not QED) corrections in SCET_I is also possible for the A_7 contribution, because the operators which give rise to the A_7 part in SCET_I have the same QCD anomalous dimension as the corresponding operators of the A_9 part. Therefore, the amplitude A_7 also receives the factor $e^{S_q(\mu_b, \mu_{hc})}$ defined in (3.20), but its QED part should be dropped.

7.2 Decay width and ultrasoft photons

So far we ignored ultrasoft photons below the soft scale μ_s . We now turn to the radiative $B_q \rightarrow \ell^+ \ell^-$ decay amplitude, and consider the matrix element with an arbitrary ultrasoft state X_s consisting of photons and possibly electrons and positrons. It factorizes into the non-radiative amplitude \mathcal{A}_i discussed before and an ultrasoft matrix element

$$\mathcal{N}_{\Delta B=1} C_i \langle \ell \bar{\ell} X_s | Q_i | \bar{B}_s \rangle = \mathcal{A}_i \langle X_s | S_{v_\ell}^\dagger(0) S_{v_{\bar{\ell}}}(0) | 0 \rangle, \quad i = 9, 10. \quad (7.8)$$

To prove this factorization formally we should match SCET_{II} at a scale of order $\Lambda_{\text{QCD}} \sim m_\ell$ to an effective theory that contains the B -meson field and heavy lepton fields with fixed velocity label, in analogy with heavy-quark effective theory. In this theory ultrasoft photons with virtuality much below $m_\ell^2 \sim \Lambda_{\text{QCD}}^2$ have leading-power couplings to the charged leptons but not to the electrically neutral B -meson. The decoupling of the ultrasoft photons from the heavy leptons, $\ell_C \rightarrow S_{v_\ell} \ell_C^{(0)}$, gives rise to the ultrasoft Wilson lines S_{v_ℓ} in (7.8). The lepton-velocity v_ℓ is defined via $p_\ell = E_\ell v_\ell$ and similarly for $v_{\bar{\ell}}$. At leading power in the $1/m_b$ expansion, the radiation originates only from the final-state leptons as the ultrasoft photons do not couple to the neutral initial state. Formally, the matching of SCET_{II} with quark fields to the EFT with point-like meson fields is nonperturbative. We can nevertheless sum the leading logarithms, because the B -meson is neutral and decoupled in the far infrared, so we know that the IR logarithms arise from perturbative QED only.

The partial decay width is obtained after squaring the full amplitude (7.8) and summing over all ultrasoft final states with total energy less than ΔE

$$\begin{aligned} \Gamma[B_q \rightarrow \mu^+ \mu^-](\Delta E) &= \frac{m_{B_q}}{8\pi} \beta_\mu \left(|A_{10} + A_9 + A_7|^2 + \beta_\mu^2 |A_9 + A_7|^2 \right) \\ &\quad \times \left| e^{S_\ell(\mu_b, \mu_c)} \right|^2 \mathcal{S}(v_\ell, v_{\bar{\ell}}, \Delta E), \end{aligned} \quad (7.9)$$

where $\beta_\mu = \sqrt{1 - 4m_\mu^2/m_{B_q}^2}$. We include here the amplitude A_7 even though we do not attempt to sum QED corrections for this amplitude. However we compute the leading

logarithmic QCD corrections to A_7 and comment on this in Section 8. The terms proportional to $|A_9 + A_7|^2$ are formally of $\mathcal{O}(\alpha_{\text{em}}^2)$. The first term in the parenthesis is due to the pseudo-scalar lepton current $[\bar{u}_c \gamma_5 v_{\bar{c}}]$ in (7.7), the second term $\beta_\mu^2 |A_9 + A_7|^2$ due to the scalar term $[\bar{u}_c v_{\bar{c}}]$. The ultrasoft function

$$\mathcal{S}(v_\ell, v_{\bar{\ell}}, \Delta E) = \sum_{X_s} |\langle X_s | S_{v_\ell}^\dagger(0) S_{v_{\bar{\ell}}}(0) | 0 \rangle|^2 \theta(\Delta E - E_{X_s}) \quad (7.10)$$

accounts for the emission of an arbitrary number of ultrasoft photons with total energy $E_{X_s} < \Delta E$.

The ultrasoft function should be further factorized to sum large logarithmic corrections with the RG technique. This could be achieved by introducing another EFT below the muon-mass scale similar to the SCET treatment of soft radiation in top-quark jets [46]. Instead, to avoid further technical complications, we use the QED exponentiation theorem to write the full soft function as the exponent of the one-loop result

$$\mathcal{S}(v_\ell, v_{\bar{\ell}}, \Delta E) = \exp \left[\frac{\alpha_{\text{em}}}{4\pi} Q_\ell^2 S^{(1)}(v_\ell, v_{\bar{\ell}}, \Delta E) \right]. \quad (7.11)$$

The one-loop result in the appropriate limit $E_\ell \gg m_\mu \gg \Delta E$ is given by (for a result in dimensional regularization, see e.g. [47])

$$S^{(1)}(v_\ell, v_{\bar{\ell}}, \Delta E) = 8 \left(1 + \ln \frac{m_\mu^2}{s_{\ell\bar{\ell}}} \right) \ln \left(\frac{\mu}{2\Delta E} \right) - 2 \left(2 + \ln \frac{m_\mu^2}{s_{\ell\bar{\ell}}} \right) \ln \frac{m_\mu^2}{s_{\ell\bar{\ell}}} - \frac{4}{3} \pi^2, \quad (7.12)$$

where $s_{\ell\bar{\ell}}$ denotes the invariant mass squared of the lepton pair. The μ dependence of the ultrasoft function is cancelled by the explicit μ_c dependence of the non-radiative amplitude, as seen in (7.13) below to the accuracy considered here, hence we set $\mu = \mu_c$. The second line of (7.9), which multiplies the reduced amplitude squared, can be rewritten as the single exponential. In the leading approximation we neglect the constant factor $-\frac{4}{3}\pi^2$ in $S^{(1)}$. Then we find

$$\begin{aligned} & \left| e^{S_\ell(\mu_b, \mu_c)} \right|^2 \mathcal{S}(v_\ell, v_{\bar{\ell}}, \Delta E, \mu_c) \\ &= \exp \left\{ \frac{\alpha_{\text{em}}}{4\pi} Q_\ell^2 \left[8 \left(1 + \ln \frac{m_\mu^2}{s_{\ell\bar{\ell}}} \right) \ln \left(\frac{\mu_c}{2\Delta E} \right) - 2 \left(2 + \ln \frac{m_\mu^2}{s_{\ell\bar{\ell}}} \right) \ln \frac{m_\mu^2}{s_{\ell\bar{\ell}}} - \frac{4}{3} \pi^2 - 8 \ln^2 \frac{\mu_b}{\mu_c} \right] \right\} \\ &= \exp \left\{ \frac{2\alpha_{\text{em}}}{\pi} Q_\ell^2 \left[\left(1 + \ln \frac{m_\mu^2}{m_{B_q}^2} \right) \ln \left(\frac{m_{B_q}}{2\Delta E} \right) \right. \right. \\ & \quad \left. \left. + 2 \ln \frac{m_{B_q}}{\mu_b} \ln \frac{\mu_b}{\mu_c} + \ln^2 \frac{m_{B_q}}{\mu_b} - \left(1 + \ln \frac{m_\mu}{\mu_c} \right) \ln \frac{m_\mu}{\mu_c} - \frac{\pi^2}{6} \right] \right\}. \end{aligned} \quad (7.13)$$

Notice that since (7.12) is given only in the one-loop and not the formal LL approximation, we use the double-logarithmic approximation (3.19) for $S_\ell(\mu_b, \mu_c)$, which gives the last term

in square brackets after the first equality. Within the same DL approximation, all terms in the last line should be dropped, since they are at most single-logarithmic, given $\mu_c \sim m_\mu$, $\mu_b \sim m_{B_q}$. We also set $s_{\ell\bar{\ell}} = m_{B_q}^2$,¹² since the dependence of the RG evolution factors and ultrasoft function on the hard scale arises from the kinematic variables entering the cusp anomalous dimension, rather than from m_b quark mass factors. This allows us to rewrite (7.9) in the conventional form ($Q_\ell^2 = 1$)

$$\Gamma[B_q \rightarrow \mu^+ \mu^-](\Delta E) = \Gamma^{(0)}[B_q \rightarrow \mu^+ \mu^-] \left(\frac{2\Delta E}{m_{B_q}} \right)^{-\frac{2\alpha_{\text{em}}}{\pi} \left(1 + \ln \frac{m_\mu^2}{m_{B_q}^2} \right)}, \quad (7.14)$$

with the non-radiative decay width

$$\Gamma^{(0)}[B_q \rightarrow \mu^+ \mu^-] \equiv \frac{m_{B_q}}{8\pi} \beta_\mu \left(|A_{10} + A_9 + A_7|^2 + \beta_\mu^2 |A_9 + A_7|^2 \right). \quad (7.15)$$

The universal ultrasoft photon corrections, which depend on ΔE , are now explicitly factorized in the usual manner [19]. In [19] and other works based on Yennie-Frautschi-Suura exponentiation [48], the scale m_{B_q} in the base $2\Delta E/m_{B_q}$ of the exponential is obtained by extrapolating the cutoff of the point-like meson theory, which should be below Λ_{QCD} , to m_{B_q} . The EFT framework developed in this paper justifies this extrapolation in part, but it also shows that there are additional, structure-dependent double logarithms. In (7.14), these process-specific resummed leading-logarithmic QED corrections that depend on the soft/collinear and hard-collinear scales are included in the amplitudes $A_{9,10}$. The decay rate is then written as the product of the resummed non-radiative decay width $\Gamma^{(0)}[B_q \rightarrow \mu^+ \mu^-]$ and the exponentiated ultrasoft photon corrections. The SCET framework can in principle be systematically extended to cover next-to-leading and higher-order logarithms, as well as power corrections m_μ/m_{B_q} .

8 Numerical results

The framework of SCET allows for a systematic factorization and resummation of leading logarithmic QED and QCD corrections to the amplitude (7.7). In particular it allowed the identification of three resummed contributions:

- i) common virtual SCET_I and SCET_{II} QED corrections among the final-state leptons to the amplitudes \mathcal{A}_9 and \mathcal{A}_{10} between hard and soft/collinear scales in the Sudakov factor $e^{S_\ell(\mu_b, \mu_c)}$, which are combined with the contributions of ultrasoft photons at the level of the decay width in Section 7.2.
- ii) virtual SCET_I QED and QCD corrections to the power-enhanced amplitude \mathcal{A}_9 between the hard and hard-collinear scales given by the overall Sudakov factor $e^{S_q(\mu_b, \mu_{hc})}$ in (6.17).

¹²The dependence of $s_{\ell\bar{\ell}}$ on ΔE is a negligible power-suppressed effect.

- iii) virtual QED and QCD corrections within SCET_{II} between the hard-collinear and soft/collinear scales, for which the RG equation was used such as to arrange that the input of the nonperturbative quantities is required at the hard-collinear scale, avoiding in this way the necessity of QCD RG evolution below the hard-collinear scale, as explained Section 6.2. This part is given by the ω -dependent soft Sudakov factor $U_s^{\text{QED}}(\mu_{hc}, \mu_s; \omega)$ in (6.18) or the ω -independent version (6.19), which are both equivalent at the LL accuracy.

We will start with the impact of points *ii*) and *iii*) on the power-enhanced amplitude \mathcal{A}_9 in Section 8.1 and turn to point *i*) afterwards in Section 8.2 when considering the branching fraction of $B_q \rightarrow \mu^+ \mu^-$.

Throughout α_s and α_{em} denote the running couplings in the $\overline{\text{MS}}$ scheme with RGEs given in Appendix A.3. We use as initial value $\alpha_s(m_Z) = 0.1181$, with $m_Z = 91.1876$ GeV and number of quark flavours $n_f = 5$, and perform the running with the four-loop expressions, including threshold corrections from quark masses ($\overline{\text{MS}}$ scheme) at the threshold crossings at $\mu_4 = \mu_b$ ($n_f = 4$) and $\mu_3 = 1.2$ GeV ($n_f = 3$). The RGEs for the hard function in SCET_I (3.16) and the matrix elements in SCET_{II} (6.12)–(6.13) had been solved to LL accuracy. In the numerical evaluation we will use values of α_{em} at the typical scales of SCET_I and SCET_{II}. For this purpose, we use as initial value $1/\alpha_{\text{em}}(m_Z) = 127.955$, and perform the RG evolution to lower scales with the one-loop expression. In addition to the quark thresholds given above, the τ -lepton is decoupled at its mass $\mu_\tau \approx 1.777$ GeV.

8.1 Resummation effects for power-enhanced amplitude

The resummation of virtual QED and QCD corrections in SCET_I to \mathcal{A}_9 in (6.17) is given by the overall Sudakov factor $e^{S_q(\mu_b, \mu_{hc})}$ from (3.20). Evaluating this factor thus provides a direct measure of the size of these corrections compared to the fixed-order result (1.1).

We calculate the Sudakov factor via numerical integration of the part of (3.15) which contains Q_q , i.e. that corresponds to $e^{S_q(\mu_b, \mu_{hc})}$. The numerical integration includes the scale dependence and threshold crossings of both gauge couplings. Since the μ_{hc} dependence of the Sudakov factor is cancelled in large parts by the one of the B -meson LCDA $\phi_+(\omega; \mu_{hc})$, which in turn is mainly driven by the scale dependence of its first inverse moment $\lambda_B(\mu_{hc})$,

$$\frac{1}{\lambda_B(\mu)} \equiv \int_0^\infty \frac{d\omega}{\omega} \phi_+(\omega; \mu), \quad (8.1)$$

the relevance of resummation is better assessed by multiplying $e^{S_q(\mu_b, \mu_{hc})}$ with the ratio $\lambda_B(\mu_0)/\lambda_B(\mu_{hc})$, where $\mu_0 = 1$ GeV is a fixed reference scale. The μ_{hc} dependence of $\lambda_B(\mu_{hc})$ due to QCD is approximated following [45], using as numerical inputs $\lambda_B(\mu_0)$ and $\sigma_1(\mu_0)$ given in Table 3 below.

The numerical impact of the resummation in SCET_I is a suppression of the fixed-order result of \mathcal{A}_9 by about 20% as tabulated in the second column of Table 2. The dependence on μ_{hc} is also shown in Figure 5 (solid line), where it reaches a maximal value of about 0.82 around $\mu_{hc} \approx 1.2$ GeV. In the relevant hard-collinear scale range $\mu_{hc} \in [1, 2]$ GeV, the scale

μ_{hc}	$\frac{\lambda_B(\mu_0)}{\lambda_B(\mu_{hc})} e^{S_q(\mu_b, \mu_{hc})}$		$e^{S_q(\mu_b, \mu_{hc})}$	α_s	$1/\alpha_{\text{em}}$
[GeV]	QCD+QED	only QCD	QCD+QED		
1.0	0.815	0.817	0.815	0.474	134.05
1.5	0.815	0.817	0.904	0.350	133.65
2.0	0.769	0.769	0.946	0.302	133.29

Table 2: The size of the SCET_I Sudakov factor for fixed $\mu_b = 5.0$ GeV and three different choices of μ_{hc} . The columns “only QCD” show the effect when setting $\alpha_{\text{em}} = 0$ in the cusp anomalous dimensions in (3.15). For convenience we provide α_s and $1/\alpha_{\text{em}}$ ($\overline{\text{MS}}$ scheme) at the scale μ_{hc} .

variation is relatively small. Note that for $\mu_{hc} < 1$ GeV the strong coupling α_s increases rapidly, reaching for example $\alpha_s \approx 0.75$ at $\mu_{hc} \approx 0.7$ GeV, such that the perturbative evaluation becomes unreliable. As expected, the Sudakov factor itself has a larger μ_{hc} dependence, varying in the larger range (0.80 – 0.95), as listed in the fourth column of Table 2 and shown in Figure 5 (dashed line). The resummation effect is by far dominated by the QCD evolution as is evident from comparing the columns “QCD+QED” and “only QCD”. The difference of both implies that the resummation of only QED effects yields tiny suppression of (0.1 – 0.3)% in agreement with the natural expectation of the size of a logarithmically enhanced QED correction $Q_q Q_\ell \times \alpha_{\text{em}}/\pi \times \ln^2(\mu_b/\mu_{hc}) \sim 0.2\%$.

The residual dependence on μ_{hc} displayed by the results in Table 2 appears due to the missing next-to-leading logarithmic corrections, as well as the approximation made to compute the scale-dependence of λ_B . In addition, the QED correction in (6.17) depends also on the first logarithmic moment of the LCDA,

$$\frac{\sigma_1(\mu)}{\lambda_B(\mu)} \equiv \int_0^\infty \frac{d\omega}{\omega} \ln\left(\frac{\mu_0}{\omega}\right) \phi_+(\omega; \mu), \quad (8.2)$$

where the latter involves the reference scale $\mu_0 = 1$ GeV. The scale dependence due to σ_1 is not captured by the results in Table 2. Further, a small residual QED μ_{hc} -dependence is compensated by the SCET_{II} QED evolution $U_s^{\text{QED}}(\mu_{hc}, \mu_s; \omega)$ in (6.17).

Turning to point *iii*), we recall that the resummation of virtual QED and QCD corrections in SCET_{II} to \mathcal{A}_9 has been organized in (6.17) such that the nonperturbative input to the B -meson LCDA is required at the scale μ_{hc} to avoid QCD evolution below μ_{hc} . The resummation of QED effects from the soft/collinear to the hard-collinear scales are contained in the Sudakov factor B -meson LCDA momentum-fraction dependent factor $U_s^{\text{QED}}(\mu_{hc}, \mu_s; \omega)$ given in (6.18) or the LL-equivalent momentum-fraction independent version (6.19).

To estimate the effect of QED resummation in SCET_{II}, we use the simple exponential model for the LCDA (see e.g. [40])

$$\phi_+(\omega) = \frac{\omega}{\omega_0^2} e^{-\omega/\omega_0}, \quad (8.3)$$

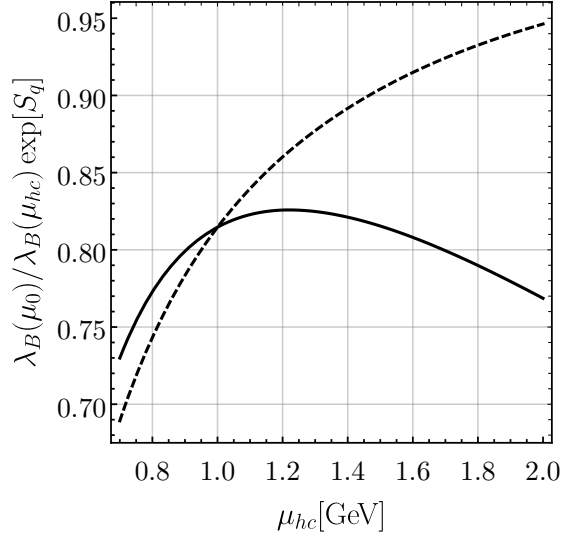


Figure 5: The SCET_I Sudakov factor $\frac{\lambda_B(\mu_0)}{\lambda_B(\mu_{hc})} e^{S_q(\mu_b, \mu_{hc})}$ (solid) and $e^{S_q(\mu_b, \mu_{hc})}$ (dashed).

where $\omega_0 = \lambda_B$ and evaluate the ratio of the amplitude (6.17) with the evolution factor to the amplitude without it,

$$r_\omega \equiv \frac{\int_0^\infty \frac{d\omega}{\omega} U_s^{\text{QED}}(\mu_{hc}, \mu_s; \omega) \phi_+(\omega) \left[\ln \frac{\omega m_{B_q}}{m_\ell^2} - 1 \right]}{\int_0^\infty \frac{d\omega}{\omega} \phi_+(\omega) \left[\ln \frac{\omega m_{B_q}}{m_\ell^2} - 1 \right]}. \quad (8.4)$$

For simplicity we assumed that C_9^{eff} is constant. On the other hand, if we use the ω -independent and equally valid expression (6.19) for the evolution factor, we simply obtain $r = U_s^{\text{QED}}(\mu_{hc}, \mu_s)$, independent of the form of the B -meson LCDA. Evaluation of (8.4) results in very small deviations of r_ω from unity. For $\mu_s = \lambda_B$ and $\mu_{hc} = 1$ GeV, the r_ω is a unity minus $(1 - 3)\%$ depending on the value of λ_B . For $\mu_{hc} = 2$ GeV, the r_ω differs from unity by about $(3 - 5)\%$. The simpler expression r agrees with these deviations from unity within about 25%, independent of whether one uses the LL or the DL versions of (6.18) and (6.19). We conclude that the numerical impact of the resummation of QED corrections in SCET_{II} compared to the fixed-order result is very small. As reference value we quote $U_s^{\text{QED}}(\mu_{hc}, \mu_s) = 1 - 0.0015$ at $\mu_{hc} = 1$ GeV for $\lambda_B = 275$ MeV.

In summary, the discussion of points *ii*) and *iii*) has shown that the main numerical effect of resummation on the power-enhanced amplitude \mathcal{A}_9 comes from the resummation of QCD corrections in SCET_I together with QCD running of the LCDA, constituting an overall suppression factor

$$S_9 \equiv \frac{\lambda_B(\mu_0)}{\lambda_B(\mu_{hc})} e^{S_q(\mu_b, \mu_{hc})} \in [0.77, 0.82], \quad (8.5)$$

that leads to a reduction of \mathcal{A}_9 of about 20%, whereas SCET_{II} QED resummation from (6.18) can be safely neglected in (6.17). Thus, from the phenomenological perspective it is

justified to consider only QCD resummation on top of the one-loop QED correction, once the leptonic Sudakov factor $e^{S_\ell(\mu_b, \mu_c)}$ is extracted, see point *i*).

This observation allows us to give a result for the \mathcal{A}_7 amplitude including QCD resummation, while the combined QCD and QED resummation is not yet feasible. Indeed, the endpoint divergences, which spoil the factorization of the \mathcal{A}_7 amplitude are only related to the QED effects.¹³ From the QCD perspective, the problem is equivalent to resummation for the heavy-to-light tensor current instead of the (axial-) vector current relevant to \mathcal{A}_9 . This implies that the QCD cusp anomalous dimension is the same as in the \mathcal{A}_9 case¹⁴ and accordingly the leading-logarithmic Sudakov factors are equal, $S_7 = S_9$. The result is then a uniform reduction of the power-enhanced QED correction “ $\mathcal{A}_9 + \mathcal{A}_7$ ” relative to the fixed-order result [21].

8.2 Branching fractions $B_q \rightarrow \mu^+ \mu^-$

We first provide the so-called non-radiative branching fraction for $B_q \rightarrow \mu^+ \mu^-$ that is found from the non-radiative decay width (7.15) as

$$\overline{\text{Br}}_{q\mu}^{(0)} \equiv \frac{\Gamma^{(0)}[B_q \rightarrow \mu^+ \mu^-]}{\Gamma_q^{\text{tot}}}. \quad (8.6)$$

For the B_d meson the total decay width Γ_d^{tot} is given in by the average width of the light and heavy B_d mass eigenstates. In case of the B_s meson the large decay-width difference requires a time-integration that can be accounted for by using instead of Γ_s^{tot} the decay width Γ_s^H of the heavy B_s -mass eigenstate [50]. According to the results of Section 8.1, the non-radiative part of the amplitude (7.7) is

$$A_{10} [\bar{u}_c \gamma_5 v_{\bar{c}}] + (S_9 A_9^{\text{fix}} + S_7 A_7^{\text{fix}}) [\bar{u}_c (1 + \gamma_5) v_{\bar{c}}], \quad (8.7)$$

where the numerically relevant resummation is now factored out explicitly as $S_{7,9}$ from the one-loop QED amplitudes $A_{7,9}^{\text{fix}}$, which were found in [21], see (1.1). We have added the fixed-order result of A_7^{fix} in the numerical analysis and keep S_7 separately, although at leading logarithmic order in QCD $S_7 = S_9$ as mentioned above.

The non-radiative time-integrated branching fraction of $B_s \rightarrow \mu^+ \mu^-$ for central values of the parameters collected in Table 3 and using the $N_f = 2 + 1 + 1$ lattice result of f_{B_s} is

$$\begin{aligned} \overline{\text{Br}}_{s\mu}^{(0)} &= 3.677 \cdot 10^{-9} \times \left(1 + \frac{\text{GeV}}{10^3 \cdot \lambda_B} [S_9 (-6.46 + 1.27\sigma_1) + S_7 (4.74 - 1.54\sigma_1 + 0.15\sigma_2)] \right) \\ &= 3.677 \cdot 10^{-9} \times (1 - 0.0166 S_9 + 0.0105 S_7) = 3.660 \cdot 10^{-9}. \end{aligned} \quad (8.8)$$

¹³ The operator basis for the amplitude \mathcal{A}_7 is more complicated than for \mathcal{A}_9 , see Appendix B, but one can prove that additional soft, collinear and hard-collinear fields that enter the SCET_I and SCET_{II} operators relevant to \mathcal{A}_7 do not carry color charge.

¹⁴ The non-cusp QCD anomalous dimensions are different for \mathcal{A}_9 and \mathcal{A}_7 , due to different Dirac structure and normalization, but in principle next-to-leading logarithmic resummation of QCD effects could be performed as well for both amplitudes, see for example [49].

Parameter	Value	Ref.	Parameter	Value	Ref.
G_F	$1.166379 \cdot 10^{-5} \text{ GeV}^{-2}$	[51]	m_Z	91.1876(21) GeV	[51]
$\alpha_s^{(5)}(m_Z)$	0.1181(11)	[51]	m_μ	105.658... MeV	[51]
$\alpha_{\text{em}}^{(5)}(m_Z)$	1/127.955(10)	[51]	m_t	173.1(6) GeV	[51]
m_{B_s}	5366.89(19) MeV	[51]	m_{B_d}	5279.63(15) MeV	[51]
$f_{B_s} _{N_f=2+1}$	228.4(3.7) MeV	[52]	$f_{B_d} _{N_f=2+1}$	192.0(4.3) MeV	[52]
$f_{B_s} _{N_f=2+1+1}$	230.3(1.3) MeV	[52]	$f_{B_d} _{N_f=2+1+1}$	190.0(1.3) MeV	[52]
$1/\Gamma_H^s$	1.615(9) ps	[53]	$2/(\Gamma_H^d + \Gamma_L^d)$	1.520(4) ps	[53]
$ V_{cb} _{\text{incl}}$	0.04200(64)	[54]	$\lambda_B(\mu_0)$	275(75) MeV	[45]
$ V_{tb}V_{ts}^*/V_{cb} $	0.982(1)	[55, 56]	$\sigma_1(\mu_0)$	1.5(1.0)	[45]
$ V_{tb}V_{td}^* $	0.0087(2)	[55, 56]	$\sigma_2(\mu_0)$	3(2)	[45]
$V_{ub}V_{ud}^*/V_{tb}V_{td}^*$	0.018 - i 0.414	[55, 56]			

Table 3: Numerical input values for parameters: Note that $\alpha_{\text{em}}^{(5)}(m_Z)$ has been determined with $\alpha_s^{(5)}(m_Z) = 0.1187(16)$ in [51] and the corresponding $\Delta\alpha_{\text{em,hadr}}^{(5)}(m_Z) = 0.02764(7)$. The B -meson decay constants are averages from the FLAG group for $N_f = 2 + 1$ from [57–61] and for $N_f = 2 + 1 + 1$ from [2, 62–64]. The $B_{s,d}$ lifetimes are prepared by HFLAV for the PDG 2018 review [51]. The same numerical values of λ_B and $\sigma_{1,2}$ at the reference scale $\mu_0 = 1 \text{ GeV}$ are used for B_s and B_d mesons. The values of the Wilson coefficients at $\mu_b = 5.0 \text{ GeV}$ are $C_{1-6} = \{-0.25, 1.01, -0.005, -0.077, 0.0003, 0.0009\}$, $C_7^{\text{eff}} = -0.302$, $C_9 = 4.344$ and $C_{10} = -4.198$ from [21].

In the first line we keep the B -meson LCDA parameters and the Sudakov factors unevaluated. The second line shows that \mathcal{A}_9 interferes destructively with \mathcal{A}_{10} whereas \mathcal{A}_7 interferes constructively. The separate contributions to the branching fraction due to \mathcal{A}_9 and \mathcal{A}_7 are rather large, about $-1.7 S_9 \%$ and $+1.0 S_7 \%$ as found previously [21]. Both contributions cancel in part and lead to an overall reduction of the branching fraction of 0.5%, when accounting for the Sudakov factor $S_9 \approx S_7 \approx 0.8$. The non-radiative branching fraction of $B_d \rightarrow \mu^+ \mu^-$ for central values of the parameters is

$$\begin{aligned}
\overline{\text{Br}}_{d\mu}^{(0)} &= 1.031 \cdot 10^{-10} \times \left(1 + \frac{\text{GeV}}{10^3 \cdot \lambda_B} [S_9 (-6.04 + 1.18\sigma_1) + S_7 (4.67 - 1.51\sigma_1 + 0.15\sigma_2)] \right) \\
&= 1.031 \cdot 10^{-10} \times (1 - 0.0155 S_9 + 0.0103 S_7) = 1.027 \cdot 10^{-10}.
\end{aligned} \tag{8.9}$$

The numerical difference between B_s and B_d decays for the contribution proportional to S_9 is due to the terms proportional to the CKM factor $V_{ub}V_{uq}^*$ in (3.10).

Let us for completeness provide also a detailed error budget of the non-radiative branch-

ing fractions $B_q \rightarrow \mu^+ \mu^-$. We find

$$\begin{aligned} \overline{\text{Br}}_{s\mu}^{(0)} = & \begin{pmatrix} 3.599 \\ 3.660 \end{pmatrix} \left[1 + \begin{pmatrix} 0.032 \\ 0.011 \end{pmatrix}_{f_{B_s}} + 0.031|_{\text{CKM}} + 0.011|_{m_t} \right. \\ & \left. + 0.006|_{\text{pmr}} + 0.012|_{\text{non-pmr}} \begin{smallmatrix} +0.003 \\ -0.005 \end{smallmatrix} |_{\text{LCDA}} \right] \cdot 10^{-9}, \end{aligned} \quad (8.10)$$

$$\begin{aligned} \overline{\text{Br}}_{d\mu}^{(0)} = & \begin{pmatrix} 1.049 \\ 1.027 \end{pmatrix} \left[1 + \begin{pmatrix} 0.045 \\ 0.014 \end{pmatrix}_{f_{B_d}} + 0.046|_{\text{CKM}} + 0.011|_{m_t} \right. \\ & \left. + 0.003|_{\text{pmr}} + 0.012|_{\text{non-pmr}} \begin{smallmatrix} +0.003 \\ -0.005 \end{smallmatrix} |_{\text{LCDA}} \right] \cdot 10^{-10}, \end{aligned} \quad (8.11)$$

where we group uncertainties as follows:

- i)* main parametric long-distance (f_{B_q}) and short-distance (CKM and m_t);
- ii)* remaining non-QED parametric (Γ_q , α_s) and non-QED non-parametric (μ_W , μ_b and higher order, see [4]);
- iii)* from the B -meson LCDA parameters λ_B and $\sigma_{1,2}$ entering the power-enhanced QED correction.

We provide two values of the branching fraction depending on the choice of the lattice calculation of f_{B_q} for $N_f = 2 + 1$ (upper) and $N_f = 2 + 1 + 1$ (lower), employing averages from FLAG 2019 [52]. Note that the small uncertainties of the $N_f = 2 + 1 + 1$ results are currently dominated by a single group [2] and confirmation by other lattice groups in the future is desirable. It can be observed that in this case the largest uncertainties are due to CKM parameters, such that in principle they can be determined, provided the experimental accuracy of the measurements is at the one-percent level. Still fairly large errors are due to the top-quark mass $m_t = (173.1 \pm 0.6)$ GeV, here assumed to be in the pole scheme [4], where an additional non-parametric uncertainty of 0.2% is included (in “non-pmr”) for the conversion to the $\overline{\text{MS}}$ scheme as in [4]. Further “non-pmr” contains a 0.4% uncertainty from μ_W variation and 0.5% further higher order uncertainty, all linearly added, see also [4].

The radiative $B_q \rightarrow \mu^+ \mu^-$ branching fraction including ultrasoft radiation with total energy $E_{X_s} < \Delta E$ is obtained from (7.15) and (8.6) as

$$\overline{\text{Br}}_{q\mu}(\Delta E) \equiv \overline{\text{Br}}_{q\mu}^{(0)} \times \Omega(\Delta E; \alpha_{\text{em}}), \quad (8.12)$$

with radiative factor

$$\Omega(\Delta E; \alpha_{\text{em}}) \equiv \left(\frac{2\Delta E}{m_{B_q}} \right)^{-\frac{2\alpha_{\text{em}}}{\pi}} \left(1 + \ln \frac{m_\mu^2}{m_{B_q}^2} \right) \quad (8.13)$$

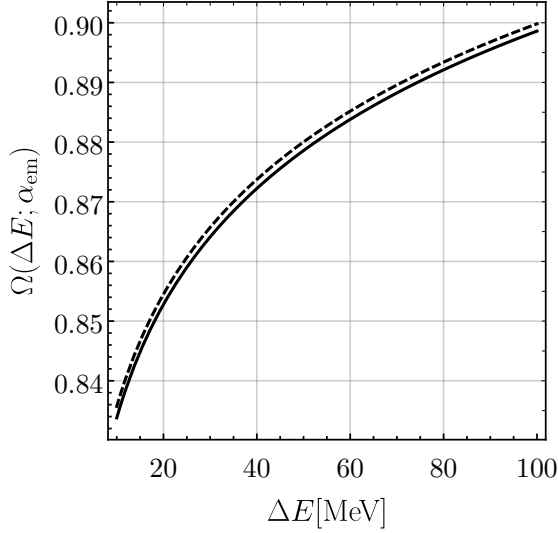


Figure 6: The radiative factor in (8.13) for $B_s \rightarrow \mu^+ \mu^-$ in the range $\Delta E \in [10, 100]$ MeV for the two values $\alpha_{\text{em}}^{-1} = 134.28$ (solid) and $\alpha_{\text{em}}^{-1} = 136.0$ (dashed).

from (7.14). ΔE corresponds to a window in the dilepton invariant mass $s_{\ell\bar{\ell}} = (p_\ell + p_{\bar{\ell}})^2$ around $s_{\ell\bar{\ell}} = m_{B_q}^2$ defining the signal region in the experimental analysis for which our effective theory framework is set up. The dependence of the radiative factor Ω on $\Delta E = (m_{B_q}^2 - s_{\ell\bar{\ell}})^{1/2}$ is shown in Figure 6 for B_s mesons. One might consider $\Delta E \simeq 60$ MeV as an example of a larger value for the theory framework that requires $\Delta E \ll \Lambda_{\text{QCD}}$. In this case the signal window contains about 88% of the non-radiative rate, whereas for example the smaller signal window with $\Delta E \simeq 10$ MeV still contains 84%. The sizes of the signal windows in the first LHCb [12, 65] and CMS [13] analyses of $B_s \rightarrow \mu^+ \mu^-$ were about $\Delta E \simeq \pm 60$ MeV and $\Delta E \simeq {}^{+83}_{-67}$ MeV around m_{B_s} , respectively.¹⁵ In comparison, the experimental resolution in the dilepton-invariant mass is reported to be about 25 MeV in LHCb and depending on the muon direction about (32 – 75) MeV in CMS. More recent experimental analyses do not use signal windows, but rather fit the modelled signal components of $B_s \rightarrow \mu^+ \mu^-$ and $B_d \rightarrow \mu^+ \mu^-$ simultaneously with background components over a wide range of $s_{\ell\bar{\ell}}$. The modelling of the components involves also the simulation of photon radiation with the help of PHOTOS [18]. We note that the systematic framework developed in this work makes is advantageous to compare experimental data in a signal window to corresponding theoretical predictions without the need for extrapolations.

Finally, we point out that the dependence on the value of α_{em} in the exponent of $\Omega(\Delta E; \alpha_{\text{em}})$ slightly changes the value of the radiative factor. The associated parametric

¹⁵ In the experimental analysis the signal window extends also above the upper boundary $(s_{\ell\bar{\ell}})_{\text{max}} = m_{B_q}^2$ of the phase space for $B_q \rightarrow \ell^+ \ell^- + n\gamma$ due to resolution effects in the reconstruction of $s_{\ell\bar{\ell}}$.

uncertainty for $\Delta E = 60$ MeV and the two values $\alpha_{\text{em}}^{-1} = \{134.28, 136.0\}$

$$\Omega(60 \text{ MeV}; \alpha_{\text{em}}) = \begin{cases} \{0.8838, 0.8852\} & \text{for } B_s \\ \{0.8848, 0.8862\} & \text{for } B_d \end{cases} \quad (8.14)$$

amounts to less than 0.2% for the two choices of α_{em} . The first choice corresponds to $\alpha_{\text{em}}(1.0 \text{ GeV})$, whereas $1/\alpha_{\text{em}}(\mu_c) = 136.0$ represents the running at one-loop to the muon mass scale, spanning a range of values that covers the renormalization scheme dependence of α_{em} . This uncertainty is comparable to the parametric QED uncertainties due to the B -meson LCDA parameters in (8.10) and (8.11). It must be added when comparing the predictions of $\overline{\text{Br}}_{q\mu}(\Delta E)$ with measurements, i.e. it must be accounted for when extracting the non-radiative rate by experiments.

8.3 Rate asymmetries in $B_q \rightarrow \mu^+ \mu^-$

The decay of neutral B_q mesons into a muon pair $\mu_\lambda^+ \mu_{\bar{\lambda}}^-$ in a helicity configuration $\lambda = L, R$ allows to investigate further observables in measurements of its time-dependent rate asymmetry

$$\frac{\Gamma[B_q(t) \rightarrow \mu_\lambda^+ \mu_{\bar{\lambda}}^-] - \Gamma[\overline{B}_q(t) \rightarrow \mu_\lambda^+ \mu_{\bar{\lambda}}^-]}{\Gamma[B_q(t) \rightarrow \mu_\lambda^+ \mu_{\bar{\lambda}}^-] + \Gamma[\overline{B}_q(t) \rightarrow \mu_\lambda^+ \mu_{\bar{\lambda}}^-]} = \frac{C_q^\lambda \cos(\Delta m_{B_q} t) + S_q^\lambda \sin(\Delta m_{B_q} t)}{\cosh(y_q t / \tau_{B_q}) + A_q^\lambda \sinh(y_q t / \tau_{B_q})}, \quad (8.15)$$

provided the initial flavour of the B_q is tagged. The decay-width difference $\Delta\Gamma_q$ enters via $y_q = \tau_{B_q} \Delta\Gamma_q / 2$, which is rather sizeable for the B_s system, $y_s = 0.066 \pm 0.004$ [51], but can be neglected for the B_d system $y_d \lesssim 0.005$ [51]. We refer to [50] for definitions and further details.

The three observables are related by $|C_q^\lambda|^2 + |S_q^\lambda|^2 + |A_q^\lambda|^2 = 1$. Note that a muon pair $\mu_\lambda^+ \mu_{\bar{\lambda}}^-$ with definite helicity $\lambda = L, R$ is not a CP eigenstate, but both are related under CP transformation as $CP(|\mu_L^+ \mu_L^- \rangle) = e^{i\delta_{CP}(\mu^+ \mu^-)} |\mu_R^+ \mu_R^- \rangle$ with a convention-dependent phase $\delta_{CP}(\mu^+ \mu^-)$. Thus the observables C_q^λ , S_q^λ and A_q^λ are not CP asymmetries. The SM predictions based on the LO QED amplitude \mathcal{A}_{10} alone lead to vanishing $C_q^\lambda = S_q^\lambda = 0$. The mass-eigenstate rate asymmetry $A_q^\lambda = 1$ because only the heavier B_q mass-eigenstate can decay into leptons. The NLO QED amplitude \mathcal{A}_9 contains in addition to the dominant amplitude involving $V_{tb} V_{tq}^*$ the term proportional to the CKM element product $V_{ub} V_{uq}^*$, and hence a second weak (CP-violating) phase, as well as scattering (CP-conserving) phases through C_9^{eff} in (3.10), potentially changing these predictions. For the future it is important to know at which level QED corrections in the SM induce a deviation from $C_q^\lambda = S_q^\lambda = 0$ and $A_q^\lambda = 1$ to disentangle them from new physics effects.

The suppression factors α_{em} and $(V_{ub} V_{uq}^*) / (V_{tb} V_{tq}^*)$ in \mathcal{A}_9 suggest that the deviations from the LO SM predictions will be very small. Due to the presence of a scattering phase we must generalize the results of [50] that were based on the assumption of only additional weak phases. The muon-helicity dependent observables are given as

$$C_q^\lambda = \frac{1 - |\xi_q^\lambda|^2}{1 + |\xi_q^\lambda|^2}, \quad S_q^\lambda = \frac{2 \text{Im } \xi_q^\lambda}{1 + |\xi_q^\lambda|^2}, \quad A_q^\lambda = \frac{2 \text{Re } \xi_q^\lambda}{1 + |\xi_q^\lambda|^2}, \quad (8.16)$$

where

$$\xi_q^\lambda = -\frac{S + \eta_\lambda P}{\bar{S} - \eta_\lambda \bar{P}}, \quad \text{with} \quad \eta_{L/R} = \pm 1. \quad (8.17)$$

The barred quantities $\bar{P} = P[\varphi_W \rightarrow -\varphi_W]$ and $\bar{S} = S[\varphi_W \rightarrow -\varphi_W]$ are obtained from the unbarred ones after reverting the signs of all CP-violating phases φ_W . We introduced here

$$P = \frac{A_{10} + A_9 + A_7}{m_\ell m_{B_q} f_{B_q} \mathcal{N}}, \quad S = \beta_\mu \frac{A_9 + A_7}{m_\ell m_{B_q} f_{B_q} \mathcal{N}}. \quad (8.18)$$

The generalized expressions (8.16) in terms of P , \bar{P} and S , \bar{S} can be derived straightforwardly. We find

$$C_q^\lambda = \frac{\bar{B}_\lambda - B_\lambda}{\bar{B}_\lambda + B_\lambda}, \quad S_q^\lambda = \frac{2 \operatorname{Im} \tilde{B}_\lambda}{\bar{B}_\lambda + B_\lambda}, \quad A_q^\lambda = \frac{2 \operatorname{Re} \tilde{B}_\lambda}{\bar{B}_\lambda + B_\lambda}, \quad (8.19)$$

where

$$B_\lambda = |P|^2 + |S|^2 + \eta_\lambda (PS^* + SP^*), \quad (8.20)$$

$$\bar{B}_\lambda = |\bar{P}|^2 + |\bar{S}|^2 - \eta_\lambda (\bar{P}\bar{S}^* + \bar{S}\bar{P}^*), \quad (8.21)$$

$$\tilde{B}_\lambda = P\bar{P}^* - S\bar{S}^* + \eta_\lambda (S\bar{P}^* - P\bar{S}^*). \quad (8.22)$$

The linear combinations $C_q \equiv \frac{1}{2}(C_q^L + C_q^R)$ and $S_q \equiv \frac{1}{2}(S_q^L + S_q^R)$ are CP-odd, while $\Delta C_q \equiv \frac{1}{2}(C_q^L - C_q^R)$ and $\Delta S_q \equiv \frac{1}{2}(S_q^L - S_q^R)$ are CP-even quantities, see for example the related discussion [66] on time-dependent rates in the $B^0 \rightarrow \pi^\mp \rho^\pm$ systems.

The assumption of only weak phases implies $\bar{P} = P^*$ and $\bar{S} = S^*$, and leads to significant simplifications as shown in [50]. In the following we do not make this general assumption, but we use that the amplitudes A_{10} and A_7 are real within the approximations adopted in this paper, i.e. do not contain neither weak nor scattering phases, and further that the amplitudes $A_{7,9} \ll A_{10}$ are suppressed by a factor α_{em} . The expansion in α_{em} yields

$$\begin{aligned} C_q^\lambda &= -\frac{\operatorname{Re}[A_9 - \bar{A}_9 + \eta_\lambda(2A_7 + A_9 + \bar{A}_9)]}{A_{10}}, \\ S_q^\lambda &= \frac{\operatorname{Im}[A_9 - \bar{A}_9 + \eta_\lambda(A_9 + \bar{A}_9)]}{A_{10}}, \\ A_q^\lambda &= 1 - \frac{2(A_7)^2 + (1 + \eta_\lambda)|A_9|^2 + (1 - \eta_\lambda)|\bar{A}_9|^2 + 2A_7 \operatorname{Re}[(1 + \eta_\lambda)A_9 + (1 - \eta_\lambda)\bar{A}_9]}{(A_{10})^2}, \end{aligned} \quad (8.23)$$

where we further use $\beta_\mu \approx 1$ in S , which is numerically well justified for muons. Note that for A_q^λ the first non-vanishing deviation from unity appears only at $\mathcal{O}(\alpha_{\text{em}}^2)$.

The expressions show that in the absence of a weak phase difference (i.e. when $\bar{A}_9 = A_9$), the QED corrections imply a modification of the observables

$$C_q^\lambda = -\eta_\lambda \frac{2 \operatorname{Re}[A_7 + A_9]}{A_{10}}, \quad S_q^\lambda = \eta_\lambda \frac{2 \operatorname{Im}[A_7 + A_9]}{A_{10}}, \quad A_q^\lambda = 1 - 2 \frac{|A_7 + A_9|^2}{(A_{10})^2}. \quad (8.24)$$

from their naive values 0, 0, 1. We added $\text{Im } A_7 = 0$ in the numerator of S_q^λ to make the result appear in line with C_q^λ and A_q^λ . As expected, the CP-odd observables C_q , S_q vanish, since there is no CP-violating phase, while $\Delta C_q = C_q^L$, $\Delta S_q = S_q^L$ are non-zero though small. C_q^λ and S_q^λ still depend on the muons' helicity through η_λ , whereas A_q^λ becomes independent on the helicity. The expressions (8.24) are very good approximations for the case of B_s mesons, where the $V_{ub}V_{us}^*$ term in the amplitude is negligible due to the strong suppression $|(V_{ub}V_{us}^*)/(V_{tb}V_{ts}^*)| \lesssim 0.005$ in (3.10). In consequence [21]¹⁶

$$C_s^\lambda = +\eta_\lambda 0.6\%, \quad S_s^\lambda = -\eta_\lambda 0.1\%, \quad A_s = 1 - 2.0 \cdot 10^{-5}. \quad (8.25)$$

While the first measurement of $A_s = 8.2 \pm 10.7$ from LHCb [16] suffers from huge errors, a future deviation from the SM prediction $A_s = 1$ at LO in QED can be safely attributed to non-standard effects in view of the tiny QED contributions.

On the other hand, for the B_d system the expressions (8.23) must be used. Here the weak phase in $(V_{ub}V_{ud}^*)/(V_{tb}V_{td}^*)$ leads to differences among the two helicities, and we therefore provide

$$\begin{aligned} C_d &= -0.08\%, \quad S_d = +0.03\%, \quad A_d^L = 1 - 1.4 \cdot 10^{-5}, \\ \Delta C_d &= +0.60\%, \quad \Delta S_d = -0.13\%, \quad A_d^R = 1 - 2.4 \cdot 10^{-5}. \end{aligned} \quad (8.26)$$

We find similar magnitudes as for the B_s system, but non-vanishing CP asymmetries C_d and S_d , which are suppressed by a factor of a few compared to the CP-conserving quantities ΔC_d , ΔS_d .

In summary we find tiny contributions from the power-enhanced NLO QED amplitudes $\mathcal{A}_{7,9}$ to the rate asymmetries in $B_q \rightarrow \mu^+\mu^-$ decays, leaving these observables as “null tests” at the percent level of the SM. The generated CP asymmetries in $B_d \rightarrow \mu^+\mu^-$ are about $C_d, S_d \approx -0.1\%$ and are strongly suppressed in $B_s \rightarrow \mu^+\mu^-$. Note that there are other, even smaller higher-order corrections to the rate asymmetries in the SM, such as for example neutral Higgs boson penguin diagrams, which give rise to higher-dimensional operators than dimension six at the electroweak scale, suppressed by $(m_b/m_W)^2 \sim 10^{-3}$.

9 Summary and conclusions

We have developed a systematic treatment of virtual and real QED effects for the power-enhanced QED contribution to $B_q \rightarrow \mu^+\mu^-$, previously reported in [21], for the case when the energy of undetected photons ΔE is small compared to the typical scale of the QCD binding energy and the muon mass. The treatment includes the resummation of large QED logarithms from various scales. The effects from the process-specific energy scales set by the external kinematics and internal dynamics of $B_q \rightarrow \mu^+\mu^-$ are factorized with the help of soft-collinear effective theory (SCET) starting at the hard scale of order of the B -meson mass m_{B_q} in a two-step matching. First hard fluctuations on the heavy meson mass scale are decoupled in the matching on SCET_I, and subsequently hard-collinear modes with virtuality $m_{B_q}\Lambda$ are decoupled in the matching onto SCET_{II}, which contains collinear

¹⁶ Note the missing factor η_λ in Eq. (20) of [21].

and soft degrees of freedom of order Λ . Finally we treat the remaining ultrasoft QED interactions in the limit of static heavy leptons.

Due to the double helicity and annihilation suppression of the $B_q \rightarrow \mu^+ \mu^-$ amplitude in the absence of QED corrections, the power-enhanced amplitude analyzed in this paper is actually an example of subleading-power resummation in SCET. The SCET framework allows us to resum the large QCD and QED logarithmic corrections systematically and reveals a lepton-mass induced operator mixing between so-called A-type and B-type SCET collinear operators as the origin of the leading logarithmic correction. We derive a SCET_{II} factorization theorem for the non-radiative amplitude, for the contributions due to the weak semileptonic operators Q_9 and Q_{10} . The formula includes “structure-dependent” logarithms beyond the standard Yennie-Frautschi-Suura (YFS) exponentiation. After squaring the amplitude, the result is organized such that the standard exponentiated logarithms are factorized and the process-specific terms are made explicit. We provide the relevant operator definitions, which facilitates the reuse of existing results within our formalism avoiding double-counting. We emphasize that the standard YFS approach contains the implicit assumption that the cutoff on virtual photon effects, which should be below the scale of the inverse size of the B -meson for the latter to be treated as point-like, can be raised to the B -meson mass scale. Our result justifies this procedure to a certain extent and gives a precise expression for the corrections to this extrapolation.

On the quantitative side, we performed the resummation at the leading-logarithmic level in both, the QCD and the QED coupling. We find that once the standard YFS exponent is extracted, the relevant effect comes from QCD logarithms. For practical purposes it is therefore sufficient to improve the previous one-loop QED calculation [21] by QCD logarithms, which results in an approximately 20% reduction of the power-enhanced amplitude. We updated the $B_{s,d} \rightarrow \mu^+ \mu^-$ branching fractions and provided an estimate of the present theoretical uncertainty. We also discussed various rate asymmetries, including CP violation at the permille level in the B_d decay mode that arises entirely from the power-enhanced QED correction. These results quantify the SM background to New Physics searches in what would be “null observables” in the absence of QED.

The derivation of the SCET_{II} factorization theorem shows the need of generalizing the concepts of the B -meson decay constant and light-cone distribution amplitudes (LCDA) in the presence of QED. We establish that even in very simple processes QED corrections are non-universal beyond the leading logarithmic approximation. The coupling of soft photons to final-state charged particles renders the B -meson matrix elements dependent on the soft Wilson lines, which carry information on the charge and direction of the final-state particles. Upon expansion in the QED coupling, this necessitates the inclusion of hadronic matrix elements, which are non-local time-ordered products. This has to be considered when these quantities are evaluated with nonperturbative methods, such as lattice gauge theory. The situation becomes even more complicated for exclusive semileptonic decays, where different process-dependent nonperturbative objects have to be defined for different phase-space regions. The number of nonperturbative objects will proliferate, as in this case it will also be necessary to include QED effects for the final-state hadrons.

Acknowledgements

This work is supported by the DFG Sonderforschungsbereich/Transregio 110 ‘‘Symmetries and the Emergence of Structure in QCD’’. The work of CB is supported by DFG under grant BO-4535/1-1.

A SCET conventions and results

Throughout we use the definitions

$$g_{\mu\nu}^\perp \equiv g_{\mu\nu} - \frac{n_+^\mu n_-^\nu}{2} - \frac{n_-^\mu n_+^\nu}{2}, \quad \varepsilon_{\mu\nu}^\perp \equiv \varepsilon_{\mu\nu\alpha\beta} \frac{n_+^\alpha n_-^\beta}{2}, \quad (\text{A.1})$$

and the convention $\varepsilon_{0123} = -1$ such that

$$\text{Tr}[\gamma_\mu \gamma_\nu \gamma_\alpha \gamma_\beta \gamma_5] = -4i\varepsilon_{\mu\nu\alpha\beta}, \quad \sigma_{\mu\nu} \gamma_5 = \frac{i}{2} \varepsilon_{\mu\nu\alpha\beta} \sigma^{\alpha\beta}. \quad (\text{A.2})$$

The running QCD and QED couplings in the $\overline{\text{MS}}$ scheme are denoted as α_s and α_{em} , respectively. They obey the RG equations

$$\frac{d\alpha_i}{d\ln\mu} = \beta_i(\alpha_s, \alpha_{\text{em}}) = -2\alpha_i \frac{\alpha_i}{4\pi} \beta_{0,i} + \mathcal{O}(\alpha_i^3), \quad i = (s, \text{em}), \quad (\text{A.3})$$

which decouple at the leading order. The one-loop contributions are

$$\beta_0 = \frac{11}{3}N_c - \frac{2}{3}n_f, \quad \beta_{0,\text{em}} = -\frac{4}{3} [N_c(n_u Q_u^2 + n_d Q_d^2) + n_\ell Q_\ell^2], \quad (\text{A.4})$$

where $N_c = 3$ and $n_f = n_u + n_d$ is the total number of active quark flavours. The separate up-type quark ($Q_u = +2/3$), down-type quark ($Q_d = -1/3$) and charged lepton ($Q_\ell = -1$) numbers are denoted as n_u , n_d and n_ℓ , respectively.

A.1 Lagrangians

The leading-power Lagrangian of a hard-collinear fermion f_C in SCET_I reads [67, 68]

$$\mathcal{L}_f^{(0)} = \bar{f}_C \left(in_- D_C + i \not{D}_{C\perp} \frac{1}{in_+ D_C} i \not{D}_{C\perp} \right) \frac{\not{n}_+}{2} f_C. \quad (\text{A.5})$$

The capital subscript C is used in SCET_I to denote collinear fields with hard-collinear and collinear scaling. The SCET_{II} fields with only collinear scaling carry index c . The field f_C represents either the light quark or the lepton fields in Table 1. The corresponding anti-hard-collinear field is denoted by $C \rightarrow \bar{C}$ and it’s Lagrangian obtained by the replacement $n_+ \leftrightarrow n_-$. The covariant derivatives are

$$in_- D = in_- \partial + eQ_f [n_- A_C + n_- A_s(x_-)] + g_s [n_- G_C + n_- G_s(x_-)], \quad (\text{A.6})$$

$$iD_C = i\partial + eQ_f A_C + g_s G_C, \quad (\text{A.7})$$

where A_μ and $G_\mu = G_\mu^A T^A$ denote the photon and gluon fields, respectively, and their subscripts C and s distinguish the hard-collinear and soft fields. The Q_f denotes the electric charge of f , whereas the generators of QCD for the fundamental representation are denoted as T^A . The QED and QCD coupling constants are $e = \sqrt{4\pi\alpha_{\text{em}}}$ and $g_s = \sqrt{4\pi\alpha_s}$, respectively. Fields without argument are taken at position x . For the soft fields, their multipole expansion in SCET_I interactions with collinear fields [68] is made explicit by the argument $x_\mp \equiv (n_\pm x) n_\mp/2$.

The operators in SCET_I have to be gauge-invariant under hard-collinear QED and QCD gauge transformations, which is achieved by combining f_C with appropriate Wilson lines of hard-collinear photons and gluons

$$W_{fC}(x) \equiv \exp \left[ie Q_f \int_{-\infty}^0 ds n_+ A_C(x + sn_+) \right], \quad (\text{A.8})$$

$$W_C(x) \equiv \mathcal{P} \exp \left[ig_s \int_{-\infty}^0 ds n_+ G_C(x + sn_+) \right], \quad (\text{A.9})$$

respectively. The Wilson lines W_{fC} in QED depend on the charge Q_f of f_C , whereas the QCD Wilson lines W_C involve the path-ordering operator \mathcal{P} . There are analogous anti-hard-collinear Wilson lines $W_{f\bar{C}}$ and $W_{\bar{C}}$, obtained by $n_+ \rightarrow n_-$. Depending on f_C , the following invariant building blocks under hard-collinear gauge transformations appear

$$\text{lepton :} \quad f_C = l_C \quad \rightarrow \quad \ell_C = W_{lC}^\dagger l_C, \quad (\text{A.10})$$

$$\text{quark :} \quad f_C = \xi_C \quad \rightarrow \quad \chi_C = [W_{\xi C} W_C]^\dagger \xi_C, \quad (\text{A.11})$$

with analogous building blocks for anti-hard-collinear leptons $\ell_{\bar{C}}$ and quarks $\chi_{\bar{C}}$ that involve $W_{f\bar{C}}$ and $W_{\bar{C}}$. The collinear fields in the main text refer to these collinear-gauge invariant fields including these collinear Wilson lines.

The leading-power Lagrangian of the soft light quark q_s with mass m_q and the heavy quark h_v

$$\mathcal{L}_s = \bar{q}_s(i\cancel{D}_s - m_q)q_s + \bar{h}_v(iv \cdot D_s)h_v \quad (\text{A.12})$$

contains the covariant derivative with soft gauge fields only. It is the same for SCET_I and SCET_{II}.

In addition we need the subleading SCET_I interaction involving both, the soft and hard-collinear light quarks [31]

$$\mathcal{L}_{\xi q}^{(1)} = \bar{q}_s(x_-) [W_{\xi C} W_C]^\dagger(x) i\cancel{D}_{C\perp} \xi_C(x) + \text{h.c.} \quad (\text{A.13})$$

and analogously for anti-hard-collinear fields with the replacements $C \rightarrow \bar{C}$, $n_+ \leftrightarrow n_-$ and $x_- \rightarrow x_+$. Further the mass-suppressed Lagrangian [69] for the hard-collinear leptons is needed

$$\mathcal{L}_m^{(1)} = m_\ell \bar{l}_C \left[i\cancel{D}_{C\perp}, \frac{1}{in_+ D_C} \right] \frac{\not{n}_+}{2} l_C. \quad (\text{A.14})$$

In SCET_I the hard-collinear and soft fields are decoupled at leading power by the field redefinitions [70]

$$f_C(x) = Y_{f+}(x_-)Y_{\text{QCD}+}(x_-)f_C^{(0)}(x), \quad f_{\bar{C}}(x) = Y_{f-}(x_+)Y_{\text{QCD}-}(x_+)f_{\bar{C}}^{(0)}(x), \quad (\text{A.15})$$

if f_C ($f_{\bar{C}}$) creates an outgoing antiparticle. If it destroys an incoming particle, \bar{Y} instead of Y is used. Here the QED Wilson lines with soft gauge fields are defined as follows:

$$\text{outgoing particles:} \quad Y_{f\pm}^\dagger(x) = \exp\left(+ieQ_f \int_0^\infty ds n_\mp A_s(x + sn_\mp) e^{-\epsilon s}\right), \quad (\text{A.16})$$

$$\text{outgoing antiparticles:} \quad Y_{f\pm}(x) = \exp\left(-ieQ_f \int_0^\infty ds n_\mp A_s(x + sn_\mp) e^{-\epsilon s}\right), \quad (\text{A.17})$$

$$\text{incoming particles:} \quad \bar{Y}_{f\pm}(x) = \exp\left(+ieQ_f \int_{-\infty}^0 ds n_\mp A_s(x + sn_\mp) e^{\epsilon s}\right), \quad (\text{A.18})$$

$$\text{incoming antiparticles:} \quad \bar{Y}_{f\pm}^\dagger(x) = \exp\left(-ieQ_f \int_{-\infty}^0 ds n_\mp A_s(x + sn_\mp) e^{\epsilon s}\right), \quad (\text{A.19})$$

where ϵ is introduced to ensure the convergence of the integral. Similarly, for QCD,

$$\text{outgoing particles:} \quad Y_{\text{QCD}\pm}^\dagger(x) = \mathcal{P} \exp\left(+ig_s \int_0^\infty ds n_\mp G_s(x + sn_\mp) e^{-\epsilon s}\right), \quad (\text{A.20})$$

$$\text{outgoing antiparticles:} \quad Y_{\text{QCD}\pm}(x) = \bar{\mathcal{P}} \exp\left(-ig_s \int_0^\infty ds n_\mp G_s(x + sn_\mp) e^{-\epsilon s}\right), \quad (\text{A.21})$$

$$\text{incoming particles:} \quad \bar{Y}_{\text{QCD}\pm}(x) = \mathcal{P} \exp\left(+ig_s \int_{-\infty}^0 ds n_\mp G_s(x + sn_\mp) e^{\epsilon s}\right), \quad (\text{A.22})$$

$$\text{incoming antiparticles:} \quad \bar{Y}_{\text{QCD}\pm}^\dagger(x) = \bar{\mathcal{P}} \exp\left(-ig_s \int_{-\infty}^0 ds n_\mp G_s(x + sn_\mp) e^{\epsilon s}\right). \quad (\text{A.23})$$

The new hard-collinear fields with superscript (0) do not have interactions with soft fields at leading power, and after the decoupling transformation the superscript is dropped. Further, in the main text we omit the label when f on $Y_{f\pm}$, whenever $f_C = \ell_C$ is a lepton or anti-lepton, see (4.5).

The SCET_{II} is obtained from SCET_I by integrating out the modes with hard-collinear virtuality. The leading-power Lagrangian of a collinear fermion f_c in SCET_{II} now includes its mass m_f [68, 69],

$$\mathcal{L}_f^{(0)} = \bar{f}_c \left[in_- D_c + (i\not{D}_{c\perp} - m_f) \frac{1}{in_+ D_c} (i\not{D}_{c\perp} + m_f) \right] \frac{\not{n}_+}{2} f_c. \quad (\text{A.24})$$

The SCET_{II} covariant derivative $iD_c = i\partial + eQ_f A_c + g_s G_c$ does not contain the soft gauge field, in distinction to the case of SCET_I in (A.6), because the interaction between a single

soft mode and collinear modes would necessarily create a mode with hard-collinear virtuality. Thus in SCET_{II} there is no need to perform a decoupling transformation to achieve factorization of soft and collinear sectors. The gauge-invariance of the SCET_{II} operators under collinear gauge transformations is achieved analogously to the case of SCET_I with the help of collinear QED and QCD Wilson lines W_{fc} and W_c , respectively, which are obtained from (A.8) and (A.9) by the replacement $C \rightarrow c$. The collinear gauge-invariant building block ℓ_c for leptons is then formed analogously to (A.10).

The collinearly gauge-invariant building block

$$\mathcal{A}_{c\perp}^\mu = e \left[A_{c\perp}^\mu - \frac{i\partial_\perp^\mu n_+ A_c}{in_+ \partial} \right], \quad (\text{A.25})$$

of the collinear QED gauge field appears in SCET_{II} operators as well as the anti-collinear version defined through the replacements $c \rightarrow \bar{c}$ and $n_+ \rightarrow n_-$. As a consequence of the decoupling of hard-collinear modes, the SCET_{II} soft fields are dressed by soft Wilson lines. For the $\bar{q}_s[\dots]h_v$ bilinear they combine to the finite-distance Wilson line $Y(x, y)$ introduced in (4.6). The relation of this finite-distance Wilson line $Y(vn_-, 0)$ that appears in (4.1), (4.2) to the infinite-distance Wilson lines defined above can be seen from the identity

$$\bar{q}_s(vn_-)Y(vn_-, 0)h_v(0) = \left[\bar{q}_s(vn_-)\bar{Y}_{q+}(vn_-)\bar{Y}_{\text{QCD}+}(vn_-) \right] \left[\bar{Y}_{\text{QCD}+}^\dagger(0)\bar{Y}_{q+}^\dagger(0)h_v(0) \right]. \quad (\text{A.26})$$

These soft Wilson lines are necessary to maintain invariance of the non-local soft operators under soft QCD and QED gauge transformations.

A.2 Renormalization conventions

The convention of the operator renormalization follows [26]. The renormalization condition of the matrix element of an operator \mathcal{O}_P with a suitable choice of external states denoted by $\langle \dots \rangle$ is given as

$$\langle \mathcal{O}_P(\{\phi_{\text{ren}}\}, \{g_{\text{ren}}\}) \rangle_{\text{ren}} = \sum_Q Z_{PQ} \prod_{\phi \in Q} Z_\phi^{1/2} \prod_{g \in Q} Z_g \langle \mathcal{O}_{Q,\text{bare}}(\{\phi_{\text{ren}}\}, \{g_{\text{ren}}\}) \rangle. \quad (\text{A.27})$$

Here ϕ_{ren} and g_{ren} denote the renormalized fields and parameters, such as coupling constant or masses, out of which the operator \mathcal{O}_Q is composed. The mixing of operators \mathcal{O}_Q into \mathcal{O}_P is given by the corresponding entries $Z_{PQ} = (\mathbf{Z})_{PQ}$ of the renormalization matrix of the operators. The anomalous dimension matrix $\mathbf{\Gamma}$ is defined as

$$\mathbf{\Gamma} = - \left(\frac{d}{d \ln \mu} \mathbf{Z} \right) \mathbf{Z}^{-1} = \mathbf{Z} \frac{d}{d \ln \mu} \mathbf{Z}^{-1}, \quad (\text{A.28})$$

which implies renormalization group equations for the operators and Wilson coefficients as

$$\frac{d}{d \ln \mu} \mathcal{O}_P = - \sum_Q \Gamma_{PQ} \mathcal{O}_Q, \quad \frac{d}{d \ln \mu} C_P = \sum_Q \Gamma_{QP} C_Q. \quad (\text{A.29})$$

Operators in SCET depend on continuous variables such as light-cone positions or their Fourier-conjugates, the momentum fractions. These are included in the index P . When necessary, the sums in the above equations should therefore be understood as convolutions either in position or in momentum space.

The renormalization condition of the one-loop matrix element of an operator \mathcal{O}_P is determined from

$$\text{finite} = \langle \mathcal{O}_{P,\text{bare}} \rangle_{1\text{-loop}} + \sum_Q \left[\delta Z_{PQ} + \delta_{PQ} \left(\frac{1}{2} \sum_{\phi \in P} \delta Z_\phi + \sum_{g \in P} \delta Z_g \right) \right] \langle \mathcal{O}_{Q,\text{bare}} \rangle_{\text{tree}}, \quad (\text{A.30})$$

where at one-loop the renormalization constants are expanded as $Z_{PQ} = \delta_{PQ} + \delta Z_{PQ}$ and $Z_i = 1 + \delta Z_i$ for $i = \phi, g$.

A.3 SCET_I renormalization

The one-loop anomalous dimension of the SCET_I operators $\mathcal{O}_{9,10}$ and $\mathcal{O}_{\bar{9},\bar{10}}$ of Section 3.1 can be obtained by adapting [26, 34, 37] to the case of QED. These operators contain two collinear sectors and one soft sector, the latter consisting of the heavy quark field h_v . For example, in $\mathcal{O}_{9,10}$, the collinear sector in n_+ direction comprises the light quark field χ_C and the lepton field ℓ_C , thus representing an $F = 2$ operator of the form considered in [26], whereas the second collinear sector (called anti-collinear) in the n_- direction contains the single anti-lepton $\ell_{\bar{C}}$. The one-loop diagrams that determine the renormalization constant, fall into two classes: *i*) with soft photon exchange between all four external lines¹⁷ and *ii*) from collinear photon exchange that is restricted to each collinear sector separately. The dependence of the soft and collinear contributions on the infrared regulator cancels in their sum.

The SCET_I operators do not mix due to their particular Dirac structure. Besides the cusp part of the anomalous dimension given in (3.12), the remainder of the QED part of the one-loop anomalous dimension in (3.14) reads

$$\begin{aligned} \gamma_i(x, y) = & \delta(x - y) \left[Q_\ell^2(4 \ln x - 6) + Q_\ell Q_q 4 \ln \bar{x} + Q_q^2(4 \ln \bar{x} - 5) \right] \\ & + 4 Q_\ell Q_q \left[\theta(x - y) \frac{\bar{x}}{y} \left(\left[\frac{1}{x - y} \right]_+ - 1 \right) + \theta(y - x) \frac{x}{y} \left(\left[\frac{1}{y - x} \right]_+ - 1 \right) \right]. \end{aligned} \quad (\text{A.31})$$

We use bar-notation for momentum fractions, $\bar{x} \equiv 1 - x$ etc. The plus distribution is defined as

$$[f(x, y)]_+ = f(x, y) - \delta(x - y) \int_0^1 dz f(z, y). \quad (\text{A.32})$$

This result can be obtained from [26]. However, there the N -jet operator does not contain soft fields. Introducing the heavy quark field as a possible building block modifies the soft, but not the collinear one-loop contribution. Since soft loops do not change the momentum

¹⁷Soft photon exchange within a single collinear direction vanishes.

fraction of the collinear fields, only the part proportional to $\delta(x - y)$ is modified. For diagrams with soft photon exchange with the soft heavy quark the coefficient of the cusp logarithm is one half of that for soft loops connecting two different collinear directions, and one has to replace $s_{ij} \rightarrow \mu(n_- v)(n_+ p_j)$. In addition, the colour generators are replaced by appropriate electric charge factors and one has to contract spinor indices according to the definition of the operator. It is permitted to use four-dimensional identities to reduce the basis of Dirac matrices. We also checked this procedure by explicit computation of the anomalous dimension of the SCET_I operators without using results of [26].

The general solution of the RGE (3.11) of the hard functions due to the cusp anomalous dimension, neglecting the running of α_{em} , can be written as

$$\frac{H_i(u, \mu)}{H_i(u, \mu_b)} = \left(\frac{m_{B_q}}{\mu_b}\right)^{a_\Gamma} \exp \left[- \int_{\alpha_s(\mu_b)}^{\alpha_s(\mu)} d\alpha_s \frac{\Gamma_{\text{cusp}}^I(\alpha_s, \alpha_{\text{em}})}{\beta_s(\alpha_s)} \int_{\alpha_s(\mu_b)}^{\alpha_s} \frac{d\alpha'_s}{\beta_s(\alpha'_s)} \right], \quad (\text{A.33})$$

with

$$a_\Gamma = \int_{\alpha_s(\mu_b)}^{\alpha_s(\mu)} d\alpha_s \frac{\Gamma_{\text{cusp}}^I(\alpha_s, \alpha_{\text{em}})}{\beta_s(\alpha_s)} \quad (\text{A.34})$$

and $\beta_s(\alpha_s)$ the beta function of the strong coupling as defined in (A.3).

A.4 SCET_{II} renormalization

The regularization of UV and IR divergences in SCET_{II} is not as simple as in SCET_I. First we note that the presence of the lepton mass in the collinear and anti-collinear contributions in Figure 4b and Figure 4c does not regularize all IR divergences. We therefore use an IR regulator inspired by introducing an off-shellness for external lines in corresponding diagrams in SCET_I before performing the decoupling transformation. In the diagrams with soft photon exchange in Figure 4a, the IR regulator has to be introduced by modifying the $i0^+$ prescription in a manner consistent with SCET_I, i.e. the appropriate Wilson lines are regularized by a parameter related to the off-shell momentum p_ℓ^2 of the original hard-collinear fields before the decoupling of the soft modes. This implies a regulator in the propagators that originate from soft Wilson lines Y_\pm in the following way:

$$\begin{aligned} \text{diagram 3 :} \quad & [n_+ \ell - i0^+] \rightarrow [n_+ \ell - \delta_{\bar{\ell}} - i0^+] \\ & [n_- \ell - i0^+] \rightarrow [n_- \ell - \delta_\ell - i0^+] \\ \text{diagram 4 :} \quad & [n_+ \ell + i0^+] \rightarrow [n_+ \ell + \delta_{\bar{\ell}} + i0^+] \\ & [n_- \ell + i0^+] \rightarrow [n_- \ell + \delta_\ell + i0^+] \\ \text{diagram 5 :} \quad & [n_+ \ell - i0^+] \rightarrow [n_+ \ell - \delta_{\bar{\ell}} - i0^+] \\ \text{diagram 6 :} \quad & [n_+ \ell - i0^+][n_- \ell + i0^+] \rightarrow [n_+ \ell - \delta_{\bar{\ell}} - i0^+][n_- \ell + \delta_\ell + i0^+], \end{aligned} \quad (\text{A.35})$$

where ℓ denotes the loop momentum, and $\delta_\ell \equiv p_\ell^2/n_+ p_\ell$ and $\delta_{\bar{\ell}} \equiv p_{\bar{\ell}}^2/n_- p_{\bar{\ell}}$. The cancellation of the IR regulators then takes place between the soft-photon exchange diagrams 3, 4 and

5 of Figure 4a. Another cancellation occurs between diagram 6 of Figure 4a and the collinear/anti-collinear diagrams in Figure 4b and Figure 4c.

The results for the renormalization constants entering (4.14) are

$$Z_s^{\text{QED}}(\omega, \omega') = \delta(\omega' - \omega) \left[Q_q^2 \left(\frac{1}{\epsilon^2} + \frac{1}{\epsilon} \ln \frac{\mu^2}{\omega^2} - \frac{1}{\epsilon} \frac{5}{2} \right) + 2Q_\ell Q_q \left(\frac{1}{\epsilon^2} + \frac{1}{\epsilon} \ln \frac{\mu^2}{\omega^2} \right) \right] - Q_q(Q_q + Q_\ell) \frac{2}{\epsilon} F(\omega, \omega') \quad (\text{A.36})$$

for the QED contribution, while the universal QCD part coincides with the well-known expression [38]

$$Z_s^{\text{QCD}}(\omega, \omega') = \delta(\omega' - \omega) C_F \left[\frac{1}{\epsilon^2} + \frac{1}{\epsilon} \ln \frac{\mu^2}{\omega^2} - \frac{1}{\epsilon} \frac{5}{2} \right] - \frac{2C_F}{\epsilon} F(\omega, \omega'). \quad (\text{A.37})$$

The common function F is

$$F(\omega, \omega') \equiv \left[\frac{\theta(\omega - \omega')}{(\omega - \omega')} + \frac{\omega \theta(\omega' - \omega)}{\omega'(\omega' - \omega)} \right]_+. \quad (\text{A.38})$$

The plus distribution for the soft convolutions is defined as

$$\int_0^\infty d\omega' [f(\omega, \omega')]_+ g(\omega') = \int_0^\infty d\omega' f(\omega, \omega') [g(\omega') - g(\omega)] . \quad (\text{A.39})$$

The collinear renormalization constants in (4.41) and (4.42) are

$$Z_{\bar{c}}^{(1)} = -\frac{\alpha_{\text{em}}}{4\pi} Q_\ell^2 \left[\frac{1}{\epsilon^2} + \frac{1}{\epsilon} \ln \frac{-\mu^2}{(n_- p_{\bar{c}})(n_+ p_c)} + \frac{3}{2\epsilon} \right], \quad (\text{A.40})$$

$$Z_{m_\chi}^{c,(1)} = -\frac{\alpha_{\text{em}}}{4\pi} Q_\ell^2 \left[\frac{1}{\epsilon^2} + \frac{1}{\epsilon} \ln \frac{-\mu^2}{(n_- p_{\bar{c}})(n_+ p_c)} - \frac{3}{2\epsilon} \right], \quad (\text{A.41})$$

$$Z_{\mathcal{A}_\chi}^{c,(1)}(w, w') = -\frac{\alpha_{\text{em}}}{4\pi} Q_\ell^2 \left\{ \left[\frac{1}{\epsilon^2} + \frac{1}{\epsilon} \ln \frac{-\mu^2}{w^2(n_- p_{\bar{c}})(n_+ p_c)} + \frac{3}{2\epsilon} \right] \delta(w - w') + \frac{1}{\epsilon} \gamma_{\mathcal{A}_\chi, \mathcal{A}_\chi}(w, w') \right\}. \quad (\text{A.42})$$

We note that $Z_{m_\chi}^{c,(1)}$ receives also a contribution due to the renormalization of the lepton mass appearing in the definition $\mathcal{J}_{m_\chi}^{A1}$. The anomalous dimension $\gamma_{\mathcal{A}_\chi, \mathcal{A}_\chi}$,

$$\frac{\gamma_{\mathcal{A}_\chi, \mathcal{A}_\chi}(w, w')}{2} = -w + \theta[w' - \bar{w}] \frac{w' - \bar{w}}{w'} + \theta[\bar{w} - w'] \frac{1}{w'} \left(\frac{w'}{\bar{w}} - w - w' \right), \quad (\text{A.43})$$

can be extracted from the results given in [26, 37], and is due to the two diagrams in Figure 4c with $A_{c\perp}$ in the loop.

B SCET operators

In this Appendix, we discuss the construction of the SCET_{II} operator basis for the power-enhanced correction to $B_q \rightarrow \mu^+ \mu^-$. We first note that classifying the operators in SCET_I \rightarrow SCET_{II} matching is substantially more complicated than classifying SCET_I operators in the matching of the effective weak Hamiltonian to SCET_I. The reason is that although SCET_I operators are non-local, the non-locality of collinear fields is related to the $\mathcal{O}(1)$ inverse derivative $1/(in_+ \partial)$. For a SCET_I operator that scales as λ^n , the power of n can therefore never be smaller than the scaling of the products of fields contained in the operator. In SCET_I \rightarrow SCET_{II} matching, however, integrating out the hard-collinear modes leads to non-locality of soft fields related to $1/(in_- \partial_s) \sim 1/\lambda^2$ from the hard-collinear propagators, hence the above statement does not hold. Part of the construction of the operator basis therefore consists in constraining the number of times such inverse derivatives can occur in the operator. A systematic procedure for constructing the SCET_{II} operator basis when there is a single collinear and a soft sector, has been described in [25]. We adapt this procedure developed for heavy-to-light form factors to the present situation. Here we are interested in SCET_{II} operators with the scaling λ^{10} of the power-enhanced $B_q \rightarrow \mu^+ \mu^-$ amplitude, which can arise in the matching of $Q_{9,10}$ and Q_7 .

We first consider the possibility of SCET_I operator without hard-collinear or hard-anti-collinear fields. Since the collinear, anti-collinear and soft fields do not interact, such operators must have the flavour quantum numbers of the external state to have non-vanishing overlap. The operator with the smallest λ scaling is $\bar{q}_s \Gamma_s h_v \bar{\ell}_c \Gamma \ell_{\bar{c}} \sim \lambda^{10}$. However, the chiral structure of the effective weak Hamiltonian implies that the operator has overlap with a pseudoscalar B meson only after a chirality flip by the lepton mass term. Since in matching to SCET_I the λ^2 -suppression cannot be compensated by $1/(in_- \partial_s) \sim 1/\lambda^2$, this results in a λ^{12} operator, which is, in fact, the operator (7.2) that contributes to the standard non-enhanced $B_q \rightarrow \mu^+ \mu^-$ amplitude in the absence of QED effects. We conclude that any SCET_I operator relevant to the power-enhanced amplitude must contain at least one hard-collinear field, which leads to non-trivial SCET_I \rightarrow SCET_{II} matching.

Any relevant SCET_I operator must contain the heavy quark field h_v , at least one hard-collinear field as concluded above, and at least one anti-collinear or anti-hard-collinear field. As always, the corresponding operators with (hard-) collinear and anti (hard-collinear) modes interchanged also exists. The following discussion is phrased for the first case and hold with obvious modifications for the second. With the power counting of fields as given in Table 1, the field content of the operators with the smallest λ scaling is

$$\begin{aligned}
\lambda^5 : \quad & \bar{\chi}_{hc} h_v \mathcal{A}_{\perp hc}, \\
\lambda^6 : \quad & 1) \bar{\chi}_{hc} h_v \bar{\ell}_{hc} \ell_{\bar{hc}}, \quad 2) \bar{\chi}_c h_v \mathcal{A}_{\perp hc}, \quad 3) \bar{\chi}_{hc} h_v \mathcal{A}_{\perp \bar{c}}, \\
& 4) \bar{\chi}_{hc} h_v \mathcal{A}_{\perp hc} \times \{\mathcal{A}_{\perp hc}, \mathcal{A}_{\perp \bar{hc}}\},
\end{aligned} \tag{B.1}$$

and so on. For every operator there is another operator with (hard-) collinear and anti (hard-) collinear fields exchanged. We then need to determine the λ suppression factors

incurred when the hard-collinear fields convert into soft and collinear fields through SCET_I time-ordered products. From the discussion below it will become clear that operators that scale as λ^7 cannot match to SCET_{II} operators with λ^{10} scaling.

We begin with the derivation of the SCET_{II} operator basis for the matching of the semi-leptonic operators $Q_{9,10}$ in the effective weak Hamiltonian, which is the case discussed in the main text. We first note that the operator with field content $\bar{\chi}_{hc} h_v \mathcal{A}_{\perp \bar{hc}}$ cannot be generated at $\mathcal{O}(\lambda^5)$ from the operators $Q_{9,10}$. To obtain $\bar{\chi}_{hc} h_v \mathcal{A}_{\perp \bar{hc}}$ from hard matching to SCET_I the lepton fields in $Q_{9,10}$ must be contracted and a anti-hard-collinear photon field attached. For the vectorial operators $Q_{9,10}$ this results in $\partial^\mu A_\mu$ or $m_l \sigma^{\mu\nu} F_{\mu\nu}$, which both lead to SCET_I operator that count as λ^7 . We will come back to the $\mathcal{O}(\lambda^5)$ operator below, where we briefly discuss the operator basis in the matching of Q_7 , but for now we proceed with the $\mathcal{O}(\lambda^6)$ operators in the above list.

The operators 2) and 3) can immediately be discarded, since the collinear (case 2)) or anti-collinear (case 3)) field content does not have the correct lepton flavour number to overlap with the $\ell^+ \ell^-$ state. For example, the collinear antiquark field $\bar{\chi}_c$ can never turn into a collinear state with lepton number one. In case of operator 4) adding more fields to the $\mathcal{O}(\lambda^5)$ operator does not allow one to overcome the above suppression. This leaves the operator $\bar{\chi}_{hc} h_v \bar{\ell}_{hc} \ell_{\bar{hc}}$ as the only candidate $\mathcal{O}(\lambda^6)$ SCET_I operator.

It is easy to see that this operator does contribute at $\mathcal{O}(\lambda^{10})$ to the amplitude in question. At tree-level, this involves the SCET_I \rightarrow SCET_{II} matching relations

$$\ell_{hc} \xrightarrow{\lambda} \ell_c, \quad \ell_{\bar{hc}} \xrightarrow{\lambda} \ell_{\bar{c}}, \quad \chi_{hc} \xrightarrow{\lambda^2} \frac{1}{in_{-\partial}} Q_q e \mathcal{A}_{\perp c} \frac{\not{n}_{-}}{2} q_s \quad (\text{B.2})$$

and their hermitian conjugates. The last relation is taken from Section 3.2.1 of [25], and describes the splitting of the hard-collinear quark field into a collinear photon and a soft quark.¹⁸ The power of λ indicated above the arrow gives the λ suppression from the left- to the right-hand side as a consequence of SCET_I \rightarrow SCET_{II} matching. Thus, the $\mathcal{O}(\lambda^6)$ SCET_I operator turns into a $\mathcal{O}(\lambda^{10})$ SCET_{II} operator with the field content of $\tilde{\mathcal{J}}_{A_X}^{B1}$ defined in (4.2). The present discussion in fact corresponds to the matching shown in the SCET_I column of Figure 3 and shows that one must obtain an inverse derivative factor $1/in_{-\partial} \sim 1/\lambda^2$, which corresponds to the factor $1/\omega$ in the tree-level matching coefficient (4.53). Another way to obtain a $\mathcal{O}(\lambda^{10})$ SCET_{II} operator consists of

$$\ell_{hc} \xrightarrow{1} \ell_{hc}, \quad \ell_{\bar{hc}} \xrightarrow{\lambda} \ell_{\bar{c}}, \quad \chi_{hc} \xrightarrow{\lambda} \frac{1}{in_{-\partial}} Q_q e \mathcal{A}_{\perp hc} \frac{\not{n}_{-}}{2} q_s \quad (\text{B.3})$$

followed by the fusion

$$\bar{\ell}_{hc} + \mathcal{A}_{\perp hc} \xrightarrow{\lambda^2} m_\ell \bar{\ell}_c \quad (\text{B.4})$$

through a hard-collinear one-loop diagram.

To find the basis of the SCET_{II} operators, these considerations have to be generalized to arbitrary loop order. To this end we follow [25] and classify all possible building blocks

¹⁸For simplicity of notation, all collinear and soft Wilson lines are set to unity here. They can be restored unambiguously by making the operator invariant under the SCET_{II} gauge symmetries.

Class	Elements	α
Γ_c	$1, \gamma_5, \gamma_\perp^\mu$	0
$\Gamma_s^{(0)}$	$1, \gamma_5, \gamma_\perp^\mu, \gamma_\perp^\mu \gamma_5, \sigma_\perp^{\mu\nu}, \not{n}_+ \not{n}_-$	0
$\Gamma_s^{(+1)}$	$\not{n}_-, \not{n}_- \gamma_5, \not{n}_- \gamma_\perp^\mu$	1
$\Gamma_s^{(-1)}$	$\not{n}_+, \not{n}_+ \gamma_5, \not{n}_+ \gamma_\perp^\mu$	-1

Table 4: Dirac matrices and their scaling α^n under “boost” or type-III RPI transformations.

\mathcal{O}_A	Object	λ	α	d
I	$(n_- \partial_s)^{-1}$	-2	-1	-1
II	$(n_+ \partial_c)^{-1}$	0	+1	-1
III	$\partial_\perp, A_{c\perp}, A_{s\perp}, m_\ell, m_q$	2	0	1
IV	$n_+ \partial_s, n_+ A_s$	2	-1	1
V	$n_- \partial_c, n_- A_c$	4	+1	1
VI	$\bar{f}_c \frac{\not{n}_+}{2} \Gamma_c f_c$	4	-1	3
VII	$\bar{f}_s \Gamma_s^{(-1)} f_s$	6	-1	3
VIII	$\bar{f}_s \Gamma_s^{(+1)} f_s$	6	+1	3
IX	$\bar{f}_s \Gamma_s^{(0)} f_s$	6	0	3

Table 5: Building blocks that can be added to (B.6). The column λ denotes the λ scaling of the object, α its scaling under type-III reparametrizations, and d its canonical dimension. The Dirac matrices Γ are defined in Table 4. The counting refers to matching of the hard-collinear sector.

according to their scaling in λ , canonical dimension d and transformation property under type-III reparametrization transformations

$$n_- \rightarrow \alpha n_-, \quad n_+ \rightarrow \alpha^{-1} n_+, \quad (\text{B.5})$$

of the reference vectors, which must be preserved in the matching due to reparametrization symmetry of SCET. Accounting for the flavour quantum numbers of the initial and final state in the $B_q \rightarrow \ell^+ \ell^-$ process, we can write the possible SCET_{II} operators in the form

$$\mathcal{O}^{(\alpha)} = [\text{objects}] \times (\bar{q}_s \Gamma_s^{(\alpha)} h_v) (\bar{\ell}_c \Gamma_c \ell_{\bar{c}}), \quad \alpha = \pm 1, 0 \quad (\text{B.6})$$

with Dirac structures given in Table 4. The “objects” can be chosen from the factors, operators and field products listed in Table 5.

The SCET_I operator $\bar{\chi}_{hc} h_v \bar{\ell}_{hc} \ell_{\bar{hc}}$, which is generated in the matching of $Q_{9,10}$ to SCET_I, has $d = 6$ and boost scaling $\alpha = 0$. Requiring these to match those of (B.6), allows us to

solve for n_1 and n_2 , the number of times the objects I and II appear in (B.6), in the form

$$n_1 = \frac{n_3 + \alpha}{2} + n_5 + n_6 + n_7 + 2n_8 + \frac{3}{2}n_9, \quad (\text{B.7})$$

$$n_2 = \frac{n_3 - \alpha}{2} + n_4 + 2n_6 + 2n_7 + n_8 + \frac{3}{2}n_9. \quad (\text{B.8})$$

Eliminating n_1, n_2 in the expression for the λ scaling $[\lambda]$ of (B.6), we obtain

$$[\lambda] = 10 - \alpha + n_3 + 2n_4 + 2n_5 + 2n_6 + 4n_7 + 2n_8 + 3n_9 \quad (\text{B.9})$$

in terms of the number of times n_i the objects III to IX appear in (B.6). Since we are looking for solutions with $[\lambda] = 10$, the following cases arise:

- $\alpha = -1$: Since all n_i are positive and non-negative integers, solutions to (B.9) have at least $[\lambda] = 12$. This case does not contribute to the power-enhanced amplitude.
- $\alpha = 0$: All n_i must be zero for a $[\lambda] = 10$ solution.
- $\alpha = +1$: The solution $[\lambda] = 9$, and $n_i = 0$ for all n_i is excluded, because $n_{1,2}$ must be integer. This leaves the $[\lambda] = 10$ solution with $n_3 = 1$, $n_i = 0$ for $i = 4, \dots, 9$. In this case further $n_1 = 1$, $n_2 = 0$.

Thus we identified the following two $\mathcal{O}(\lambda^{10})$ SCET_{II} operators:

$$\mathcal{O}^{(0)} = [\bar{q}_s \Gamma_s^{(0)} h_v] [\bar{\ell}_c \Gamma_c \ell_{\bar{c}}], \quad (\text{B.10})$$

$$\mathcal{O}^{(+1)} = \frac{\mathcal{O}_{\text{III}}}{in_- \partial_s} [\bar{q}_s \Gamma_s^{(+1)} h_v] [\bar{\ell}_c \Gamma_c \ell_{\bar{c}}]. \quad (\text{B.11})$$

Note that this analysis implicitly assumed that in the anti-collinear direction the SCET_I \rightarrow SCET_{II} matching was trivial, $\ell_{hc} \rightarrow \ell_{\bar{c}}$. This is justified, since any non-trivial matching would lead to further λ suppression.

At this point we have to invoke helicity conservation, which implies that for $\mathcal{O}^{(0)}$ only $\Gamma_c = \gamma_{\perp}^{\mu}$ has a non-vanishing matching coefficient to any order in α_{em} . However, this Dirac structure cannot contribute to the decay rate of a (pseudo-) scalar B -meson, which excludes this operator.

In the case of $\mathcal{O}^{(+1)}$, the helicity structure of the lepton current depends on \mathcal{O}_{III} . For $\mathcal{O}_{\text{III}} = m_{\ell}$ helicity conservation implies $\Gamma_c \in \{1, \gamma_5\} \equiv \Gamma^{S/P}$, and the operator has a non-vanishing matrix element for the $B_q \rightarrow \ell^+ \ell^-$ transition. For all other members of object class III, only $\Gamma_c = \gamma_{\perp}^{\mu}$ is allowed by helicity conservation. However, only $\mathcal{O}_{\text{III}} = A_{c\perp}$ has a non-vanishing matrix element for the (pseudo-) scalar B -meson decay. In summary, we find the following SCET_{II} operators with λ^{10} suppression:

$$\mathcal{O}_-^{A1} = m_{\ell} \left[\frac{1}{in_- \partial_s} \bar{q}_s \not{p}_- \Gamma^{S/P} h_v \right] [\bar{\ell}_c \Gamma^{S/P} \ell_{\bar{c}}], \quad (\text{B.12})$$

$$\mathcal{O}_-^{B1} = T_{\mu\nu} \left[\frac{1}{in_- \partial_s} \bar{q}_s \not{h}_- \Gamma^{S/P} h_v \right] \left[\mathcal{A}_{c\perp}^\nu \bar{\ell}_c \gamma_\perp^\mu \ell_{\bar{c}} \right], \quad (\text{B.13})$$

with $\Gamma^{S/P} \in \{1, \gamma_5\}$ and $T_{\mu\nu} \in \{g_{\mu\nu}^\perp, \varepsilon_{\mu\nu}^\perp\}$. When the Wilson lines and non-localities are restored these two operators correspond to (4.1) and (4.2) in the main text. The present analysis also implies that to any order in the matching, only a single power of $1/in_- \partial_s$ can appear, modified by logarithms, together with the leading-twist B -meson LCDA. Hence, similar to the case of heavy-to-light form factors discussed in [25], the power-enhanced correction from the operators $Q_{9,10}$ can be expressed in terms of the inverse moment λ_B and the logarithmic moments, (8.1) and (8.2), respectively. Upon exchanging the collinear and anti-collinear sectors, we obtain the corresponding two operators

$$\mathcal{O}_+^{\overline{A1}} = m_\ell \left[\frac{1}{in_+ \partial_s} \bar{q}_s \not{h}_+ \Gamma^{S/P} h_v \right] \left[\bar{\ell}_c \Gamma^{S/P} \ell_{\bar{c}} \right], \quad (\text{B.14})$$

$$\mathcal{O}_+^{\overline{B1}} = T_{\mu\nu} \left[\frac{1}{in_+ \partial_s} \bar{q}_s \not{h}_+ \Gamma^{S/P} h_v \right] \left[\mathcal{A}_{\bar{c}\perp}^\nu \bar{\ell}_c \gamma_\perp^\mu \ell_{\bar{c}} \right]. \quad (\text{B.15})$$

The all-order analysis of the $\mathcal{O}(\lambda^5)$ operator $\bar{\chi}_{hc} h_v \mathcal{A}_{\perp \bar{hc}}$ from (B.1), which arises in SCET_I from the tree-level matching of Q_7 , is substantially more complicated. This is because the operator involves a hard-collinear quark and an anti-hard-collinear photon field, which both must undergo not-trivial SCET_I \rightarrow SCET_{II} matching to obtain an operator that overlaps with the external state of $B_q \rightarrow \ell^+ \ell^-$ decay. Since the collinear and anti-collinear sector interact with the same soft fields, the analysis above must be extended to keep track from which sector a soft field and its corresponding non-localities arises. In particular, since the collinear final state must have lepton number +1, and the hard-collinear sector of the SCET_I does not carry lepton number, likewise for the anti-collinear direction, the SCET_{II} operator must necessarily contain a soft lepton pair, which is generated in SCET_I \rightarrow SCET_{II} matching. We are therefore led to consider operators of the form

$$\mathcal{O}(s, t, u) = [\text{objects}] \times [\bar{q}_s(sn_\pm) \Gamma_s h_v(0)] [\bar{\ell}_c(tn_+) \Gamma'_s \ell_s(un_-)] [\bar{\ell}_c(0) \Gamma_c \ell_{\bar{c}}(0)], \quad (\text{B.16})$$

where here we kept the position arguments to indicate the non-locality of the fields. Not counting the “objects”, this operator has dimension $d = 9$ and $[\lambda] = 16$, while the initial operator has $d = 5$. For this operator to contribute to the power-enhanced amplitude, it must contain a number of inverse derivatives $1/(in_- \partial_s)$ acting on soft fields that arise from hard-collinear matching, or $1/(in_+ \partial_s)$ from the matching of the anti-hard-collinear sector.

That this possibility is indeed realized can be seen from tree-level matching. The relevant splitting of the hard-collinear quark field is (B.3) above, followed by

$$A_{\perp hc}^\mu \xrightarrow{\lambda^2} \frac{Q_\ell e}{(in_+ \partial_c)(in_- \partial_s)} \left\{ \bar{\ell}_c \gamma_\perp^\mu \ell_s + \text{h.c.} \right\} \quad (\text{B.17})$$

from Section 3.2.2 of [25]. For the splitting of the anti-hard-collinear photon, (B.17) adapted to the anti-collinear sector applies. All together this provides a λ^5 suppression of the initial

operator, resulting in $[\lambda] = 10$ and the correct dimension. Putting everything together, we obtain

$$\bar{\chi}_{hc} h_v \mathcal{A}_{\perp \bar{hc}} \rightarrow \bar{q}_s \overleftarrow{in_- \partial_s^{-1}} h_v \left[\frac{1}{(in_+ \partial_c)(in_- \partial_s)} \bar{\ell}_c \ell_s \right] \left[\frac{1}{(in_- \partial_{\bar{c}})(in_+ \partial_s)} \bar{\ell}_s \ell_{\bar{c}} \right]. \quad (\text{B.18})$$

The QED one-loop calculation of the matrix element of Q_7 performed in [21] corresponds to evaluating the one-loop SCET_{II} matrix element of this operator, obtained by contracting the soft lepton fields. The endpoint divergence in the one-loop integral found there is a consequence of the large number of inverse derivative operators in (B.18). We performed a general analysis of SCET_I \rightarrow SCET_{II} also for Q_7 and find that the above operator together with those discussed above for $Q_{9,10}$ are the only SCET_{II} operators relevant to the power-enhanced $B_q \rightarrow \ell^+ \ell^-$ amplitude.

References

- [1] T. Inami and C. S. Lim, *Effects of Superheavy Quarks and Leptons in Low-Energy Weak Processes* $K_L \rightarrow \mu^+ \mu^-$, $K^+ \rightarrow \pi^+ \nu \bar{\nu}$ and $K^0 \leftrightarrow \bar{K}^0$, *Prog. Theor. Phys.* **65** (1981) 297.
- [2] A. Bazavov et al., *B- and D-meson leptonic decay constants from four-flavor lattice QCD*, *Phys. Rev.* **D98** (2018) 074512 [[1712.09262](#)].
- [3] A. J. Buras, M. Gorbahn, U. Haisch and U. Nierste, *Charm quark contribution to $K^+ \rightarrow \pi^+ \nu \bar{\nu}$ at next-to-next-to-leading order*, *JHEP* **11** (2006) 002 [[hep-ph/0603079](#)].
- [4] C. Bobeth, M. Gorbahn, T. Hermann, M. Misiak, E. Stamou and M. Steinhauser, *$B_{s,d} \rightarrow \ell^+ \ell^-$ in the Standard Model with Reduced Theoretical Uncertainty*, *Phys. Rev. Lett.* **112** (2014) 101801 [[1311.0903](#)].
- [5] A. Sirlin, *Current Algebra Formulation of Radiative Corrections in Gauge Theories and the Universality of the Weak Interactions*, *Rev. Mod. Phys.* **50** (1978) 573.
- [6] A. Sirlin, *Large m_W , m_Z Behavior of the $\mathcal{O}(\alpha)$ Corrections to Semileptonic Processes Mediated by W* , *Nucl. Phys.* **B196** (1982) 83.
- [7] W. J. Marciano and A. Sirlin, *Radiative corrections to $\pi_{\ell 2}$ decays*, *Phys. Rev. Lett.* **71** (1993) 3629.
- [8] C. Bobeth, M. Gorbahn and E. Stamou, *Electroweak Corrections to $B_{s,d} \rightarrow \ell^+ \ell^-$* , *Phys. Rev.* **D89** (2014) 034023 [[1311.1348](#)].
- [9] T. Hermann, M. Misiak and M. Steinhauser, *Three-loop QCD corrections to $B_s \rightarrow \mu^+ \mu^-$* , *JHEP* **12** (2013) 097 [[1311.1347](#)].
- [10] C. Bobeth, P. Gambino, M. Gorbahn and U. Haisch, *Complete NNLO QCD analysis of $\bar{B} \rightarrow X_s \ell^+ \ell^-$ and higher order electroweak effects*, *JHEP* **04** (2004) 071 [[hep-ph/0312090](#)].
- [11] T. Huber, E. Lunghi, M. Misiak and D. Wyler, *Electromagnetic logarithms in $\bar{B} \rightarrow X_s \ell^+ \ell^-$* , *Nucl. Phys.* **B740** (2006) 105 [[hep-ph/0512066](#)].

- [12] LHCb collaboration, *Measurement of the $B_s^0 \rightarrow \mu^+\mu^-$ branching fraction and search for $B^0 \rightarrow \mu^+\mu^-$ decays at the LHCb experiment*, *Phys. Rev. Lett.* **111** (2013) 101805 [1307.5024].
- [13] CMS collaboration, *Measurement of the $B_s \rightarrow \mu^+\mu^-$ branching fraction and search for $B^0 \rightarrow \mu^+\mu^-$ with the CMS Experiment*, *Phys. Rev. Lett.* **111** (2013) 101804 [1307.5025].
- [14] LHCb, CMS collaboration, *Observation of the rare $B_s^0 \rightarrow \mu^+\mu^-$ decay from the combined analysis of CMS and LHCb data*, *Nature* **522** (2015) 68 [1411.4413].
- [15] ATLAS collaboration, *Study of the rare decays of B_s^0 and B^0 into muon pairs from data collected during the LHC Run 1 with the ATLAS detector*, *Eur. Phys. J.* **C76** (2016) 513 [1604.04263].
- [16] LHCb collaboration, *Measurement of the $B_s^0 \rightarrow \mu^+\mu^-$ branching fraction and effective lifetime and search for $B^0 \rightarrow \mu^+\mu^-$ decays*, *Phys. Rev. Lett.* **118** (2017) 191801 [1703.05747].
- [17] ATLAS collaboration, *Study of the rare decays of B_s^0 and B^0 mesons into muon pairs using data collected during 2015 and 2016 with the ATLAS detector*, *JHEP* **04** (2019) 098 [1812.03017].
- [18] P. Golonka and Z. Was, *PHOTOS Monte Carlo: A Precision tool for QED corrections in Z and W decays*, *Eur. Phys. J.* **C45** (2006) 97 [hep-ph/0506026].
- [19] A. J. Buras, J. Girrbach, D. Guadagnoli and G. Isidori, *On the Standard Model prediction for $Br(B_{s,d} \rightarrow \mu^+\mu^-)$* , *Eur. Phys. J.* **C72** (2012) 2172 [1208.0934].
- [20] Y. G. Aditya, K. J. Healey and A. A. Petrov, *Faking $B_s \rightarrow \mu^+\mu^-$* , *Phys. Rev.* **D87** (2013) 074028 [1212.4166].
- [21] M. Beneke, C. Bobeth and R. Szafron, *Enhanced electromagnetic correction to the rare B-meson decay $B_{s,d} \rightarrow \mu^+\mu^-$* , *Phys. Rev. Lett.* **120** (2018) 011801 [1708.09152].
- [22] M. Beneke, *Soft-collinear factorization in B decays*, *Nucl. Part. Phys. Proc.* **261-262** (2015) 311 [1501.07374].
- [23] K. G. Chetyrkin, M. Misiak and M. Münz, *Weak radiative B-meson decay beyond leading logarithms*, *Phys. Lett.* **B400** (1997) 206 [hep-ph/9612313].
- [24] C. Bobeth, M. Misiak and J. Urban, *Photonic penguins at two loops and m_t dependence of $Br(B \rightarrow X_s \ell^+ \ell^-)$* , *Nucl. Phys.* **B574** (2000) 291 [hep-ph/9910220].
- [25] M. Beneke and T. Feldmann, *Factorization of heavy to light form-factors in soft collinear effective theory*, *Nucl. Phys.* **B685** (2004) 249 [hep-ph/0311335].
- [26] M. Beneke, M. Garry, R. Szafron and J. Wang, *Anomalous dimension of subleading-power N-jet operators*, *JHEP* **03** (2018) 001 [1712.04416].
- [27] M. Beneke and V. A. Smirnov, *Asymptotic expansion of Feynman integrals near threshold*, *Nucl. Phys.* **B522** (1998) 321 [hep-ph/9711391].

- [28] B. Jantzen, *Foundation and generalization of the expansion by regions*, *JHEP* **12** (2011) 076 [1111.2589].
- [29] H. H. Patel, *Package-X: A Mathematica package for the analytic calculation of one-loop integrals*, *Comput. Phys. Commun.* **197** (2015) 276 [1503.01469].
- [30] H. H. Patel, *Package-X 2.0: A Mathematica package for the analytic calculation of one-loop integrals*, *Comput. Phys. Commun.* **218** (2017) 66 [1612.00009].
- [31] M. Beneke, A. P. Chapovsky, M. Diehl and T. Feldmann, *Soft collinear effective theory and heavy to light currents beyond leading power*, *Nucl. Phys.* **B643** (2002) 431 [hep-ph/0206152].
- [32] R. J. Hill and M. Neubert, *Spectator interactions in soft collinear effective theory*, *Nucl. Phys.* **B657** (2003) 229 [hep-ph/0211018].
- [33] S. Alte, M. König and M. Neubert, *Effective Field Theory after a New-Physics Discovery*, *JHEP* **08** (2018) 095 [1806.01278].
- [34] M. Beneke, M. Garny, R. Szafron and J. Wang, *Violation of the Kluberg-Stern–Zuber theorem in SCET*, 1907.05463.
- [35] A. J. Buras and M. Münz, *Effective Hamiltonian for $B \rightarrow X_s e^+ e^-$ beyond leading logarithms in the NDR and HV schemes*, *Phys. Rev.* **D52** (1995) 186 [hep-ph/9501281].
- [36] M. Beneke, T. Feldmann and D. Seidel, *Systematic approach to exclusive $B \rightarrow V l^+ l^-$, $V \gamma$ decays*, *Nucl. Phys.* **B612** (2001) 25 [hep-ph/0106067].
- [37] M. Beneke, M. Garny, R. Szafron and J. Wang, *Anomalous dimension of subleading-power N -jet operators. Part II*, *JHEP* **11** (2018) 112 [1808.04742].
- [38] B. O. Lange and M. Neubert, *Renormalization group evolution of the B meson light cone distribution amplitude*, *Phys. Rev. Lett.* **91** (2003) 102001 [hep-ph/0303082].
- [39] M. G. Echevarría, A. Idilbi and I. Scimemi, *Soft and Collinear Factorization and Transverse Momentum Dependent Parton Distribution Functions*, *Phys. Lett.* **B726** (2013) 795 [1211.1947].
- [40] A. G. Grozin and M. Neubert, *Asymptotics of heavy meson form-factors*, *Phys. Rev.* **D55** (1997) 272 [hep-ph/9607366].
- [41] M. Beneke and T. Feldmann, *Symmetry breaking corrections to heavy to light B meson form-factors at large recoil*, *Nucl. Phys.* **B592** (2001) 3 [hep-ph/0008255].
- [42] M. Beneke, *Lectures at the Helmholtz International Summer School on Heavy Quark Physics, Dubna, Russia*, <http://theor.jinr.ru/~hq2005/>, 6 – 16 June 2005.
- [43] T. Becher and M. Neubert, *Drell-Yan Production at Small q_T , Transverse Parton Distributions and the Collinear Anomaly*, *Eur. Phys. J.* **C71** (2011) 1665 [1007.4005].
- [44] T. Becher, G. Bell and M. Neubert, *Factorization and Resummation for Jet Broadening*, *Phys. Lett.* **B704** (2011) 276 [1104.4108].

- [45] M. Beneke and J. Rohrwild, *B meson distribution amplitude from $B \rightarrow \gamma \ell \nu_\ell$* , *Eur. Phys. J.* **C71** (2011) 1818 [1110.3228].
- [46] S. Fleming, A. H. Hoang, S. Mantry and I. W. Stewart, *Jets from massive unstable particles: Top-mass determination*, *Phys. Rev.* **D77** (2008) 074010 [hep-ph/0703207].
- [47] A. von Manteuffel, R. M. Schabinger and H. X. Zhu, *The two-loop soft function for heavy quark pair production at future linear colliders*, *Phys. Rev.* **D92** (2015) 045034 [1408.5134].
- [48] D. R. Yennie, S. C. Frautschi and H. Suura, *The infrared divergence phenomena and high-energy processes*, *Annals Phys.* **13** (1961) 379.
- [49] G. Bell, M. Beneke, T. Huber and X.-Q. Li, *Heavy-to-light currents at NNLO in SCET and semi-inclusive $\bar{B} \rightarrow X_s l^+ l^-$ decay*, *Nucl. Phys.* **B843** (2011) 143 [1007.3758].
- [50] K. De Bruyn, R. Fleischer, R. Knegjens, P. Koppenburg, M. Merk, A. Pellegrino et al., *Probing New Physics via the $B_s^0 \rightarrow \mu^+ \mu^-$ Effective Lifetime*, *Phys. Rev. Lett.* **109** (2012) 041801 [1204.1737].
- [51] PARTICLE DATA GROUP collaboration, *Review of Particle Physics*, *Phys. Rev.* **D98** (2018) 030001.
- [52] FLAVOUR LATTICE AVERAGING GROUP collaboration, *FLAG Review 2019*, 1902.08191.
- [53] HFLAV collaboration, *Averages of b-hadron, c-hadron, and τ -lepton properties as of summer 2016*, *Eur. Phys. J.* **C77** (2017) 895 [1612.07233].
- [54] P. Gambino, K. J. Healey and S. Turczyk, *Taming the higher power corrections in semileptonic B decays*, *Phys. Lett.* **B763** (2016) 60 [1606.06174].
- [55] J. Charles et al., *Current status of the Standard Model CKM fit and constraints on $\Delta F = 2$ New Physics*, *Phys. Rev.* **D91** (2015) 073007 [1501.05013].
- [56] UTFIT collaboration, *Unitarity Triangle analysis in the Standard Model from the UTFit collaboration*, *PoS ICHEP2016* (2016) 554.
- [57] C. McNeile, C. T. H. Davies, E. Follana, K. Hornbostel and G. P. Lepage, *High-Precision f_{B_s} and HQET from Relativistic Lattice QCD*, *Phys. Rev.* **D85** (2012) 031503 [1110.4510].
- [58] FERMILAB LATTICE, MILC collaboration, *B- and D-meson decay constants from three-flavor lattice QCD*, *Phys. Rev.* **D85** (2012) 114506 [1112.3051].
- [59] H. Na, C. J. Monahan, C. T. H. Davies, R. Horgan, G. P. Lepage and J. Shigemitsu, *The B and B_s Meson Decay Constants from Lattice QCD*, *Phys. Rev.* **D86** (2012) 034506 [1202.4914].
- [60] N. H. Christ, J. M. Flynn, T. Izubuchi, T. Kawanai, C. Lehner, A. Soni et al., *B-meson decay constants from 2 + 1-flavor lattice QCD with domain-wall light quarks and relativistic heavy quarks*, *Phys. Rev.* **D91** (2015) 054502 [1404.4670].

- [61] Y. Aoki, T. Ishikawa, T. Izubuchi, C. Lehner and A. Soni, *Neutral B meson mixings and B meson decay constants with static heavy and domain-wall light quarks*, *Phys. Rev.* **D91** (2015) 114505 [[1406.6192](#)].
- [62] ETM collaboration, *Mass of the b-quark and B-meson decay constants from $N_f = 2 + 1 + 1$ twisted-mass lattice QCD*, *Phys. Rev.* **D93** (2016) 114505 [[1603.04306](#)].
- [63] HPQCD collaboration, *B-Meson Decay Constants from Improved Lattice Nonrelativistic QCD with Physical u, d, s, and c Quarks*, *Phys. Rev. Lett.* **110** (2013) 222003 [[1302.2644](#)].
- [64] C. Hughes, C. T. H. Davies and C. J. Monahan, *New methods for B meson decay constants and form factors from lattice NRQCD*, *Phys. Rev.* **D97** (2018) 054509 [[1711.09981](#)].
- [65] LHCb collaboration, *First Evidence for the Decay $B_s^0 \rightarrow \mu^+ \mu^-$* , *Phys. Rev. Lett.* **110** (2013) 021801 [[1211.2674](#)].
- [66] M. Beneke and M. Neubert, *QCD factorization for $B \rightarrow PP$ and $B \rightarrow PV$ decays*, *Nucl. Phys.* **B675** (2003) 333 [[hep-ph/0308039](#)].
- [67] C. W. Bauer, S. Fleming, D. Pirjol and I. W. Stewart, *An Effective field theory for collinear and soft gluons: Heavy to light decays*, *Phys. Rev.* **D63** (2001) 114020 [[hep-ph/0011336](#)].
- [68] M. Beneke and T. Feldmann, *Multipole expanded soft collinear effective theory with non-abelian gauge symmetry*, *Phys. Lett.* **B553** (2003) 267 [[hep-ph/0211358](#)].
- [69] A. K. Leibovich, Z. Ligeti and M. B. Wise, *Comment on quark masses in SCET*, *Phys. Lett.* **B564** (2003) 231 [[hep-ph/0303099](#)].
- [70] C. W. Bauer, D. Pirjol and I. W. Stewart, *Soft collinear factorization in effective field theory*, *Phys. Rev.* **D65** (2002) 054022 [[hep-ph/0109045](#)].